A PHENOMENOLOGICAL MODEL FOR FRACTION JETTING ON DISTILLATION SIEVE TRAYS FOR MULTI-REGIME MASS TRANSFER MODELING APPLICATIONS

By

ANAND N. VENNAVELLI

Bachelor of Technology in Chemical Engineering
Osmania University
Hyderabad, Andhra Pradesh, India
2002

Master of Science in Chemical Engineering
Oklahoma State University
Stillwater, Oklahoma, United States
2006

Submitted to the Faculty of the
Graduate College of
Oklahoma State University
in partial fulfillment of
the requirements for
the Degree of
DOCTOR OF PHILOSOPHY
May, 2011

A PHENOMENOLOGICAL MODEL FOR FRACTION JETTING ON DISTILLATION SIEVE TRAYS FOR MULTI-REGIME MASS TRANSFER MODELING APPLICATIONS

Dissertation Approved:

Dr. James R. Whiteley

Dissertation advisor

Dr. Jan Wagner

Dr. Karen A. High

Dr. Ahmad Shariat

Dr. David G. Lilley

Dr. Mark Payton

Dean of the Graduate College

ACKNOWLEDGMENTS

I would like to thank my advisor, Dr. Rob Whiteley, for his encouragement and support throughout my Ph.D. program. I'd also like to thank my committee members Dr. Karen High, Dr. Jan Wagner, Dr. David Lilley, and Dr. Ahmad Shariat for their input and advice.

Heartfelt thanks to my family and friends for their understanding and support. I'd like to thank my wife, Kinnera, for her constant support.

Finally, I'd like to thank Fractionation Research Inc. (FRI) for the financial support to this project.

TABLE OF CONTENTS

LIST OF TABLES

LIST OF FIGURES

Figure Page

NOMENCLATURE

a	Interfacial area per unit volume of dispersion (m^2 / m^3)
a_i	Interfacial area per tray area (m^2 / m^2)
a'	Total interfacial area (m^2)
b	Weir length per unit bubbling area (m / m^2)
d_{32L}	Sauter mean diameter of the large bubble (m)
D_G	Vapor diffusivity (m^2/ s)
d_h	Hole diameter (m)
d_j	Jet diameter (m)
D_L	Liquid diffusivity (m^2/ s)
E_b	E_{OG} for the bubbling zone (fractional)
E_j	E_{OG} for the jetting zone (fractional)
E_{LB}	Efficiency of the large bubbling zone (fractional)
E_{oc}	Efficiency predicted from a model (fractional)
E_{OG}	Vapor phase point efficiency (fractional)
E_{om}	Measured efficiency (fractional)
E_{SB}	Efficiency of the small bubbling zone (fractional)
F_b	Bubbling area based F-factor $u_b\rho_G^{0.5}$ $(Pa)^{0.5}$
f_j	Fraction jetting
FP	Flow parameter $\left(\frac{\rho_G}{\rho_L}\right)^{0.5}$ at total reflux
Fr'	Modified Froude number $u_b\sqrt{\rho_G}/\sqrt{g\rho_L h_{cl}}$

FSB	Fraction small bubbles
g	Acceleration due to gravity (m / s^2)
h_{cl}	Clear liquid height (m)
h	Height above the tray floor (m)
h_f	Froth height (m)
h_w	Height of the outlet weir (m)
k	Breakage constant for turbulent breakup (1 / s)
k_{Gj}	Vapor phase mass transfer coefficient in the jetting zone (m / s)
k_{LLB}	Vapor phase mass transfer coefficient of the large bubbles (m / s)
k_G	Vapor phase mass transfer coefficient (m / s)
k_{Lj}	Liquid phase mass transfer coefficient in the jetting zone (m / s)
k_{LLB}	Liquid phase mass transfer coefficient of the large bubbles (m / s)
k_L	Liquid phase mass transfer coefficient (m / s)
k_{OGj}	Overall vapor phase mass transfer coefficient in the jetting zone (m / s)
L	Liquid flow rate per weir length (m^3 / m /s)
m	Slope of equilibrium curve
n	Number of data points
p	Hole pitch (m)
Pe_G	Peclet number
Q_L	Liquid flow rate (m^3 / s)
Sh_∞	Asymptotic Sherwood number $k_G d_{32L}/D_G$
t_G	Mean vapor residence time (s)
t_{GLB}	Residence time of the large bubbles (s)
u_b	Vapor velocity based on bubbling area (m / s)

u_s Vapor velocity through hole(s) (m / s)

u_{LB} Velocity of the large bubbles (m / s)

V_b Vapor flow as bubbles (m^3 / s)

V_j Vapor flow as jets (m^3 / s)

V_{LB} Volume of the large bubbles (m^3)

W Width of the outlet weir (m)

y^* Vapor composition of the more volatile component in equilibrium with the liquid leaving the tray

y_0 Vapor composition of the more volatile component entering a tray

y_b Vapor composition of the more volatile component leaving the bubbling zone

y_i Intefacial vapor composition of the more volatile component

y_j Vapor composition of the more volatile component leaving the jetting zone

Greek letters

β Parameter in the fraction jetting model

ε Gas holdup fraction: volume of gas per unit volume of two-phase dispersion

ε_L Liquid holdup fraction: volume of liquid per unit volume of two-phase dispersion

η Volume of the vapor per volume of the liquid in the dispersion

μ_L Liquid viscosity (Pa.s)

ϕ Fractional hole area: ratio of hole area to bubbling area

ρ_F Dispersion density (kg/m^3)

$\rho_G \rho_L$ Vapor and liquid densities (kg/m^3)

σ Surface tension ($N.m^{-1}$)

CHAPTER 1

INTRODUCTION

Distillation is the the work-horse of separation in the process industries. According to Mix et al. (1978), distillation accounts for 3% of total energy consumed in the United States. Seader and Henley (2006) estimate the energy consumption by distillation to be equivalent to 13 million bbl/day of crude oil, and at a crude oil price of $40/bbl, approximately, to be $20 trillion per year. The potential for savings in capital costs, operating costs, and energy consumption from improvements in distillation design and operation is, therefore, considerable.

Internals used in a distillation column to promote vapor-liquid contact are broadly classified into two classes — trays and packing. Combinations of trays and packings in a single column have also been used. Trays and packings each offer a unique set of advantages and disadvantages, and the several criteria that need to be considered in the choice of internals are discussed elsewhere (Lockett, 1986). This work is focused on the distillation columns which employ trayed internals.

Sieve, valve, bubble cap, and dual flow trays are some of the different tray types used in distillation columns (Kister, 1992). Sieve trays are fabricated by punching holes into a flat plate. The liquid flows onto a tray from an inlet downcomer and flows across the tray and to the next tray through an outlet downcomer. The vapor rising through the sieve holes prevents the liquid from weeping. In valve and bubble cap trays, additional construction above the holes prevents liquid weeping at lower rates, but also results in additional pressure drop, because the vapor has to maneuver through these constructions. In the dual flow trays, there are no downcomers and the liquid and vapor flow counter currently through the holes.

The interacting liquid and vapor on a tray create a two-phase dispersion on the tray. Important design considerations, such as capacity or efficiency, are fundamentally dependent on the phase velocities, interfacial area, transfer-coefficients, and contact times. The success of an improved design method, therefore, is directly tied to the accuracy of the models for the two-phase characteristics.

The bi-phase on a tray has been categorized into several flow regimes - emulsion, foam, bubble, froth, and spray. The flow regime identifies the nature and behavior of the continuous and the dispersed phases in the bi-phase. An operating tray can function in any of the five flow regimes reported on a tray (Kister, 1992; Lockett, 1986) depending on the vapor-to-liquid ratio and the physical properties of the system. Of the different flow regimes on a tray, the froth and the spray regimes are the most commonly occurring on an industrial tray.

Flow regimes have been used as a basis for fundamental modeling as they provide a generalization of the bi-phase behavior. Categorizing models by flow regimes, however, has a fundamental disadvantage because of the need to predict the transition between flow regimes in order to apply the appropriate model. A discontinuity at the flow regime boundaries exists, and the gradual transitions in the efficiency and capacity observed experimentally cannot be explained by this sudden change in bi-phase behavior at the flow regime boundary.

Nevertheless, several empirical and theoretical studies, have been performed to investigate the regime transitions, particularly the froth-spray transition, on sieve trays. Excellent reviews of the transition studies are available (Hofhuis and Zuiderweg, 1979; Lockett, 1981; Prado et al., 1987). A majority of the froth-spray transition work is on sieve trays. However, the froth-spray transition studies have also been extended to valve trays (Dhulesia, 1983). Despite the several studies on the froth-spray transition over the years, no reliable theoretical model exists (Lockett, 1981, 1986).

A fundamental drawback of all the froth-spray transition studies is that they assume

that the froth-spray transition is sudden and characterized by an operating point. While the theoretical considerations developed for the froth-spray transition still apply, a new approach is needed that considers the gradual transitions in the flow regimes rather than a sudden and well-defined transition point.

The gradual change in the properties from one flow regime to another is due to the gradual change in the vapor transport mechanisms. The broad definitions of the flow regimes do not clearly delineate the various vapor transport mechanisms that exist. For instance, the classical hydraulic model, which considers the bi-phase as an emulsion of bubbles is applied to the entire froth regime because the froth regime is generally defined as a liquid continuous regime. Studies in the froth regime (Ashley and Haselden, 1972; Hofhuis and Zuiderweg, 1979; Raper et al., 1979, 1982), however, showed that the vapor transport in the froth regime is not entirely in the form of bubbles. As the gas velocity increases, intermittent vapor jets begin to form, and the vapor jets dominate the bi-phase before transition to spray. To accommodate the vastly different vapor transport mechanisms, Hofhuis and Zuiderweg (1979) proposed that the froth regime be divided into two subregimes: (i) the bubbling froth, where the vapor transport is entirely in the form of bubbles, and (ii) the mixed-froth, where the vapor transport is both in the form of bubbles and jets. The mixed-froth regime described by Hofhuis and Zuiderweg (1979) is the transition zone where the jets are beginning to form at one boundary and the jets are totally dominant at the other. Even at conditions in the bubbling subregime, a bimodal bubble distribution exists and the properties of the large bubbles may be different from those of the small bubbles (Ashley and Haselden, 1972). In the mixed froth regime, the transport by bubbles and jets is markedly different.

The ability to accurately and reliably predict the efficiency and capacity of trays in the froth regime fundamentally should include and account for all of the various vapor transport mechanisms that may be present. Incorrectly approximating the entire froth regime using a single model based on bubble transport mechanisms is fundamentally flawed. Sim-

ilarly, categorizing models by a single mode of vapor transport is ineffective because vapor transport via multiple mechanisms simultaneously exists.

Alternatively, accounting for contributions from all mechanisms of vapor transport leads to multi-regime models that can be simplified to the existing single-regime models when only one mode of vapor transport is active, but can also be applied when multiple modes of vapor transport are possible. Therefore, rather than forcing the transport mechanisms to be bubble or jets based on the prevalent flow regime, a new approach to account for the vapor transport mechanisms using a fraction jetting (and fraction bubbling) has been used (Garcia and Fair, 2000b; Prado and Fair, 1990; Syeda et al., 2007).

The fraction jetting model can also explain the effect of rate, geometry, and physical properties on efficiency in a manner that was not explained hitherto because changes in rate, geometry, or physical properties not only affect transfer-coefficient, residence times, contact times, or interfacial area, but also the fraction jetting and therefore the relative contributions of the different modes of vapor transport.

A fundamental fraction jetting model can also provide insights into key factors promoting or inhibiting modes of vapor transport and, thereby, increasing the maximum efficiencies observed on the trays by modest changes to design.

Fraction jetting models also facilitate multi-regime models, such as the Syeda et al. (2007) sieve tray efficiency model, that are valid for both froth and spray regimes by accounting for the contributions of the jets from when they begin to form in the froth regime, rather than when they are noticeably formed at the spray transition. This is a better way to gradually transition between regimes and to use the same model in both regimes.

The hypothesis of this work is that an improved fraction jetting model will lead to more reliable multi-regime models. Predicting the fraction of the vapor transported as jets, or fraction jetting, on a tray operating in the mixed-froth regime can bridge froth and spray regime models, explain gradual changes in tray efficiency during the froth-spray transition, and eliminate the need to predict the froth-spray transition point when separate froth and

spray regime models are used.

Existing fraction jetting models have several shortcomings. Only two models for fraction jetting exist in the literature (Prado and Fair, 1990; Syeda et al., 2007). The current fraction jetting models are empirical and developed from limited data. Prado et al. (1987) data used for the Prado et al. model were collected at the sieve holes on a tray, whereas the Raper et al. (1982) data used for the Syeda et al. model were collected in the dispersion. The models therefore are developed from inherently different fraction jetting measurements and, as such, are not directly comparable. However, both models were developed from air-water data and are entirely empirical.

The empirical nature of any model implies limited extrapolative or predictive capability. This is of importance for the fraction jetting models because the data from which these empirical models were developed are all from the air-water system and do not have sufficient variability in terms of the factors affecting fraction jetting. The reliability of the empirical models improves only when there is a large amount of quality data with a wide range of the variables that have a stake are represented.

Therefore, there is a need to phenomenologically account for the factors affecting fraction jetting and include them in the fraction jetting model in a reliable way. The current models are lacking in this regard.

1.1 Research Objectives

The objectives of this work are to:

1. Develop a fundamental model for fraction jetting
2. Determine the physical significance of the parameters in the fraction jetting model
3. Demonstrate the applicability of the fraction jetting model as an alternative to existing fraction jetting model

1.2 Contributions of this work

The main contribution of this work is a new phenomenological one-parameter model to describe the fraction jetting on distillation trays. The physical significance of the parameter in the model is explained in terms of the change in dominant mode of vapor transport from bubbles to jets.

Fraction jetting models are often used as intermediate models in the hydraulic and efficiency models developed from a mechanistic framework and incorporate jetting such as Syeda et al. (2007), Prado and Fair (1990), and Garcia and Fair (2000b) models. In this work, the fraction jetting model is developed such that it can be directly applicable to the existing mechanistic models that rely on a fraction jetting model for efficiency prediction. The applicability and the advantages of the new fraction jetting model are demonstrated using the Syeda et al. (2007) sieve tray efficiency model.

The liquid and vapor rates, tray geometry, and the system physical properties all affect the fraction jetting and consequently the effective mechanism of vapor-liquid contact on a tray. Change in the operating condition therefore has (i) a direct effect through a change in the bi-phase properties and (ii) an indirect effect through a change in the fraction jetting. The indirect effects are not well understood. In this work, using the predictions of the fraction jetting model, the indirect effects of fraction jetting are explained.

This work provides a platform for design of better hardware to promote or inhibit jetting because it identifies fraction jetting as an additional handle for design and modeling. In addition, this work provides a basis to explain the rate and physical property effects in terms of the contact mechanisms on the tray.

The scientific contributions of the research stem from an improved understanding of the jetting phenomenon and the ability to explain indirect effects of rate, geometry, and physical properties in terms of jetting. The work also provides a fundamental basis for fraction jetting models and a launch pad for the development of new multi-regime models.

Furthermore, the fundamental concept is also valid for other separation processes such as absorption or stripping.

The economic contributions of this research are expected not only from improved designs for trays, but also from improved overall distillation column designs. An understanding of fraction jetting promotes our ability to push the operation envelope for higher capacity and efficiency gains. The large scale economics of distillation operation implies that even minor increases in efficiency or capacity can lead to a large economic benefit. Since distillation is a mature technology already in place for over 200 years, the profit margins are tight and there is a continuous need for improvement. The fraction jetting model is expected to bring new opportunities for distillation research and development. Conversations with the leading distillation research experts at FRI (FRI, 2010) also led the author to believe that jetting is observed at almost all rates and systems and may be the missing piece in current distillation models. Finally, the models incorporating jetting via the fraction jetting concept are closer to reality and, for that reason, have greater model reliability.

The broader impacts of this research are to make distillation systems more efficient and process industries more competitive. According to Kister (1992), "distillation is the king of separations," and no existing technology can replace distillation in the near future (Kunesh et al., 1995). Improved designs for distillation lead to better efficiency, reliability, and sustainability, and favorably impact the society through reduced emissions, lesser carbon footprint to achieve the same separation, and the more tangible economic benefits in an energy driven economy.

1.3 Organization

In Chapter 2, an analysis of the needs and gaps in the literature are presented along with a review of the state-of-the-art on vapor jetting on distillation trays. In Chapter 3, a new fraction jetting model is described. In Chapter 4, the new fraction jetting model is applied to the Syeda et al. (2007) sieve tray efficiency model and the results are discussed.

In addition, the scope of the study and limitations of the proposed model are discussed. Summary, conclusions, and directions for future work are described in Chapter 5.

CHAPTER 2

VAPOR JETTING ON DISTILLATION TRAYS

The bi-phases on a tray can function in several possible flow regimes on a distillation tray depending on the physical properties and the liquid-to-vapor ratio. Each flow regime has a characteristic dominant mechanism of vapor and liquid transport.

In this chapter, a review of the flow regimes and the transitions between the froth and spray regimes on distillation trays with emphasis on vapor transport mechanisms is presented. In addition, the concept of fraction jetting, its measurement, modeling, and applications are presented. Finally, an analysis of the needs and gaps is presented.

2.1 Basic definitions

In this section, some of the commonly used terms in this thesis and their physical significance are presented.

F-factor The F-factor is a term to denote the vapor load. The F-factor is the square-root of the kinetic energy of the vapor and is defined as

$$\text{F-factor } F_b = u_b\sqrt{\rho_G} \tag{2.1}$$

where

F_b is the F-factor,

u_b is the vapor velocity based on the bubbling area, and

ρ_G is the vapor density.

In some cases, the F-factor is defined using vapor velocity based on the hole area and

is termed as the hole F-factor (F_h) and is defined as

$$F_h = u_h \sqrt{\rho_G} \tag{2.2}$$

The F-factor is expressed in m/s $(\mathrm{kg/m^3})^{0.5}$, or equivalently, $(\mathrm{Pa})^{0.5}$

Clear liquid height (h_{cl}) The clear liquid height is the level to which the liquid falls if the vapor flow stops and the liquid is prevented from weeping. The clear liquid height is a measure of the liquid head on the tray and is an important variable in most capacity and efficiency models. The clear liquid height is defined for both liquid continuous and vapor continuous regimes. In general, the clear liquid height is the ratio of the volume of the liquid in the dispersion to the bubbling area.

The clear liquid height is measured in m.

Hold-up fraction The hold up fraction relates the volumes of the liquid, the vapor, and the dispersion. Accordingly, there are three definitions: (i) gas hold up fraction (ε)— the volume of the gas in a unit volume of the two-phase dispersion, (ii) liquid hold up fraction (ε_l or α_e) — the volume of the liquid in a unit volume of dispersion, and (iii) $\eta = \frac{\varepsilon}{1-\varepsilon}$, the ratio of the gas to the liquid volumes in the dispersion.

Fraction jetting (f_j) The fraction jetting is the ratio of the volume of the gas transported in the form of jets to the total volume of the gas transported. The fraction jetting is the spray-like nature of the froth. The fraction jetting (f_j), volume fraction of the gas transported as jets, is defined as

$$f_j = \frac{V_j}{V_b + V_j} \tag{2.3}$$

where

V_j is the vapor flow as jets ($\mathrm{m^3}$ / s), and

V_b is the vapor flow as bubbles ($\mathrm{m^3}$ / s).

2.2 Flow regimes

On a distillation tray, the flow regime describes the two-phase mixture, which could be liquid-continuous-vapor-dispersed, vapor-continuous-liquid-dispersed, or both. The two-phase dispersions on a tray are classified into five flow regimes (Lockett, 1986): emulsion, foam, bubble, spray, and froth.

In the bubble, emulsion, and the foam regimes, the liquid is the continuous phase and the vapor is the dispersed phase. In each of the three regimes, vapor rises as bubbles through the liquid. In the bubble regime, the liquid is slow moving and relatively quiescent, but in the emulsion regime, the liquid has a high horizontal momentum. The foam regime, also liquid continuous and vapor dispersed, occurs when bubble coalescence tendencies are significant.

In the spray regime, the vapor is the continuous phase and the liquid is the dispersed phase. Jets of vapor rise through the tray openings and atomize the liquid on the tray projecting liquid droplets into the intertray spacing. The liquid droplets are simultaneously subject to drag, gravity, and buoyancy forces and, as a result, fall back on to the tray to repeat the projection process or get entrained to the tray above.

In the froth regime, liquid and vapor continuous dispersions could coexist. The vapor transport in the froth regime, bounded by the bubble and spray regimes on a regime diagram, gradually changes from bubble dominated to jet dominated with increasing F-factor. However, jetting begins well before the transition to the spray regime. For this reason, the froth regime was also referred to as being made up of two subregimes — the bubbling-froth where the vapor transport is only by bubbles and the mixed-froth — where the vapor transport is by both bubbles and jets (Hofhuis and Zuiderweg, 1979). In the froth regime at lower rates, the vapor transport is primarily in the form of bubbles (Figure 2.1(a)). As the vapor rates are increased, intermittent vapor jets begin to form, and eventually, the jets break through the liquid layer on the tray (Figure 2.1(b)). At much higher rates, the vapor jets dominate the bi-phase on the tray and the bi-phase resembles a spray (Figure 2.1(c)).

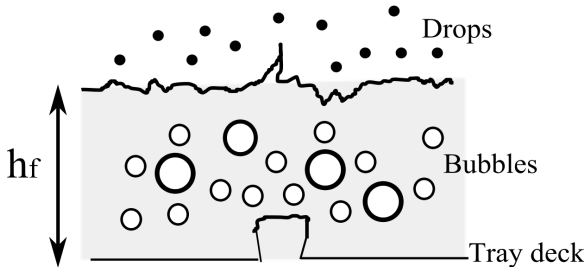

(a) two-phase structure in the bubbling zone

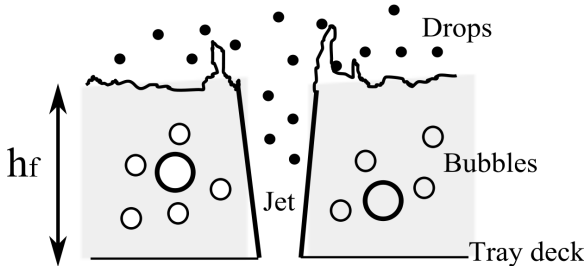

(b) two-phase structure in the jetting zone

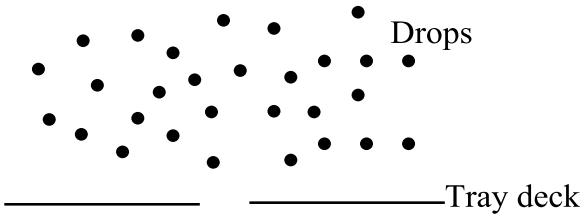

(c) two-phase structure in the spray

Figure 2.1: Two-phase structure on a tray.

When more than 60% of the tray is jetting, a visible transition in the froth structure occurs (Prado et al., 1987) and the transition to the spray regime is initiated. Further increase in the vapor rate leads the operation into a vapor-continuous-liquid-dispersed spray regime.

Of the various flow regimes on a tray, the froth regime is considered to be the most common to occur on industrial trays and is also the most complex (Kister, 1992). The operation in the froth regime is characterized by constant fluctuations in the froth height (Wijn, 1998). The local properties of the froth may vary considerably from the average depending on the bubble sizes, coalescence and breakup of bubbles (Hu et al., 2007; Wijn, 1998), froth stabilization effects (Zuiderweg, 1982), surface tension and surface tension gradients (Syeda et al., 2004), and random movements in the dispersion.

Not surprisingly, several variations of the froth bi-phase have been proposed and used for modeling. Most notable among them are treating the froth as (i) an emulsion of bubbles (AIChE, 1958), (ii) large bubbles, small bubbles, and jets (Ashley and Haselden, 1972; Prado and Fair, 1990; Syeda et al., 2007), (iii) a vapor continuous region populated with projected droplets over the liquid continuous region on the tray deck (Bennett et al., 1997), and (iv) a vertical froth density distribution with a high liquid level zone and a low liquid level zone (Van Sinderen et al., 2003). Specifying the prevalent flow regime on a tray and the appropriate hydraulic contact mechanisms on a tray in the froth regime has implications on the choice of the models as described in the next section.

As a result, several studies were undertaken to study the froth-spray transitions. Early work was focused on bubble cap trays and later on sieve trays. The froth-spray transition studies are described in the next section.

2.3 Froth-spray transition studies

The froth-spray transitions are the most studied flow regime transitions on trays since Zuiderweg and Harmens (1958) first indicated that a phase inversion occurs from a liquid continuous (froth) to a vapor continuous (spray) dispersion on sieve trays.

The froth-spray transition has been attributed to the drop coalescence phenomenon occurring at a certain level above the tray (Andrew, 1969; Porter and Wong, 1969), to the interaction between the gas core of the jet and the liquid film adjacent to the gas core (Sundar and Tan, 1999; Tan and Sundar, 2001), but mostly to the mechanisms resulting from the two opposing forces due to the vapor inertia and the gravitational force on the liquid, i.e., to the jet penetration theory described later in this section.

Owing to the gradual nature of the froth-spray transition, several criteria have been used to define it. The common techniques that have been used for detecting the regime transitions on trays are changes in light transmission (Porter and Wong, 1969), electrical conductivity (Loon et al., 1973; Pinczewski and Fell, 1972; Prado and Fair, 1987; Raper et al., 1982), residual pressure drop (Payne and Prince, 1975), liquid holdup profile (Barber and Wijn, 1979), and orifice pulsation frequency (Pinczewski and Fell, 1972). Additionally, acoustic and differential pressure signals (Al-Masry et al., 2007) and visual observations (Barber and Wijn, 1979) have also been used.

The different techniques for the froth-spray transition studies led to several correlations for predicting the froth-spray transition point. Lockett (1986) and Prado et al. (1987) present an excellent review of the froth-spray transition studies. In this section, a brief review of the froth-spray transitions studies is presented.

Lockett (1981) performed theoretical modeling of the froth-spray transition using the jet penetration theory. Lockett was able to reduce the jet penetration theory equation, using various values of the two parameters in the equation, to match the existing froth-spray correlations by Barber and Wijn (1979), Hofhuis and Zuiderweg (1979), Payne and Prince (1977), and Wong and Kwan (1979).

According to the jet penetration theory, a force balance between forces favoring and resisting jet formation on a tray determines the froth-spray transition. Vapor jetting prevails when the momentum of the vapor jet exceeds the momentum of the liquid trying to form a bridge across the vapor jet. At near spray-like conditions, the vapor jets are continuous

and penetrate completely through the froth. However, at lower rates, the force due to the weight of the liquid tends to collapse the jet. The jet penetration theory predicts that at the transition point, the two forces are equal.

The equations for the jet penetration model for froth-spray transition are described as follows: The momentum of the gas jet, with a cross sectional area A_j is

$$u_{\text{gas}}^2 \rho_G A_j \tag{2.4}$$

where

u_{gas}^2 is the vapor velocity at a height h above the tray floor (m/s), and

ρ_G is the vapor density (kg/m^3).

Similarly, the weight of the fluid above the gas jet that forms a bridge at a height h is

$$g\rho_F(h_f - h)A_j \tag{2.5}$$

where

ρ_F is the froth density (kg/m^3),

h_f is the froth height (m), which is constant for a given liquid and vapor rate.

h is the height above the tray floor (m), and

g is the acceleration due to gravity (m/s^2).

Therefore, according to the jet penetration theory,

$$u_{\text{gas}}^2 \rho_G = g\rho_F(h_f - h) \tag{2.6}$$

A uniform froth-density is assumed so that

$$\frac{d(\rho_G u_{\text{gas}}^2)}{dh} = -\rho_F g \tag{2.7}$$

However, the assumption of the uniform froth density is a gross over-simplification according to Lockett.

In the jet penetration theory, the following equation was used to describe the expansion of the jet issuing from an orifice:

$$\left(\frac{d_j}{d_h}\right)^n = a\left(\frac{h}{d_h}\right) + 1 \tag{2.8}$$

where

n and a are variables describing the cone angle of the jet,

d_j is the diameter of the jet at a height h above the tray floor (m),

d_h is the hole diameter (m).

The function shown in Equation (2.8) for a=1, and for various values of n is shown in Figure 2.2.

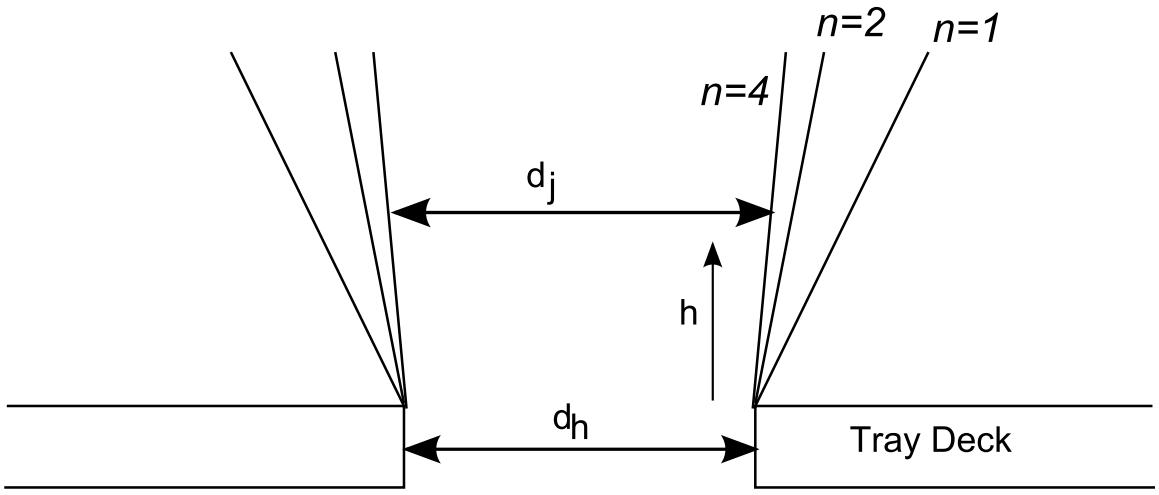

Figure 2.2: Jet expansion above a sieve hole described by Equation (2.8) for a=1, and for various n. Source: Lockett (1981)

From gas continuity in the jet, and no change in the gas density,

$$u_j d_j^2 = u_h d_h^2 \tag{2.9}$$

where

u_j is the vapor velocity in the jet (m/s), and

u_h is the vapor velocity through the holes (m/s).

From Equations (2.6)–(2.9), and using $\rho_F = \rho_L(1-\varepsilon)$ and $h_{cl} = h_f(1-\varepsilon)$, the final

expression according to the jet penetration theory was obtained as

$$\frac{h_{cl}}{d_h} = \frac{(4+n)/n}{(4/n)^{4/(4+n)}} \left(\frac{\rho_G}{\rho_L}\right)^{n/(4+n)} \frac{u_h^{2n/(4+n)}}{a^{4/(4+n)}} \frac{(1-\varepsilon)^{4/(4+n)}}{(gd_h)^{n/(4+n)}} - \frac{1-\varepsilon}{a} \tag{2.10}$$

where

ρ_L is the liquid density (kg/m^3), and

ε is the gas hold up fraction.

Equation (2.10) expresses the froth-spray transition in terms of the vapor and liquid rates. The clear liquid height at transition can be determined from any of the clear liquid height correlations available in the literature (Lockett, 1986). Lockett recommends the Hofhuis and Zuiderweg (1979) correlation for use in Equation (2.10). The operating condition that satisfies the Equation (2.10) corresponds to the froth-spray transition point.

The published froth-spray correlations correspond to $n = 1, 2$, or 4 in Equation (2.10). The Barber and Wijn (1979) correlation corresponds to $n = 1$ and was derived with a constant cone angle of the jet:

$$\frac{h_{cl}}{d_h} = 1.35 \left(\frac{\rho_G}{\rho_L}\right)^{0.25} \frac{u_h^{0.4}}{(gd_h)^{0.2}} \left(\frac{p}{d_h}\right)^{0.33} - 0.59 \left(\frac{p}{d_h}\right)^{0.33} \tag{2.11}$$

where

p is the hole pitch.

Hofhuis and Zuiderweg (1979) correlation, Equation (2.12), corresponds to $n = 2$.

$$\frac{h_{cl}}{d_h} = 1.07 \left(\frac{\rho_G}{\rho_L}\right)^{0.33} \frac{u_h^{0.66}}{(gd_h)^{0.33}} \tag{2.12}$$

The Payne and Prince (1977) correlation, based on the slug-annular flow transition in vertical two-phase pipe flow, is

$$\frac{h_{cl}}{d_h} = 1.5 \left(\frac{\rho_G}{\rho_L}\right)^{0.5} \frac{u_h(1-\varepsilon)^{0.5}}{(gd_h)^{0.5}} \tag{2.13}$$

The Wong and Kwan correlation, developed from an earlier equation by Porter and Wong (1969), which is based on a fluidized bed model for the spray regime, is

$$\frac{h_{cl}}{d_h} = 30.5 \left(\frac{\rho_G}{\rho_L}\right)^{0.5} \frac{u_h(1-\varepsilon)}{g^{0.5}} + 2.06(1-\varepsilon) \tag{2.14}$$

The correlations by Payne and Prince (1977), Equation (2.13), and Wong and Kwan (1979), Equation (2.14), correspond to $n = 4$.

However, Lockett (1986) argued that none of the above correlations are satisfactory in explaining the experimental data and proposed a simple empirical expression:

$$\frac{h_{cl}}{d_h} = 2.78 \left(\frac{\rho_G}{\rho_L} \right)^{0.5} u_h \tag{2.15}$$

Most of the correlations for the froth-spray transition include the clear liquid height, which, in turn, is a function of the liquid and vapor rates and tray geometry. Pinczewski and Fell (1982) proposed a correlation that does not include clear liquid height. The froth-spray transition is correlated directly in terms of the vapor and liquid rates. The correlation is

$$u_b \rho_G^{0.5} = 2.75 \left(\frac{Q_L}{W} \rho_L^{0.5} \right)^{0.91 \frac{d_h}{\phi}} \tag{2.16}$$

where

u_b is the vapor velocity based on the bubbling area (m/s),

Q_L is the liquid volumetric flow rate (m^3/s),

W is the outlet weir length (m), and

ϕ is the fractional open area.

Johnson (1981) proposed an empirical model for the froth-spray transition that includes a dependence on surface tension:

$$u_b = 0.04302 \rho_G^{-0.5} \rho_L^{0.692} \sigma^{0.06} \phi^{0.25} L^{0.05} d_h^{-0.1} \tag{2.17}$$

where

σ is the surface tension (N/m), and

L is the liquid volumetric flow rate per unit weir length (m^3/s/m-weir).

The effect of surface tension on the froth-spray transition, however, is unclear from the transition correlations. Jeronimo and Sawistowski (1973) proposed an equation with a

greater dependence on surface tension than Equation (2.17):

$$u_b = \frac{\frac{0.655}{\phi}\left(\frac{g(\rho_L-\rho_G)\sigma^2}{d_h\rho_G^3}\right)^{1/6}}{1+0.000104L^{-0.59}\phi^{-1.79}} \tag{2.18}$$

Porter and Wong (1969), Prince et al. (1979), and Lockett (1981) found no dependence of surface tension on the froth-spray transition. The effect of variables included in the empirical correlations, however, cannot be reliable because the effect of the ratio such as $\frac{\rho_G}{\rho_L}$ can be correlated in terms of other physical properties (Lockett, 1986). The theoretical jet penetration theory equation does not consider surface tension forces to play a part in the froth-spray transition. The froth-spray transition correlations by Sundar and Tan (1999) and Tan and Sundar (2001), derived from a force balance on a liquid film adjacent to the gas core, however, include surface tension using the Kutateledze number. The Sundar and Tan (1999) correlation is

$$\frac{h_{cl}}{d_h} = 0.794\,Ku + 2.124 \tag{2.19}$$

The Tan and Sundar (2001) correlation is

$$\frac{h_f}{d_h} = 1.85\,Ku + 1.96 \tag{2.20}$$

where Ku is the Kutateledze number defined by

$$Ku = \frac{u_h\rho_G^{0.5}}{(\sigma g(\rho_L-\rho_G))^{0.25}} \tag{2.21}$$

The Kutateledze number is the ratio of the forces due to gas inertia to the forces due to surface tension and buoyancy.

In summary, several correlations exist for froth-spray transition on sieve trays. The correlations express the froth-spray transition in terms of the liquid and vapor rates and the clear liquid height. Surface tension has also been included in some correlations. The correlations allow the designer to characterize the flow regimes into froth or spray by predicting the transition point. The implications of such flow regime characterization are described in the next section.

2.4 Implications of the flow regime on modeling

The hydraulic and mass transfer properties of the trays are a function of the properties of the two-phase dispersion on a tray. Fundamental modeling requires characterization of the continuous and the dispersed phases, or, in effect, the hydraulic nature of the bi-phase. Therefore, the flow regime, which characterizes the dispersion, is central to fundamental hydraulic and mass transfer models on trays.

A change of the flow regime in the normal operating region implies a change in the dispersion structure on the tray at the point of phase inversion warranting separate models for each flow regime. To address the flow regimes in modeling, researchers chose one of the following options: (a) a semi-empirical model that extrapolates into adjoining regimes (Chen and Chuang, 1993), or (b) a separate model for each regime (Bekassymolnar and Mustafa, 1991; Zuiderweg, 1982) coupled with correlations described in Section 2.3.

Proponents of the first approach argue that despite the change in the flow regime and the associated transport phenomenon, the observed properties such as efficiency change only gradually. As a result, models developed for one flow regime have been incorrectly extrapolated into another taking advantage of the gradual transition in the capacity and efficiency during regime change. However, this approach is fundamentally flawed because a model developed on the assumption of liquid continuous phase, for instance, is unreliable when the liquid becomes a dispersed phase.

On the other hand, the two model approach assumes that a flow regime transition point exists and occurs suddenly. The uncertainty in the predicted transition point, in addition to the likely presence of a transition zone instead of a transition point, invariably implies that the separate model approach is only reliable when the flow regime is known for certain and not during the transition zones.

The alternate approach, the approach used in this work, is that the change in flow regime is not sudden, but gradually changes with the change in operating conditions as the dom-

inant modes of vapor transport change. By accounting for all transport mechanisms, the regimes are bridged as the vapor transport mechanism changes.

The studies of flow regime transitions, however, are not completely invalid with such an assumption. As Prado et al. (1987) have shown, the "visible" transition to spray from froth occurs about 50-60% of fraction jetting. Therefore, the ideas developed for the froth-spray transitions, particularly the theoretical considerations based on the jet penetration theory, are also valid for fraction jetting. The modeling work on the froth-spray transition studies provides insight into the variables affecting the transition.

The rest of the chapter is focused on fraction jetting that describes the regime change between the froth and the spray — the most likely flow regimes to occur on industrial trays (Kister, 1992).

Fraction jetting was defined in Section 2.1. The fraction jetting is zero when all the vapor is transported as bubbles and one when the entire vapor is transported as jets. Jetting studies on sieve trays indicate that low fraction jetting is favored by large clear liquid heights, and by low gas velocities (Lockett, 1986). Greater horizontal liquid momentum also favors low fraction jetting as the tendency to form a liquid bridge across the tray open is high (Lockett, 1981, 1986).

The next section describes fraction jetting measurement, modeling, and applications. The summary of needs and gaps conclude the chapter.

2.5 Measurement of fraction jetting

The optical probe and the conductivity (or electric-resistivity) probe have been primarily used for quantitative study of bubble properties in the two-phase mixture on trays. The optical probe is similar in construction to the conductivity probe and is used when the liquid involved is non-conducting or flammable. The detailed description of the techniques is found in Lockett (1986). Yang et al. (2007) presents a review of the applications of the bubble probe and other bubble property measurement techniques in two-phase flows.

The measurement of fraction jetting using the conductivity probe is indirect. The conductivity probe, also called the bubble probe, accounts for all vapor transported as bubbles. The vapor that is not accounted for is the vapor that bypasses the probe in the form of jets. The measurement of the fraction jetting using the bubble probe data is described in this section.

The bubble probe was first designed by Burgess and Calderbank (1975) and Calderbank and Pereira (1977). The limitations of the first bubble probe was that it was difficult to measure closely space bubbles (Calderbank, 1978).

2.5.1 Raper et al. measurement method

Raper et al. (1982) used a mini-computer software that keeps track of preceding bubbles and allows closely spaced bubbles to be accepted. The Raper et al. probe is placed at the center row of tray openings and approximately midway through the froth vertically. The bubble probe used by Raper et al. is essentially a collection of vapor-liquid continuity detectors placed as shown in the Figure 2.3. The continuity detector 1 is surmounted by another three detectors $2, 3,$ and 4. The probe is positioned vertically so that the detector 1 is at the midpoint of the froth. It is not necessary for all continuity detectors to be placed in the liquid phase. The multiple detectors provide a means of rejecting non vertical bubbles (Raper et al., 1982).

The time it takes for the leading surface of a bubble to pass detector 1 yields bubble central axis length. The time it takes for the leading edge of the bubble to pass from detector 1 to detectors $2, 3,$ or 4 gives the bubble velocity.

The bubble probe gives the distribution of the bubble sizes and bubble velocities. Using the gas hold up fraction, measured independently by Raper et al. using gamma-ray densitometry, the total flux of bubbles crossing a horizontal plane in the dispersion is

$$N_T = \frac{\varepsilon}{\sum_{i=1}^{n} \frac{f_{bi} V_{Bi}}{U_{Bi}}} \tag{2.22}$$

where

N_T is the total number of bubbles passing a unit horizontal plane in dispersion per second,

ε is the gas holdup fraction,

f_{bi} is the size distribution frequency of the bubbles of size d_{Bi},

V_{Bi} is the volume of the bubbles of size d_{Bi} (m^3), and

U_{Bi} is the rise velocity of the bubbles of size d_{Bi} (m/s).

The apparent superficial velocity, V_s' , across the plane is

$$V_s' = N_T \sum_{i=1}^{n} f_{bi} V_{Bi} \tag{2.23}$$

The apparent superficial velocity is the fraction of the superficial velocity accounted by the bubbles. The fraction jetting is obtained from the vapor unaccounted by the bubble probe as

$$f_{j,meas} = \frac{V_s - V_s'}{V_s} \tag{2.24}$$

Using the bubble probe data and Equation (2.24), Raper et al. (1982) measured fraction jetting on sieve, valve, and bubble cap trays.

2.5.2 Prado et al. measurement method

Prado et al. (1987) also used the bubble probe and the mini-computer software to measure the fraction jetting data on sieve trays. The technique used by Prado et al. was similar to that used by Pinczewski and Fell (1972). An electrical resistance probe was bolted to the underside of a tray so that the tip of the probe protruded through the orifice. These probes were inserted into eight holes on a given tray.

When liquid surrounded the orifice, the circuit was closed, whereas when bubbles or jets were formed, the circuit was open. Analog pulses were recorded by a pulse counter as zeros (for liquid) or ones (for vapor).

An equal volume of the gas was assigned to every sampled ‘one.’ From the total sampling time, gas flow rate, and total number of sampled ‘ones,’ a volume of the gas per ‘one’

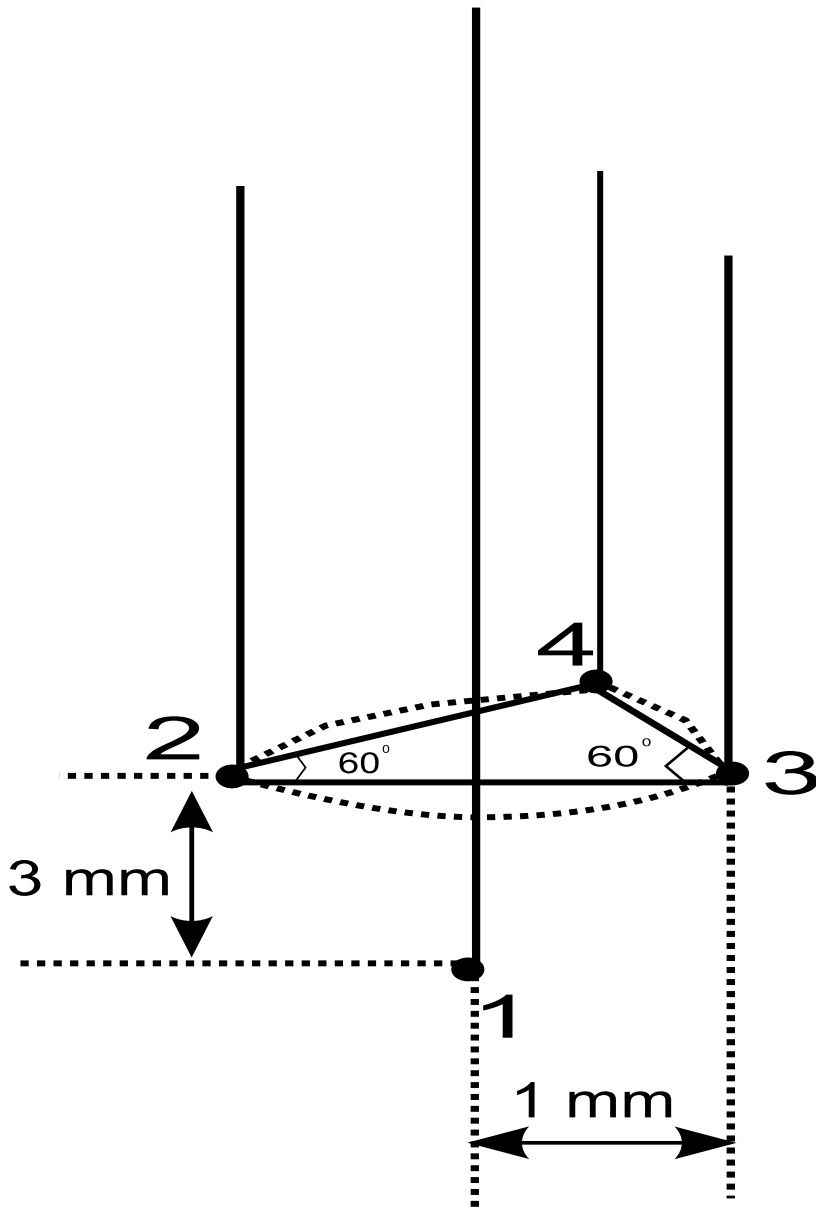

Figure 2.3: Schematic of the bubble probe used by Raper et al. Source: Raper et al. (1982)

was determined. Converting the chains of ones into equivalent spherical bubble diameters produced a binormal distribution of bubble sizes. The equivalent bubble volumes greater than that of the second (larger) mode of the binormal bubble size distribution were counted as jets.

The liquid cover or hole inactivity was obtained as the number of zeros divided by the total number of zeros and ones. The fractions of small bubble, large bubble, and jetting were obtained by dividing the number of ones for each characteristic hole activity by the total number of zeros and ones.

The location of the conductivity probe affects the utility measured fraction jetting data. The Prado et al. data are obtained with the conductivity probe located at the holes. However, the measurement of the fraction jetting at the holes is different from the fraction jetting in the dispersion. Because of the measurement location, Prado et al. report, in addition to bubbling and jetting, a fraction of liquid cover, which indicates that there is not enough information whether a particular hole is bubbling or jetting. On the other hand, the measurements of the Raper et al. data are based on the conductivity probe placed at the midpoint of the froth.

All fraction jetting data are collected on air-water systems. However, several models used in distillation that are developed from air-water have been found to be very much applicable to hydrocarbon systems that exhibit relatively low non-ideality as long as the physical property effects are accurately incorporated.

Table 2.1: Description of fraction jetting data. The instrument used in both cases is the conductivity probe.

Source	Tray types	Datapoints	No. Probes	Location
Raper et al. (1982)	Sieve, valve, and bubblecap	29	1	In the dispersion
Prado et al. (1987)	Sieve	429	8	In the orifice

2.6 Modeling fraction jetting

Only two models for fraction jetting are found in the literature — Prado and Fair (1987) and Syeda et al. (2007). Both models are empirical models. The Prado and Fair (1987) model was developed from Prado's data and includes eight estimated parameters. The Syeda et al. (2007) model was developed from Raper's data and includes three parameters.

In this section, the two model equations are presented, and the advantages and the limitations of the models are discussed.

As described in Section 2.5, the data collected for the Prado et al. model are inherently different from the Raper et al. data because of the different measurement locations employed.

For the fraction jetting model to be used in capacity and efficiency correlations, the data of Raper et al. measured in the midpoint of the froth are more appropriate. For a fraction jetting model that is to be used for orifice phenomenon, the Prado et al. data are more appropriate.

A brief review of the two models along with the model equations is presented here.

2.6.1 Prado et al. fraction jetting model

The Prado et al. model equations are shown in Equations (2.25)–(2.27).

$$f_j = \frac{u_b - u_{b,0}}{u_{b,100} - u_{b,0}} \tag{2.25}$$

$$u_{b,0} = 0.1\rho_G^{-0.5}\rho_L^{0.692}h_w^{0.132}d_h^{-0.26}\phi^{0.992}L^{0.27} \tag{2.26}$$

$$u_{b,100} = 1.1\rho_G^{-0.5}\rho_L^{0.692}h_w^{0.132}d_h^{-0.26}\phi^{0.992}L^{0.27} \tag{2.27}$$

where

u_b is the vapor velocity based on bubbling area (m/s),

$u_{b,0}$ is the vapor velocity based on bubbling area at 0% jetting (m/s), and

$u_{b,100}$ is the vapor velocity based on bubbling area at 100% jetting (m/s).

The Prado et al. model has eight estimated parameters. The variables included in Prado's fraction jetting model are the most common variables used in several froth-spray transition studies. The Prado model, Equation (2.25), can be expressed in terms of the F-factor by multiplying throughout by $\rho_G^{0.5}$, so that

$$f_j = \frac{F_b - F_{b,0}}{F_{b,100} - F_{b,0}} \tag{2.28}$$

$$F_{b,0} = 0.1\rho_L^{0.692}h_w^{0.132}d_h^{-0.26}\phi^{0.992}L^{0.27} \tag{2.29}$$

$$F_{b,100} = 1.1\rho_L^{0.692}h_w^{0.132}d_h^{-0.26}\phi^{0.992}L^{0.27} \tag{2.30}$$

where

$F_b = u_b\rho_G^{0.5}$ is the F-factor based on bubbling area ($\text{Pa}^{0.5}$),

$F_{b,0} = u_{b,0}\rho_G^{0.5}$ is the F-factor based on bubbling area at 0% jetting ($\text{Pa}^{0.5}$), and

$F_{b,100} = u_{b,100}\rho_G^{0.5}$ is the F-factor based on bubbling area at 100% jetting ($\text{Pa}^{0.5}$).

The Prado model assumes a linear dependence of the fraction jetting on the F-factor for a given liquid rate and geometry. Prado et al. indicate that there is a change in the dispersion structure that is visually observed at about 50-60% jetting corresponding to a regime (Prado et al., 1987). Prado's model assumes the same linear dependence on F-factor before and after the change.

In addition, the Prado data used for the Prado model were based on the orifice phenomenon and included a fraction of liquid cover in addition to bubbling and jetting. The fraction liquid cover indicated the amount of inactive holes or insufficient information whether a particular hole is jetting or bubbling.

2.6.2 Syeda et al. fraction jetting model

The Syeda model equation is

$$f_j = -0.1786 + 0.9857\left(1 - e^{-1.43F_b}\right) \tag{2.31}$$

The Syeda model was developed from Raper et al.'s data and has three fitted parameters. The Syeda model is artificially limited to a value of 0.8 for F-factors beyond 3.0 and is therefore asymptotically inconsistent. The model assumes a simple exponential relationship of the jetting fraction with the vapor F-factor. The Syeda model only considers the F-factor as a variable in the fraction jetting model. However, the Syeda model captures the nonlinear rate of fraction jetting dependence on the F-factor by using an exponential relationship, albeit empirically.

2.7 Analysis of needs and gaps

Neither the Syeda nor the Prado models has a theoretical basis. These two are the only fraction jetting models available to date. Therefore, there is clearly a need for a new fraction jetting model that is based on theory and also incorporates all the factors that affect the fraction jetting in a consistent manner. Furthermore, the new fraction jetting model should have good predictive capabilities and therefore a theoretical basis is desired. Such a model will also help design of new experiments to study fraction jetting by providing a basis for how each of the variables hydrodynamically affect the fraction jetting observed experimentally.

The models for tray capacity and efficiency are dependent on the prevailing flow regime. Separate models for each flow regime have been developed and they require models to detect the flow regime transitions. Of particular interest is the commonly occurring froth-spray transition. However, the flow regime transitions are not sudden but occur gradually over a wide operating range. Therefore, a fraction jetting model that can bridge the various mechanisms of vapor transport has been used. This led to multi-regime models that are dependent on the accurate representation of the various vapor transport mechanisms at any operating condition. The most recent sieve tray efficiency models used a fraction jetting model for the purpose of bridging the froth and spray regimes and are therefore applicable to both regimes.

The fraction jetting model is a critical component used in the recent sieve tray efficiency models to relate the contributions of the jetting zone and the bubbling zone to the observed overall effect. However, not much modeling effort was expended on the fraction jetting model.

The fraction jetting model that is used to obtain the overall effect of the bubble and the jet models, however, is currently the weak link of the multi-regime models. A new fraction jetting model can significantly improve the reliability of multi-regime models and also provides an opportunity for new multi-regime mechanistic models. Improvements in accurately predicting the jetting fraction not only brings the model to represent reality closely, but also, as a result, provide more reliable models.

In Chapter 3, this need is addressed and a new fundamental model for fraction jetting is presented.

CHAPTER 3

FRACTION JETTING MODEL

In this chapter, a new single parameter fraction jetting model is described. The data of Raper et al. (1982) are used to develop the model. The model structure is developed to fundamentally explain the rate and physical property effects on fraction jetting.

The model structure is presented in Section 3.1, estimating the parameter is presented in Section 3.2, and results and discussion are presented in Section 3.3.

The new fraction jetting model is developed such that it can be directly used in a multi-regime mass transfer model in which a fraction jetting model is employed. The application of the new fraction jetting model in the multi-regime mass transfer efficiency model is presented in Chapter 4 using the Syeda et al. (2007) sieve tray efficiency model.

3.1 Model Structure

The premise of the froth-spray transition and the fraction jetting concepts is that the formation of vapor jets with an increase in vapor rate during the normal operation of a tray in the mixed-froth regime is responsible for the changes in the hydraulic and mass transfer properties in the two-phase mixture. However, a key distinction between the froth-spray transitions models and the fraction jetting model is that the transition point is not a specific operating point according to the fraction jetting model, but the transition is an operating range over which fraction jetting goes from zero to one.

Based on the studies from two-phase flow in pipes, the transition between flow regimes is understood to occur due to hydrodynamic instabilities (Drazin, 2002). Depending on

which of the forces such as inertia, viscous, surface tension acting on the bi-phases are dominant, the nature of the instability that leads to the transition can be determined.

Porter and Wang (1969) found that surface tension and viscous forces have a negligible effect on the froth-spray transition. According to Lockett (1986), suggestions that the Rayleigh instabilities of the gas jet are responsible for froth-spray transitions (Spells and Bakowski, 1950) are also unfounded.

According to the jet penetration model, the force of the weight of the liquid above a jet tends to form a liquid bridge across the jet and acts to collapse it. The force of the gas momentum acts to resist the liquid bridge formation. A stable jet is formed when the gas momentum exceeds the liquid weight force.

The success of the jet penetration theory implies that the forces due to the momentum of the vapor and the weight of the liquid are responsible for the froth-spray transition (Lockett, 1986).

The theoretical considerations for the froth-spray transition studies based on the jet penetration model will be still valid for the fraction jetting model. The forces affecting froth-spray transition, which are also the forces that determine the jetting phenomenon, are hypothesized to be responsible for fraction jetting.

Therefore, it follows that the modified Froude number is the dimensionless number appropriate for correlating fraction jetting. The modified Froude number was previously used by Hofhuis and Zuiderweg (1979) and Colwell (1981) as an independent variable in their mixed-froth regime hydraulic correlations. The modified Froude number is the ratio of the inertia of the vapor (square root of the kinetic energy of the vapor) to the resistance to the vapor through the dispersion on the tray due to the presence of the liquid (square root of the potential energy of the liquid on the tray).

The modified Froude number is defined in its general form as

$$Fr' = \frac{u_{gas}\sqrt{\rho_G}}{\sqrt{g h_{liq} \rho_L}} \tag{3.1}$$

where

Fr' is the modified Froude number,

u_{gas} is a characteristic gas velocity (m/s),

h_{liq} is a characteristic liquid holdup (m),

g is the acceleration due to gravity, and

ρ_G and ρ_L are the vapor and liquid densities (kg/m^3).

The modified Froude number represents the propensity of the vapor to be transported in the form of jets rather than bubbles. In other words, the ratio of the volume of the vapor transported as jets to the ratio of the volume of the vapor transported as bubbles is proportional to the modified Froude number. The phenomenological relation can be represented in equation form as

$$\frac{V_j}{V_b} \propto Fr' \tag{3.2}$$

where

V_j is the vapor flow as jets (m^{3}s^{-1}), and

V_b is the vapor flow as bubbles (m^{3}s^{-1}).

From Equations (2.3) and (3.2),

$$\frac{1}{f_j} - 1 = \frac{V_b}{V_j} \propto \frac{1}{Fr'} \tag{3.3}$$

Or,

$$\frac{1}{f_j} - 1 = \frac{V_b}{V_j} = \frac{\beta}{Fr'} \tag{3.4}$$

where

f_j is the fraction jetting, and

β is the proportionality constant.

The proportionality constant β is the value of the modified Froude number where $V_b = V_j$. For $Fr' > \beta$, the volume of the vapor transported as jets is greater than that transported as bubbles; for $Fr' < \beta$, the volume of the vapor transported as jets is less than

that transported as bubbles; and for $Fr' = \beta$, equal volumes of the vapor is transported as jets and bubbles. The parameter β, therefore, signifies the operating point in terms of the modified Froude number where the dominant mode of vapor transport changes from bubbling to jetting, or vice-versa.

At the value of $Fr' = \beta$, the fraction jetting is equal to one-half. The above physical significance for β indicates that the change in the dominant mode of vapor transport occurs at a fraction jetting of one-half, which is consistent with the observations in the literature that a change in the light transmission properties occurs at about 50-60% jetting and also a visual change in the dispersion structure observed (Prado and Fair, 1990; Prado et al., 1987).

Rearranging Equation (3.4), the final form of the fraction jetting model structure is obtained as

$$f_j = \frac{Fr'}{\beta + Fr'} \tag{3.5}$$

3.2 Estimating β

The modified Froude number, defined in its general form in Equation (3.1), varies both vertically in the dispersion and across the tray due to the variations in the u_{gas} and h_{liq}. Dispersion density changes, momentum transfer between the vapor and the liquid, local pressure variations, and dispersion height gradients all affect the local u_{gas} and h_{liq}. Therefore, a vapor velocity and a liquid height that correlate with the average modified Froude number in the dispersion are desired for a given operating point.

From various hydraulic and mass transfer correlations, the average properties of the dispersion are well correlated by the vapor velocity based on the bubbling area, u_b, and the clear liquid height, h_{cl}. Therefore, the modified Froude number is defined as

$$Fr' = \frac{u_b \sqrt{\rho_G}}{\sqrt{g h_{cl} \rho_L}} \tag{3.6}$$

The definition of the modified Froude number, Equation (3.6), has also been used in previous gas hold up fraction correlations by Colwell (1981) and Hofhuis and Zuiderweg (1979) as the independent variable. The modified Froude number was also used by Zuiderweg (1982) in their spray regime entrainment correlation where vapor jetting is the dominant phenomenon.

For estimating β , the experimental fraction jetting data of Raper et al. (1982) on sieve trays are used. The data were measured in the dispersion using the electrical conductivity bubble probe as described in Section 2.5.1. The fraction jetting data were plotted against the modified Froude number, which was calculated from Raper's data and a clear liquid height calculated from the Bennett et al. (1983) correlation. The data used for the correlation are listed in Appendix A.

Using the MATLAB^{TM} function nlinfit, an optimum value of β is obtained to minimize the sum squared error defined by

$$\text{Sum Squared Error} = \sum_{i}^{n} \left(f_{j,m} - f_{j,p}\right)^2 \tag{3.7}$$

where

$f_{j,m}$ is the fraction jetting measured Raper et al. (1982) data, and

$f_{j,p}$ is the fraction jetting predicted using the new fraction jetting model.

The maximum likelihood (ML) criterion is satisfied by the parameter obtained by minimizing the objective function in Equation (3.7), the least-squares estimate, assuming that the measurement errors in the fraction jetting measurements are normally distributed.

The new fraction jetting model is given by

$$f_j = \frac{Fr'}{0.0449 + Fr'} \tag{3.8}$$

Furthermore, the uncertainty estimate of the parameter in Equation (3.8) can be calculated using the studentized residuals. Using the MATLAB^{TM} function nlparci, the 95% confidence limits on the parameter are obtained as

$$\beta = 0.0449 \pm 0.0073 \tag{3.9}$$

As described in Section 3.1, the numerical value of the parameter β represents a change in the dominant mode of vapor transport from bubbles to jets.

3.3 Results and Discussion

This section presents the analysis and discussion for the fraction jetting model described in Section 3.2.

3.3.1 Model fit

The goodness of fit is shown in Figure 3.1.

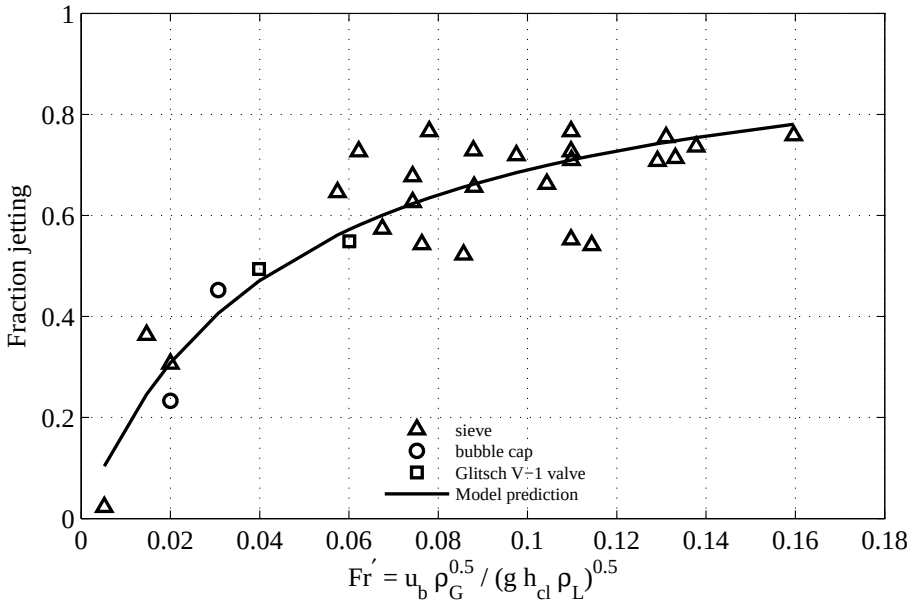

Figure 3.1: Fit of the new jetting fraction model using the sieve tray data of Raper et al. (1982). The curve represents Equation (3.8), $f_j = \frac{Fr'}{0.0449+Fr'}$

.

The goodness of fit of the new fraction jetting model (Figure 3.1) for the Raper et al. data indicates a good fit over the entire experimental data range.

The new fraction jetting model is compared with the Syeda et al. fraction jetting model in the parity plot shown in Figure 3.2. The new fraction jetting model and the Syeda et al. model provide comparable fit to the Raper et al. data.

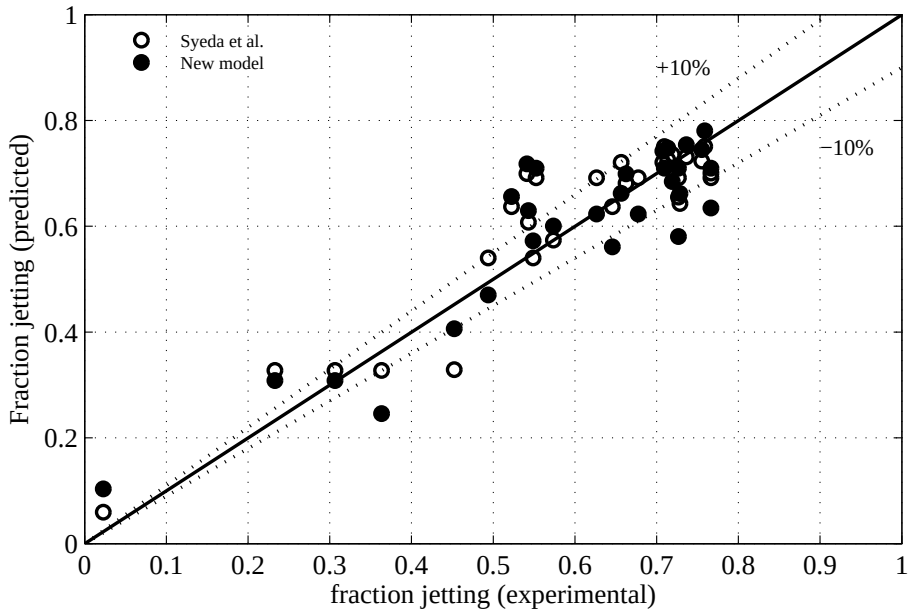

Figure 3.2: A parity plot of the new fraction jetting model predictions and the Syeda et al. model predictions compared to Raper et al. experimental data.

For comparison, the predictions of the Syeda et al. (2007) fraction jetting model are shown in Figure 3.3.

Furthermore, the value of β obtained from minimizing the sum squared error coincides with the observed change in the rate of change of the fraction jetting and this is attributed to the change in the dominant mode of vapor transport.

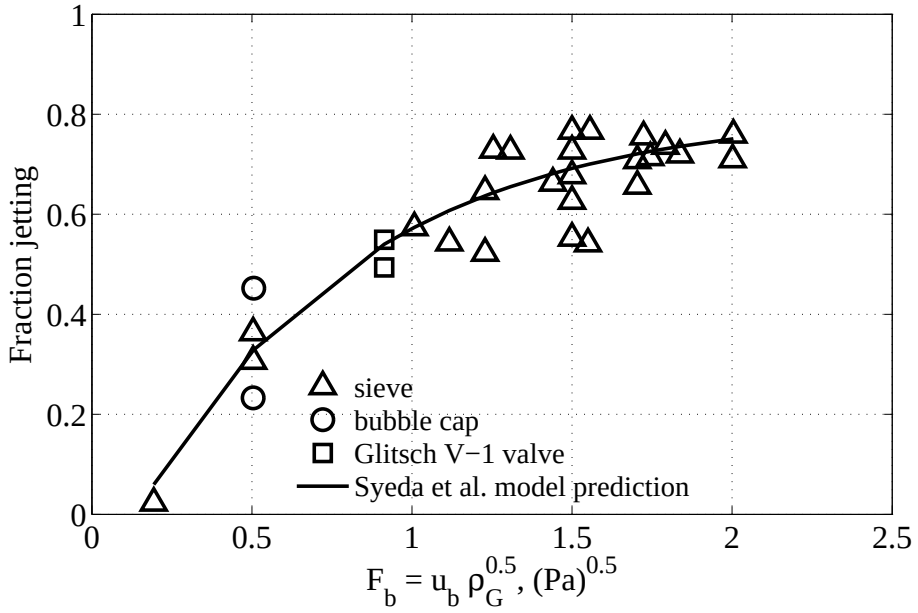

Figure 3.3: Fit of the Syeda et al. model using Raper et al. (1982) data. The curve represents the equation $f_j = -0.1786 + 0.9857\left(1 - e^{-1.43F_b}\right)$.

As can be seen from Figure 3.3, the change in the rate of fraction jetting with F-factor is also captured in the Syeda et al. model, albeit empirically.

Furthermore, the Syeda et al. fraction jetting model plateaus at a fraction jetting of 0.8 at F-factors beyond 3.0. The artificial limit of 0.8 is a result of the empirical model structure. The new fraction jetting model, however, does not have such an artificial limit on fraction jetting and predicts a fraction jetting of 1.0 as the F-factor approaches infinity. This is illustrated as follows

$$\lim_{F_b \to +\infty} f_j = \lim_{Fr' \to +\infty} \frac{Fr'}{0.0449 + Fr'} = 1.0 \tag{3.10}$$

However, for the Syeda et al. model,

$$\begin{aligned} \lim_{F_b \to +\infty} f_j &= \lim_{F_b \to +\infty} -0.1786 + 0.9857(1 - e^{-1.43F_b}) \\ &= -0.1786 + 0.9857 = 0.8071 \neq 1.0 \end{aligned} \tag{3.11}$$

3.3.2 Model consistency

The phenomenological method presented here also can be used to explain the relatively good predictions of the Syeda et al. model. The exponential relationship used in the Syeda et al. model has a remarkable similarity to the gas holdup fraction models such as the Bennett et al. (1983) model for sieve trays, i.e.,

$$\varepsilon = 1 - \exp\left(-12.55\left(\frac{F_b}{\sqrt{\rho_L - \rho_G}}\right)^{0.91}\right) \tag{3.12}$$

where

ε is the gas hold up fraction (volume of the vapor in the dispersion / volume of the dispersion), and

F_b is the F-factor based on the bubbling area, $(\text{Pa})^{0.5}$.

The ratio of the volume of the liquid in the dispersion to the volume of the vapor in the dispersion, η, is

$$\eta = \frac{1-\varepsilon}{\varepsilon} \tag{3.13}$$

Or equivalently,

$$\varepsilon = \frac{\eta}{1+\eta} \tag{3.14}$$

Theoretical investigations of the conditions under which the energy of the two phases on the tray is the minimum have to led to the relations where η was a function of the Froude number (Azbel, 1963). Therefore, the gas hold up fraction can be expressed in terms of the Froude number as

$$\varepsilon = \frac{\eta}{1+\eta} \propto \frac{Fr'}{1+Fr'} \tag{3.15}$$

An examination of the Equations (3.12) and Equation (3.15), in part, explains why the fraction jetting may be correlated with the F-factor using an exponential relationship as in the Syeda et al. model.

3.3.3 Parameter consistency

Correlations based on Equation (3.15) have been used to predict the gas hold up fraction or the liquid holdup fraction on trays (Colwell, 1981; Hofhuis and Zuiderweg, 1979). The correlation by Hofhuis and Zuiderweg is shown in Figure 3.4. In this correlation, the modified Froude number is used to predict the liquid hold up fraction (ε_l). If the beta value of Equation (3.8) is plotted on the Hofhuis and Zuiderweg correlation plot, it coincides with an inflexion zone where a rate of change occurs. This provides further evidence that the modified Froude number at the numerical value of 0.0449 is indicative of a change in the dominant mode of vapor transport from bubbles to jets.

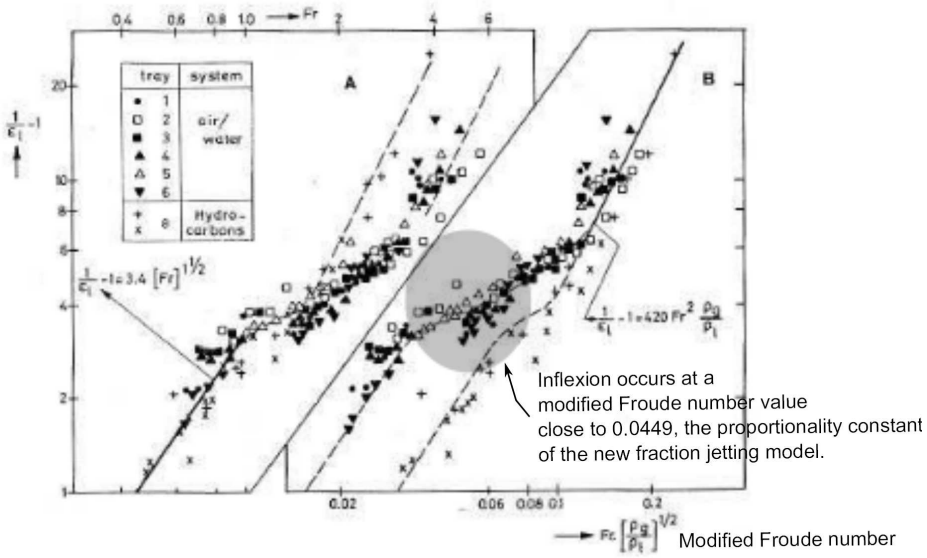

Figure 3.4: Correlation of gas hold up fraction with Froude number. Source: Hofhuis and Zuiderweg (1979).

3.3.4 Residual analysis

A residual analysis for the new fraction jetting model is done to validate the goodness of fit. The purpose of the residual analysis is to provide insight regarding

1. Randomness of the residual — A random distribution of the residuals implies that the information in the data is adequately captured in the model and the variability in the residuals is random and probably a result of insufficient variation in the data or measurement errors.

2. Systemic bias — A residual plot not centered around the mean (or zero) indicates the presence of a systemic bias.

The bias plot of the residual versus the predicted value indicates the randomness of the predictions at all fraction jetting values (Figure 3.5). The randomness of the residual is confirmed by the normal probability plot shown in Figure 3.6, which indicates the degree of normality of the residuals. It can be concluded from the bias plot and the normality plot that the effects of each of the model variables is well captured as indicated in the random residuals.

Additional bias plots in which the residual fraction jetting is plotted against (i) clear liquid height (ii) the vapor velocity based on the bubbling area and (iii) the fractional open hole area are included in Appendix C. Furthermore, the bias plots are all centered at zero indicating that there are no systemic biases in the model. The same conclusion is also drawn from the parity plot of Figure 3.2.

3.3.5 Effect of clear liquid height model and tray geometry

Although the new fraction jetting model has only one parameter determined from the experimental data, the use of clear liquid height in the equation means that it has to be determined from a correlation, or measured. The clear liquid height correlation used, therefore, becomes another parameter in the model.

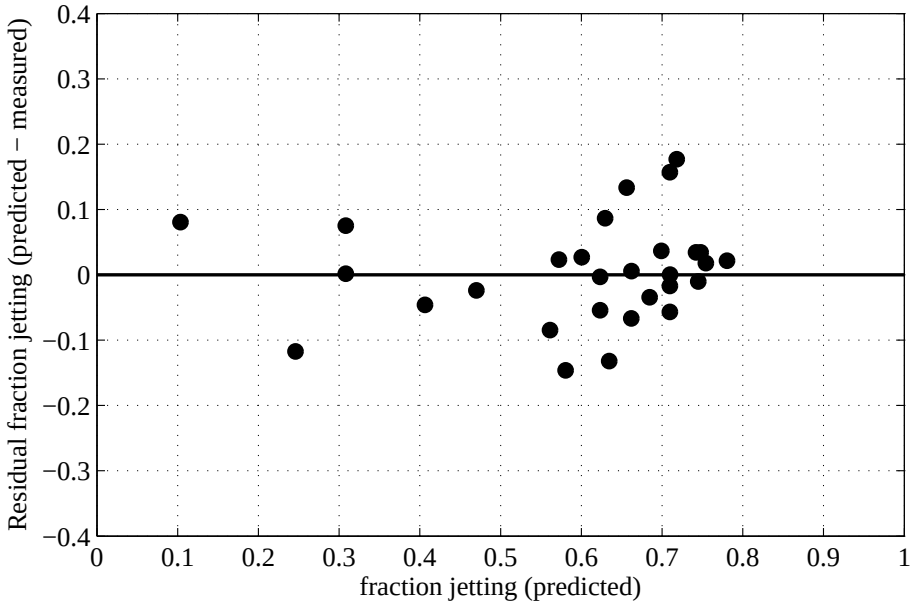

Figure 3.5: Bias plot of the new jetting fraction model with respect to the predicted fraction jetting value. The residual is calculated as predicted-measured. Raper et al. data.

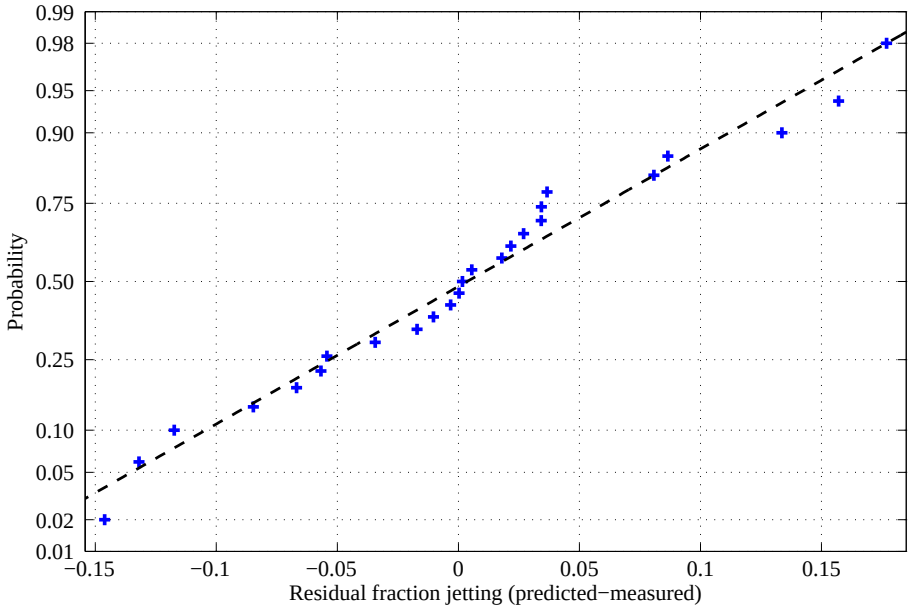

Figure 3.6: Normal probability plot of the residual fraction jetting. The residual is calculated as predicted-measured. Raper et al. data. The solid line indicates the expected probability value from normally distributed data.

The clear liquid height models are of two types (i) based on the Francis weir equation (Bennett et al., 1983; Colwell, 1981) and (ii) Zuiderweg's type (Dhulesia, 1984; Hofhuis and Zuiderweg, 1979; Zuiderweg, 1982). A comparison of the clear liquid height models shows, however, that the choice of a clear liquid height model does not greatly affect the fraction jetting predictions as shown in the Figure 3.7.

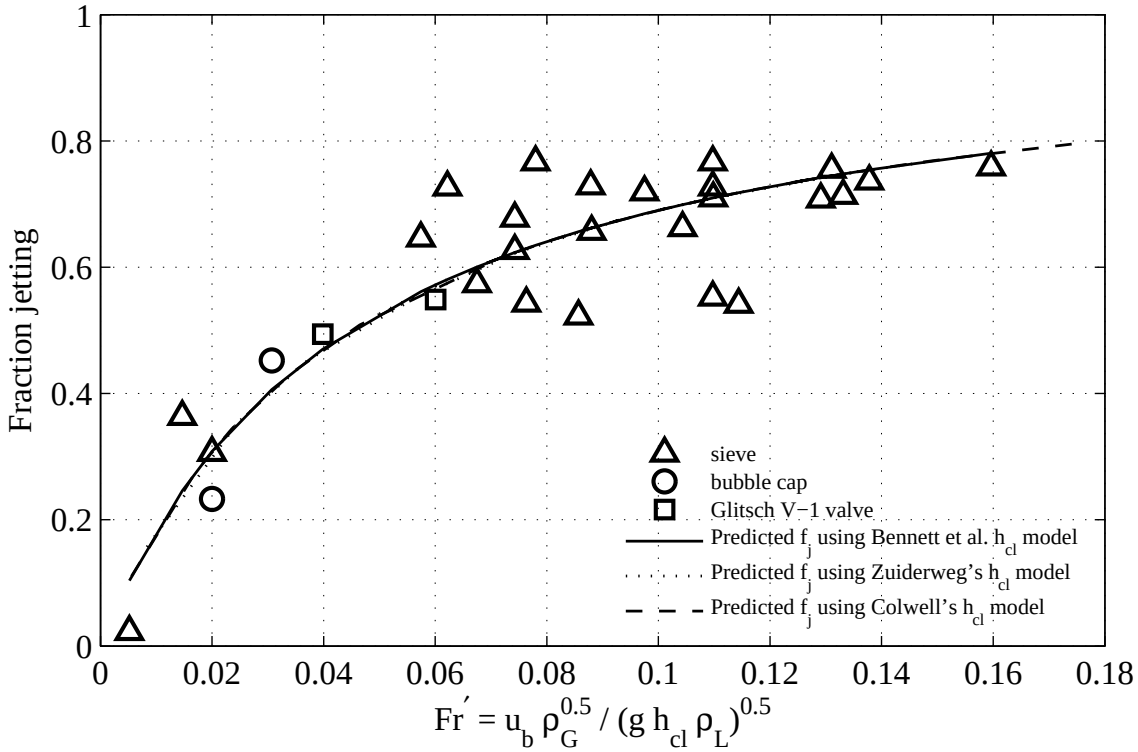

Figure 3.7: The new fraction jetting model predictions with different clear liquid height calculations indicate that the choice of the clear liquid height model is unimportant.

Studies on the properties of the jets (Lockett, 1981) indicate that hole diameter also has an important effect on hole properties. The hole diameter and fractional hole area also appear in many froth-spray transition studies. The effect of hole diameter, however, is not captured in the new fraction jetting model.

The effect of hole area on fraction jetting may have been indirectly captured using a clear liquid height model, however, the data of Raper et al. show enough scatter that no net hole area effect is observed in the data. The bias plot with respect to the hole area also indicates that the data do not show a significant effect of hole area (See Appendix C).

3.4 Summary

A new phenomenological model for the fraction jetting has been presented. The model is capable of predicting jetting fractions based on the modified Froude number. The implications for the model have been presented as well.

The key results are listed as follows:

1. The new fraction jetting model structure fits the Raper et al. data. over the entire experimental data range.

2. The quality of the residuals indicate that there is no systemic bias in the predictions.

3. The randomness of the residuals indicates that the variability in the dependent variable due to the variability in the independent variables has been adequately captured.

4. The form of the model is consistent with the previous models for ε_L and with the Syeda's fraction jetting model.

5. The value of 0.0449 for the modified Froude number connects with completely indepenent set of data by Hofhuis and Zuiderweg (1979).

The model will be used in the next section to combine the jetting properties with bubbling zone properties.

CHAPTER 4

APPLICATION OF THE FRACTION JETTING MODEL

Syeda et al. (2007) sieve tray efficiency model provides a different fundamental tray model that can capture the crown pattern of efficiency rate curves, i.e., the pattern characterized by an initial increase followed by a decrease in efficiency with increasing vapor rate thereby resembling a crown shape.

The fraction jetting data used were obtained using the air-water system. However, the sieve tray efficiency model is developed using FRI's tray efficiency data on isobutane/n-butane system and the cyclohexane/n-heptane system at various pressures.

Evaluation of the new fraction jetting model in Syeda's sieve tray efficiency model will provide insight regarding the ability to capture the crown patterns.

In this chapter, the sieve tray efficiency model of Syeda et al. (2007) is modified by using the new fraction jetting model (Equation 3.8) in place of Syeda's original fraction jetting model (Equation 2.31). The Syeda sieve tray efficiency model is described in Section 4.2 along with the model equations. The implications of using the new fraction jetting model in place of the Syeda et al. fraction jetting model are described and the efficiency predictions with the new model are presented.

4.1 Combining efficiencies of bubbling and jetting zones

The fraction jetting model conveniently bridges the efficiencies of the bubble and jet zones to an observed efficiency using an equation such as

$$(1 - f_j)E_b + f_j E_j = E_{OG} \tag{4.1}$$

where

f_j is the fraction jetting,

E_b is the efficiency of the bubbles,

E_j is the efficiency of the jets, and

E_{OG} is the point efficiency.

If the efficiency of the bubbling and the jetting zones are known, then Equation (4.1) can be used to determine the point efficiency that results from both mechanisms. Equation (4.1), initially proposed by Ashley and Haselden (1972) and later by Raper et al. (1982), is the central idea behind the sieve tray efficiency model of Syeda et al. (2007).

The development of Equation (4.1) is as follows:

Consider the elemental strip shown in Figure 4.1. It is assumed that the liquid is perfectly mixed in the vertical direction and has a concentration of x.

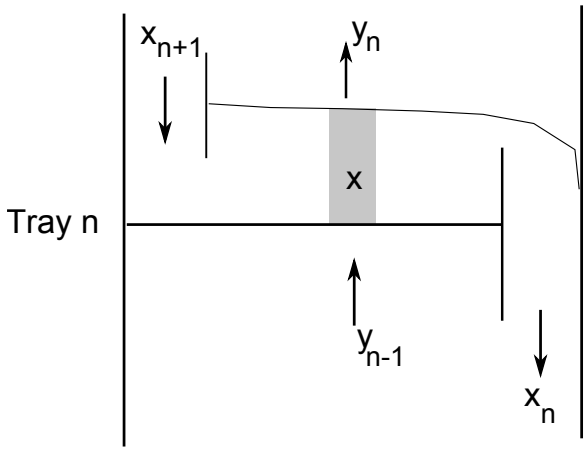

Figure 4.1: Elemental strip for point efficiency defintion.

By definition, the point efficiency is

$$E_{OG} = \frac{y_n - y_{n-1}}{y^* - y_{n-1}} \tag{4.2}$$

where

y_{n-1} is the composition of the entering vapor (mole fraction),

y_n is the composition of the leaving vapor (mole fraction),

y^* is the equilibrium vapor composition with respect to the liquid concentration x (mole fraction), and

E_{OG} is the efficiency of the shaded strip in Figure 4.1.

Equation (4.2) is valid regardless of the mode of vapor transport. The mass transfer efficiency is determined not only by the driving force available for mass transfer, but also by the interfacial area, and the contact times. When there are multiple modes of vapor transport, the concentration change achieved is different for each mode despite the same driving force because of the differences in the interfacial area and the contact times.

For the case when $f_j = 0$, Equation (4.2) can be written as

$$E_b = \frac{y_{bn} - y_{n-1}}{y^* - y_{n-1}} \tag{4.3}$$

where

y_{bn} is the concentration of the leaving vapor if the vapor transport is entirely in the form of bubbles, and

E_b is the point efficiency of the bubbles.

Similarly, for the case when $f_j = 1$, Equation (4.2) can be written as

$$E_j = \frac{y_{jn} - y_{n-1}}{y^* - y_{n-1}} \tag{4.4}$$

where y_{jn} is the concentration of the leaving vapor if the vapor transport is entirely in the form of jets, and

E_j is the point efficiency of the jets.

When both jets and bubbles exist over an operating cycle, the vapor phase material balance for the more volatile component can be written as

$$y_{bn}V_b + y_{jn}V_j = y_n(V_b + V_j) \tag{4.5}$$

where

V_j is the vapor flow as jets (m^3/s), and

V_b is the vapor flow as bubbles (m^3/s).

By definition, since

$$f_j = \frac{V_j}{V_b + V_j} \tag{2.3}$$

where f_j is the fraction jetting.

Therefore,

$$y_{bn}(1 - f_j) + y_{jn} f_j = y_n \tag{4.6}$$

From Equations (4.2), (4.3), and (4.4),

$$(1 - f_j)[E_b(y^* - y_{n-1}) + y_{n-1}] + f_j[E_j(y^* - y_{n-1}) + y_{n-1}] = (y^* - y_{n-1})E_{OG} + y_{n-1} \tag{4.7}$$

which leads to Equation (4.1).

$$(1 - f_j)E_b + f_j E_j = E_{OG} \tag{4.1}$$

4.2 Syeda et al. model

The Syeda et al. sieve tray efficiency model uses Equation (4.1) to obtain the point efficiency as a combination of the jetting and the bubbling efficiencies. The hydraulic picture on the tray is assumed to be composed of a jetting zone and a bubbling zone. The bubble zone is, in turn, considered to be composed of two sub zones, one containing small bubbles and the other large bubbles. In all zones, the two-resistance theory is assumed to be valid. A brief review of the two-resistance theory is discussed in Section 4.2.1.

4.2.1 Two-resistance theory

According to the two-resistance theory, the entire resistance to mass-transfer is concentrated in films on either side of the vapor-liquid interface as shown in Figure 4.2.

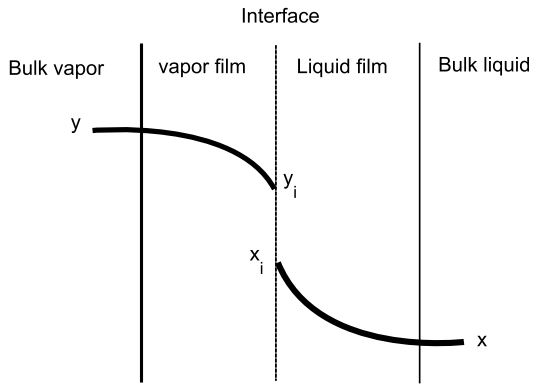

Figure 4.2: Liquid-vapor film representation for the two-resistance theory. y and x are the bulk vapor and liquid compositions, and y_i and x_i are the interfacial vapor and liquid compositions.

Equilibrium is assumed at the interface, and equimolal counter diffusion exists throughout the films. The resistance to mass-transfer in each phase, or equivalently the overall resistance, can be expressed in terms of the mass-transfer coefficients, interfacial area, and the residence times of the liquid and vapor phases.

The point efficiency, which is the approach to equilibrium in the shaded region on Figure 4.1, is expressed by Equation (4.8).

$$E_{\mathrm{OG}} = 1 - \exp\left(-N_{OG}\right) \tag{4.8}$$

where

E_{OG} is the point efficiency (fractional),

N_{OG} is the number of overall vapor phase transfer units.

The number of overall vapor phase transfer units are related to the individual vapor and liquid phase transfer units as

$$\frac{1}{N_{OG}} = \frac{1}{N_G} + \frac{\lambda}{N_L} \tag{4.9}$$

where

N_G is the number of vapor phase transfer units,

N_L is the number of liquid phase transfer units,

$\lambda = mG/L$ is the stripping factor,

m is the slope of the equilibrium line, and

G/L is the ratio of the vapor to liquid molar flow rates.

Equation (4.9) is a direct consequence of the application of the two-resistance theory, to obtain the total resistance to mass transfer as the sum of the resistances in the vapor and liquid phases.

The individual phase transfer units are obtained as

$$N_G = k_G a_{iG} t_G \tag{4.10}$$

$$N_L = k_L a_{iL} t_L \tag{4.11}$$

where

k_G is the vapor phase mass transfer coefficient (m/s),

k_L is the liquid phase mass transfer coefficient (m/s),

a_{iG} is the interfacial area per unit volume of the vapor (m^2/m^3),

a_{iL} is the interfacial area per unit volume of the liquid (m^2/m^3),

t_G is the vapor residence time (s), and

ρ_G and ρ_L are the vapor and liquid densities (kg/m^3).

Furthermore, from a material balance,

$$a_{iL} t_L = \frac{\rho_L G_f}{\rho_G L_f} a_{iG} t_G \tag{4.12}$$

where

G_f is the vapor rate (kg/s), and

L_f is the liquid rate (kg/s).

Detailed development and the assumptions involved in the derivation of Equation (4.8) are discussed in the literature (Lockett, 1986). In summary, the two-resistance theory relates the overall (vapor phase) point efficiency to the mass-transfer coefficients of the individual phases, the interfacial area, and the (vapor phase) residence time.

4.2.2 Approaches to tray efficiency modeling

Models that employ the two-resistance theory can be broadly classified as those that predict the volumetric mass-transfer coefficients ($k_G a$ and $k_L a$) and those that predict the mass-transfer coefficients (k_G and k_L) separately from the interfacial area (a) for use in Equation (4.8).

The volumetric mass transfer coefficients ($k_G a$ and $k_L a$) are predicted using independent empirical correlations developed from experimental absorption or stripping data. When used for distillation, volumetric mass transfer coefficients obtained from absorption or stripping data are known to incorrectly predict low liquid phase resistance and, consequently, over-predict efficiency (Chen et al., 1994; Kister, 1992; Lockett, 1986). The AIChE (1958) and Chan and Fair (1984) are the most popular sieve tray efficiency models that use volumetric mass transfer coefficients. The success of these models was primarily rooted in the large database of commercial scale efficiency data used for model development and the lack of alternative fundamental models at that time.

Models that predict k_G and k_L separately from a usually predict the mass-transfer coefficients from the penetration theory or the surface renewal theory. The interfacial area and the residence time are predicted using empirical correlations (Hughmark, 1965; Todd and Van Winkle, 1972; Zuiderweg, 1982), or from the properties of the two-phase dispersion such as the bubble diameter or drop diameter, the froth density, and the froth height.

Models using the two-phase dispersion properties assume a contact mechanism of the two phases to define the dispersion structure. Therefore, these models are also known as mechanistic models. The Prado and Fair (1990), Garcia and Fair (2000a,b), Syeda et al. (2007), Chen and Chuang (1993) models are examples of the mechanistic class, which includes all sieve tray models of the last decade.

4.2.3 Syeda et al. sieve tray efficiency model equations

The equations of the Syeda et al. (2007) sieve tray efficiency model are described in this section.

Equation (4.8) is applied in each of the bubbling and jetting zones. Furthermore, in the bubbling zone, the small bubble efficiency, E_{SB}, is taken as one with the assumption that the small bubbles are so small that they emerge saturated through the froth (Lockett and Ahmed, 1983). Two fractions to characterize the two phases on the tray are used — the fraction small bubbling that determines the amount of vapor in the form of small bubbles in the bubbling zone, and fraction jetting that determines the amount of vapor in the form of jets. The fraction jetting model of Syeda et al. was discussed in Section 2.6.

The model equations are as follows:

$$d_{32L} = 0.887 d_H^{0.846} u_H^{0.21} \tag{4.13}$$

where

d_{32L} is the sauter mean diameter of the large bubbles (m),

d_H is the hole diameter (m), and

u_H is the vapor velocity based on the hole area (m/s).

$$u_{LB} = 2.5 V_{LB}^{1/6} + u_b \tag{4.14}$$

where

u_{LB} is the rise velocity of the large bubbles (m/s),

V_{LB} is the volume of the large bubbles (m^3), and

u_b is the vapor velocity based on the bubbling area (m/s).

$$a_{iG} = \frac{6}{d_{32L}} \tag{4.15}$$

where

a_{iG} is the interfacial area per unit volume of vapor (m^2/m^3).

$$t_{GLB} = \frac{h_f}{u_{LB}} \tag{4.16}$$

where

t_{GLB} is the residence time of the large bubbles (s), and

h_f is the dispersion height (m).

$$k_{LLB} = 1.13 \left(\frac{D_L}{t_G} \right)^{0.5} \tag{4.17}$$

where

k_{LLB} is the liquid side mass transfer coefficient of the large bubbles (m/s), and

D_L is the molecular diffusivity of the liquid (m^2/s).

The vapor phase mass transfer coefficient is determined from the numerical solution presented by Zaritzky and Calvelo (1979). The same correlation was also used by Prado and Fair (1990) and Garcia and Fair (2000a) in their sieve tray efficiency models for vapor phase mass transfer coefficient of large bubbles. The asymptotic Sherwood number is predicted from the gas Peclet number (Pe_G) in the correlation.

For $40 < Pe_G < 200$, the following polynomial is used:

$$Sh_\infty = -11.878 + 25.879(\log Pe_G) - 5.64(\log Pe_G)^2 \tag{4.18}$$

where

$Sh_\infty = k_{GLB} d_{32L} / D_G$ is the asymptotic Sherwood number,

D_G is the molecular diffusivity of the vapor (m^2/s), and

$Pe_G = d_{32L} u_{LB} / D_G$ is the Peclet number.

For the range $Pe_G > 200$,

$$Sh_\infty = 17.9 \tag{4.19}$$

The Bennett et al. (1983) correlation is used for the froth height correlation. This is the same correlation used for the new fraction jetting model presented in the previous chapter.

$$h_f = h_w + C \left(\frac{Q_L}{W \alpha_e} \right)^{0.67} \tag{4.20}$$

where

h_f is the dispersion height (m),

h_w is the outlet weir height (m),

Q_L is the volumetric flow rate of the liquid (m^3/s), and

W is the length of the outlet weir (m).

α_e, the liquid hold up fraction, is obtained from

$$\alpha_e = \exp\left[-12.55\left(u_b\left(\frac{\rho_G}{\rho_L-\rho_G}\right)^{0.5}\right)^{0.91}\right] \tag{4.21}$$

and C, the constant in Equation (4.20), is obtained as

$$C = 0.501 + 0.438\exp(-137.8\,h_w) \tag{4.22}$$

The fraction of small bubbles is estimated from the first order binary breakage rate. The breakage rate is derived from the functionality given by Hesketh et al. (1991):

$$k\bar{\Delta t} = 0.16\frac{3.8\rho_L^{0.1}\rho_G^{0.3}}{\sigma^{0.4}}(u_b g)^{0.6} t_{GLB} \tag{4.23}$$

where

k is the first order bubble breakage rate constant (1/s),

$\bar{\Delta t}$ is the time when half of the total secondary bubbles are formed in the froth from the initial number of bubbles (s).

The fraction of small bubbles in the bubbling zone, FSB, is

$$FSB = \frac{2(1-\exp(-k\bar{\Delta t}))}{2(1-\exp(-k\bar{\Delta t})) + 125\exp(-k\bar{\Delta t})} \tag{4.24}$$

The fraction of small bubbles given by Equation (4.24) is used to determine the efficiency of the bubbling zone (E_b)

$$E_b = FSB\,E_{SB} + (1-FSB)\,E_{LB} \tag{4.25}$$

In the jetting zone, the Zuiderweg (1982) spray regime model is used to estimate the efficiency of the jets. The Zuiderweg model equations are

$$k_{Gj} = \frac{0.13}{\rho_G} - \frac{0.065}{\rho_G^2} \qquad (1 < \rho_G < 80 \text{ kg/m}^3) \tag{4.26}$$

$$k_{Lj} = \frac{2.6 \times 10^{-5}}{\mu_L^{0.25}} \tag{4.27}$$

$$E_j = 1 - \exp\left(-\frac{ah_f K_{OGj}}{u_b}\right) \tag{4.28}$$

$$ah_f = \frac{40}{\phi^{0.3}} \left(\frac{F_b^2 h_L FP}{\sigma}\right)^{0.37} \tag{4.29}$$

$$h_L = 0.6 h_w^{0.5} \left(\frac{p}{b} FP\right)^{0.25} \tag{4.30}$$

where

k_{Gj} is the vapor phase mass transfer coefficient (m/s),

k_{Lj} is the liquid phase mass transfer coefficient (m/s),

$k_{OGj} = 1/(1/k_{Gj} + m/k_{Lj})$ is the overall vapor phase mass transfer coefficient (m/s),

m is the slope of the equilibrium curve,

ρ_G is the vapor density (kg/m^3),

μ_L is the liquid viscosity (Pa-s),

E_j is the efficiency of the jets (fractional),

a is the interfacial area per volume of the two phase mixture (m^2/m^3),

h_f is the dispersion height (m),

h_w is the outlet weir height (m),

p is the hole pitch (m),

ϕ is the fractional hole area,

σ is the surface tension (N/m),

h_L is the clear liquid height (m),

b is the weir length per unit bubbling area (1/m), and

FP is the flow parameter, $\left(\frac{\rho_G}{\rho_L}\right)^{0.5}$ at total reflux.

Syeda's fraction jetting model, Equation (2.31), is used for the fraction jetting

$$f_j = -0.1786 + 0.9857(1 - e^{-1.43F_b}) \tag{2.31}$$

where

f_j is the fraction jetting,

F_b is the F-factor based on the bubbling area ($Pa^{0.5}$)

The efficiencies of the bubbling zone, Equation (4.25), and the efficiency of the jetting zone, Equation (4.28), are combined to obtain the point efficiency as

$$E_{OG} = f_j E_j + (1 - f_j) E_b \tag{4.1}$$

4.3 Methodology and Data

The results presented in this chapter are obtained by replacing Equation (2.31) of the Syeda et al. sieve tray efficiency model with Equation (3.8). In addition, the printing errors in the published Syeda et al. model have been identified (Syeda, 2010) and subsequently corrected (See Appendix B). No other changes to the model structure or model equations are made.

The data used for the efficiency predictions are the same as those used by Syeda et al. to develop the sieve tray model. The data were obtained on a 1.22 m diameter column (FRI data) on two binary hydrocarbon systems — cyclohexane/n-heptane (C6/C7) system and isobutane/n-butane (IC4/NC4) system . The data are categorized by system, pressure, and fractional hole area into seven sets:

1. isobutane/n-butane (IC4/NC4) system at 1138 kPa, 8.3% hole area
2. isobutane/n-butane (IC4/NC4) system at 1138 kPa, 14% hole area
3. isobutane/n-butane (IC4/NC4) system at 2068 kPa, 8.3% hole area
4. isobutane/n-butane (IC4/NC4) system at 2758 kPa, 8.3% hole area

5. cyclohexane/n-heptane (C6/C7) system at 34 kPa, 14% hole area

6. cyclohexane/n-heptane (C6/C7) system at 165 kPa, 14% hole area

7. cyclohexane/n-heptane (C6/C7) system at 165 kPa, 8.3% hole area

The IC4/NC4 system data at 2068 kPa and 2758 kPa pressures as corrected by Syeda et al. using the Hoek and Zuiderweg (1982) method for vapor entrainment were used. The data are representative of the physical properties of most industrial columns (Sakata and Yanagi, 1972; Syeda et al., 2007; Yanagi and Sakata, 1982). The data are described in Appendix D.

4.4 Results and Discussion

The following results and discussion are presented in this section:

1. A comparison of the point efficiency (E_{OG}) predictions with the two fraction jetting models.

2. A comparison of the predictions of the two fraction jetting models for the hydrocarbon systems.

3. The impact of fraction jetting on point efficiency predictions

4.4.1 E_{OG} predictions

Figures 4.3–4.9 show predictions of the Syeda et al. model with the original fraction jetting model used by Syeda et al. model and with their fraction jetting model replaced by Equation (3.8). In addition, the predictions reported by Syeda et al. (2007), which have been read from the smoothed prediction curves, are also included.

For all efficiency data, it can be seen that the Syeda et al. point efficiency (E_{OG}) predictions are similar using both fraction jetting models. There is also a close agreement with the sieve tray efficiency predictions reported by Syeda et al.

Since the objective is to verify the impact of replacing the Syeda et al. fraction jetting model with the new fraction jetting model in the Syeda et al. sieve tray efficiency model, average and maximum deviations between the efficiency predictions of the Syeda et al. sieve tray efficiency model obtained using the two fraction jetting models are compared for each of the seven data sets as shown in Table 4.1. From Table 4.1, it can be seen that the average absolute deviations do not exceed 0.031 for all systems and pressures.

Table 4.1: Maximum and average absolute deviations between the point efficiency predictions of the Syeda et al. sieve tray efficiency model using the new fraction jetting model and using Syeda's fraction jetting model.

System	Pressure kPa	Hole area %	Maximum absolute deviation	Average absolute deviation
IC4/NC4	1,138	14.0	0.046	0.014
IC4/NC4	2,068	8.3	0.032	0.013
IC4/NC4	1,138	8.3	0.055	0.014
IC4/NC4	2,758	8.3	0.038	0.014
C6/C7	165	8.3	0.034	0.018
C6/C7	165	14.0	0.070	0.020
C6/C7	34	14.0	0.040	0.031

Therefore, the new fraction jetting model can directly replace the Syeda et al. fraction jetting model in the Syeda et al. sieve tray efficiency model without negatively impacting the point efficiency predictions. The implications of this result are that the phenomenological fraction jetting model can now be used to extend the Syeda et al. sieve tray efficiency

model and eliminate the artificial limit of 0.8 on the fraction jetting predictions of the Syeda et al. model.

The point efficiency predictions of the Syeda et al. model obtained using the model equations agree with those reported by the authors for the iso-butane/n-butane system at 2068 kPa, 2758 kPa, and 1138 kPa for both 8.3% and 14% hole areas. The point efficiency predictions of the Syeda et al. model obtained using the model equations, however, were considerably lower than those reported by the authors for the cyclohexane/n-heptane system at all pressures and hole areas. The reason for the underpredicted results were traced back to the fraction of small bubble model reported by the authors in the original paper (Syeda, 2010). The corrections in the original version of the model are listed in Appendix D. However, the absolute predicted value of the Syeda et al. efficiency predictions is not of importance for this study.

A key feature of the Syeda et al. sieve tray efficiency model is its ability to predict the crowned efficiency patterns observed in the experimental data. The sieve tray efficiency model uses the fraction jetting to combine the bubble zone and jetting zone efficiencies to obtain the point efficiency. Using the new fraction jetting model in place of Syeda et al.'s fraction jetting model retains the crowned pattern prediction capability of the sieve tray efficiency model as seen in Figures 4.3–4.9. The result reconfirms that the new fraction jetting model can effectively replace Syeda's fraction jetting model in Syeda's sieve tray efficiency model.

4.4.2 Comparison of the fraction jetting predictions

The difference in the point efficiency predictions using the new fraction jetting model and Syeda et al.'s fraction model are because of the differences in the predicted fraction jetting.

Both the new fraction jetting model and Syeda et al.'s fraction jetting model were developed using Raper et al.'s air-water data. However, the fraction jetting in the sieve tray

efficiency model is predicted for hydrocarbon systems.

The fraction jetting predictions using the new model and using the Syeda et al. fraction jetting model are given in Tables 4.2– 4.8.

At higher rates and F-factors, the predictions of the Syeda et al. model are artificially limited to 0.8 because of the model structure of the Syeda et al. model. The new fraction jetting model, however, does not have that limitation and can predict fraction jetting values higher than 0.8 at the high F-factor conditions.

The sensitivity of the efficiency model to the fraction jetting model used is also dependent on the difference in the bubbling and jetting efficiencies used in Equation (4.1). If the values of the bubbling and the jetting efficiencies are same, even large changes in fraction jetting does not affect the efficiency prediction. For instance, the jetting and bubbling efficiencies for the iso-butane/n-butane system at 1138 kPa and 14% hole area, given in Table 4.2, can differ by as much as 46 percentage points. The difference in the bubbling and jetting modes is typical of other systems as well, which are presented in the Tables 4.2–4.8. Therefore, the new fraction jetting model can replace the Syeda fraction jetting model in the Syeda sieve tray efficiency model without negatively impacting the efficiency predictions even when the sensitivity of point efficiency predictions to fraction jetting predictions are high as indicated by the markedly different bubbling and jetting zone efficiencies.

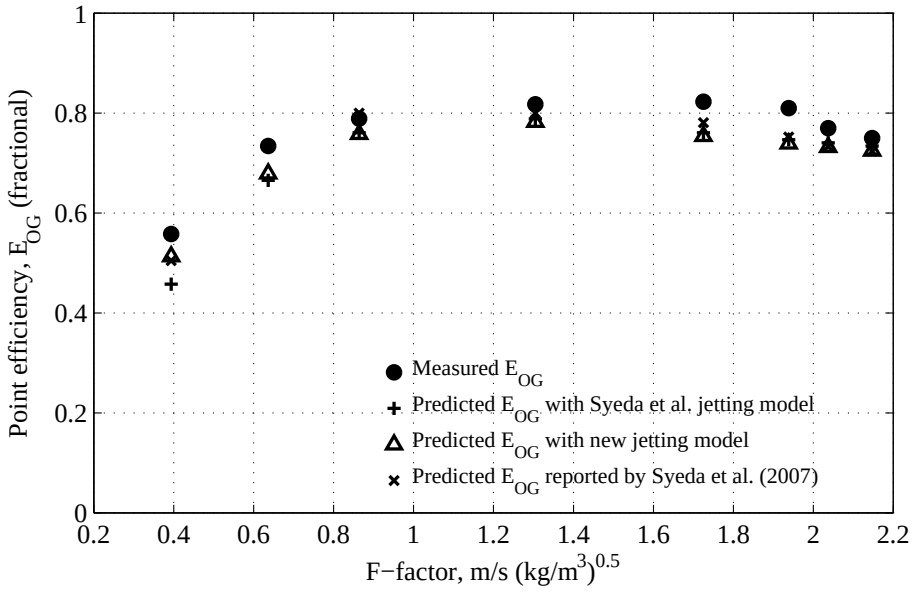

Figure 4.3: Comparison of efficiency predictions for the IC4/NC4 system 1138 kPa, 8.3% open hole area

Table 4.2: IC4/NC4 system 1138 kPa, 8.3% hole area. Comparison of the bubbling and jetting efficiencies.

F_b (m/s)(kg/m^3)$^{0.5}$	FSB	f_j (Syeda et al.)	f_j (new model)	E_b	E_j	E_{OG} (Syeda et al.)	E_{OG} (new model)
0.394	0.331	0.246	0.366	0.344	0.806	0.458	0.513
0.636	0.589	0.410	0.490	0.596	0.766	0.665	0.679
0.864	0.783	0.521	0.573	0.786	0.737	0.761	0.758
1.305	0.957	0.654	0.679	0.957	0.700	0.789	0.782
1.725	0.994	0.723	0.744	0.994	0.672	0.761	0.754
1.938	0.998	0.745	0.769	0.998	0.661	0.747	0.739
2.037	0.999	0.754	0.779	0.999	0.656	0.741	0.732
2.147	0.999	0.761	0.789	0.999	0.651	0.734	0.725

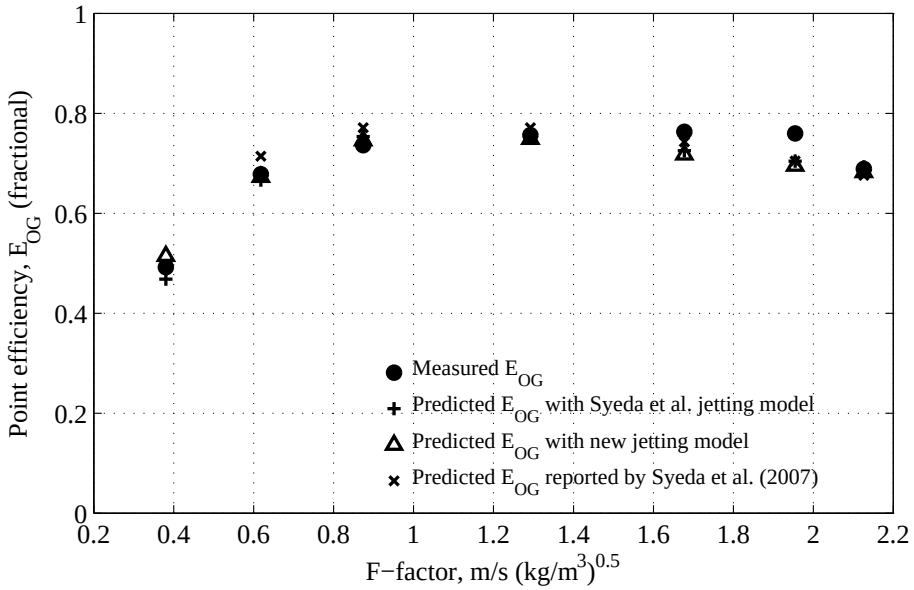

Figure 4.4: Comparison of efficiency predictions for the IC4/NC4 system 1138 kPa, 14% open hole area

Table 4.3: IC4/NC4 system 1138 kPa, 14% hole area. Comparison of the bubbling and jetting efficiencies.

F_b (m/s)(kg/m^3)$^{0.5}$	FSB	f_j (Syeda et al.)	f_j (new model)	E_b	E_j	E_{OG} (Syeda et al.)	E_{OG} (new model)
0.381	0.365	0.235	0.360	0.381	0.752	0.468	0.515
0.618	0.628	0.400	0.483	0.635	0.713	0.666	0.673
0.874	0.832	0.525	0.576	0.835	0.681	0.754	0.746
1.292	0.967	0.652	0.677	0.967	0.645	0.757	0.749
1.677	0.995	0.718	0.738	0.995	0.619	0.725	0.718
1.955	0.999	0.747	0.770	0.999	0.605	0.704	0.695
2.126	1.000	0.760	0.787	1.000	0.596	0.693	0.682

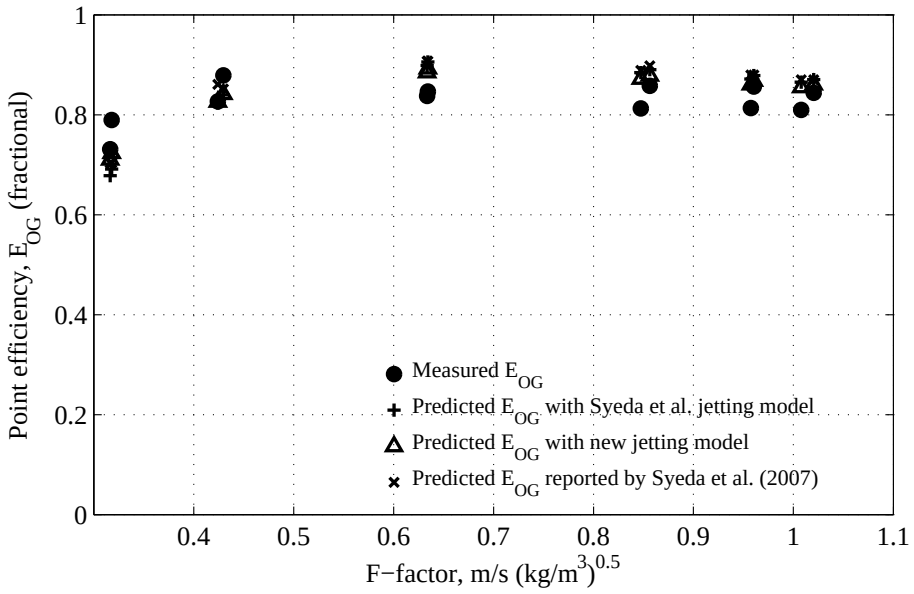

Figure 4.5: Comparison of efficiency predictions for the IC4/NC4 system 2068 kPa, 8.3% open hole area

Table 4.4: IC4/NC4 system 2068 kPa, 8.3% hole area. Comparison of the bubbling and jetting efficiencies.

F_b (m/s)(kg/m^3)$^{0.5}$	FSB	f_j (Syeda et al.)	f_j (new model)	E_b	E_j	E_{OG} (Syeda et al.)	E_{OG} (new model)
0.318	0.645	0.181	0.326	0.652	0.871	0.692	0.723
0.430	0.834	0.274	0.398	0.837	0.848	0.840	0.842
0.634	0.967	0.409	0.498	0.967	0.817	0.906	0.893
0.856	0.995	0.517	0.577	0.995	0.793	0.891	0.878
0.960	0.998	0.557	0.607	0.998	0.784	0.879	0.868
1.020	0.999	0.578	0.623	0.999	0.777	0.871	0.861
0.316	0.632	0.180	0.324	0.638	0.861	0.678	0.710
0.424	0.815	0.270	0.394	0.818	0.839	0.823	0.826
0.634	0.962	0.409	0.497	0.963	0.806	0.899	0.885
0.847	0.994	0.514	0.574	0.994	0.781	0.885	0.872
0.957	0.998	0.556	0.605	0.998	0.771	0.872	0.860
1.008	0.998	0.574	0.618	0.998	0.767	0.865	0.855

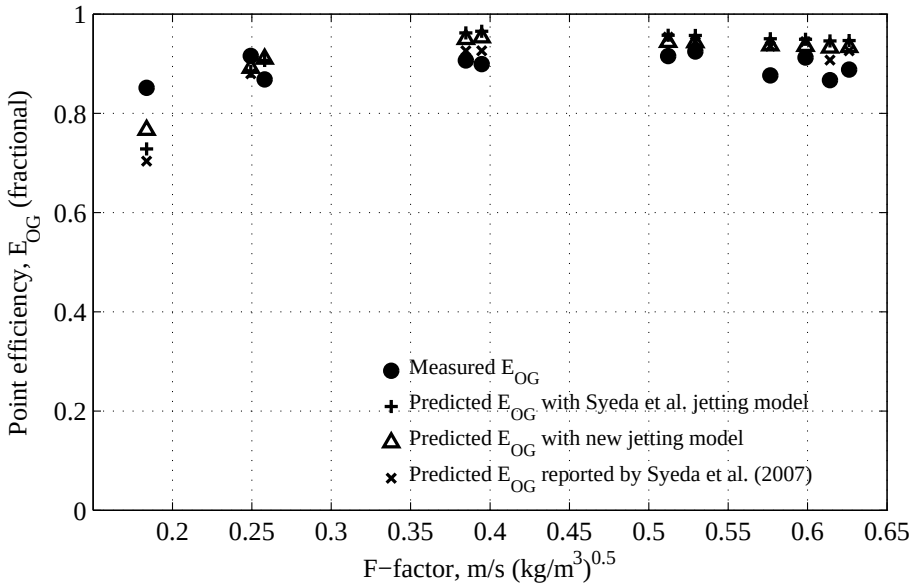

Figure 4.6: Comparison of efficiency predictions for the IC4/NC4 system 2758 kPa, 8.3% open hole area

Table 4.5: IC4/NC4 system 2758 kPa, 8.3% hole area. Comparison of the bubbling and jetting efficiencies.

F_b (m/s)(kg/m^3)$^{0.5}$	FSB	f_j (Syeda et al.)	f_j (new model)	E_b	E_j	E_{OG} (Syeda et al.)	E_{OG} (new model)
0.258	0.902	0.126	0.290	0.904	0.924	0.907	0.910
0.395	0.988	0.247	0.388	0.988	0.898	0.966	0.953
0.529	0.998	0.345	0.462	0.998	0.878	0.957	0.943
0.599	0.999	0.388	0.493	0.999	0.870	0.949	0.936
0.626	1.000	0.404	0.504	1.000	0.868	0.947	0.933
0.184	0.712	0.049	0.222	0.717	0.938	0.728	0.767
0.249	0.878	0.117	0.281	0.880	0.922	0.885	0.892
0.385	0.983	0.239	0.379	0.983	0.896	0.962	0.950
0.512	0.997	0.333	0.449	0.997	0.878	0.957	0.944
0.577	0.999	0.375	0.480	0.999	0.870	0.950	0.937
0.614	0.999	0.397	0.498	0.999	0.865	0.946	0.932

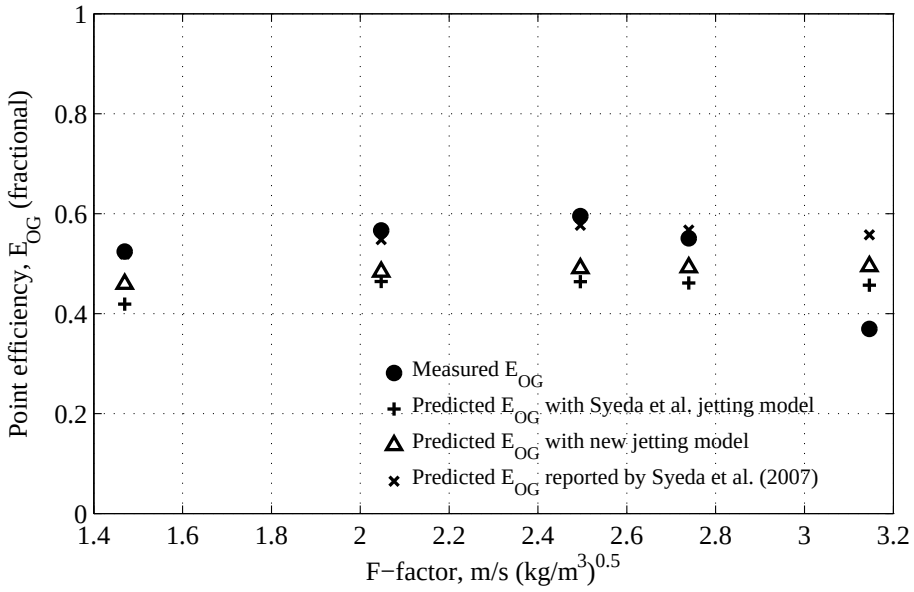

Figure 4.7: Comparison of predictions for C6/C7 system 34 kPa, 14% open hole area

Table 4.6: C6/C7 system 34 kPa, 14% hole area. Comparison of the bubbling and jetting efficiencies.

F_b (m/s)(kg/m^3)$^{0.5}$	FSB	f_j (Syeda et al.)	f_j (new model)	E_b	E_j	E_{OG} (Syeda et al.)	E_{OG} (new model)
1.470	0.013	0.687	0.757	0.027	0.598	0.419	0.459
2.047	0.029	0.754	0.789	0.046	0.601	0.465	0.484
2.495	0.032	0.779	0.830	0.047	0.582	0.464	0.491
2.740	0.034	0.787	0.847	0.049	0.573	0.461	0.493
3.146	0.038	0.796	0.871	0.052	0.561	0.457	0.495

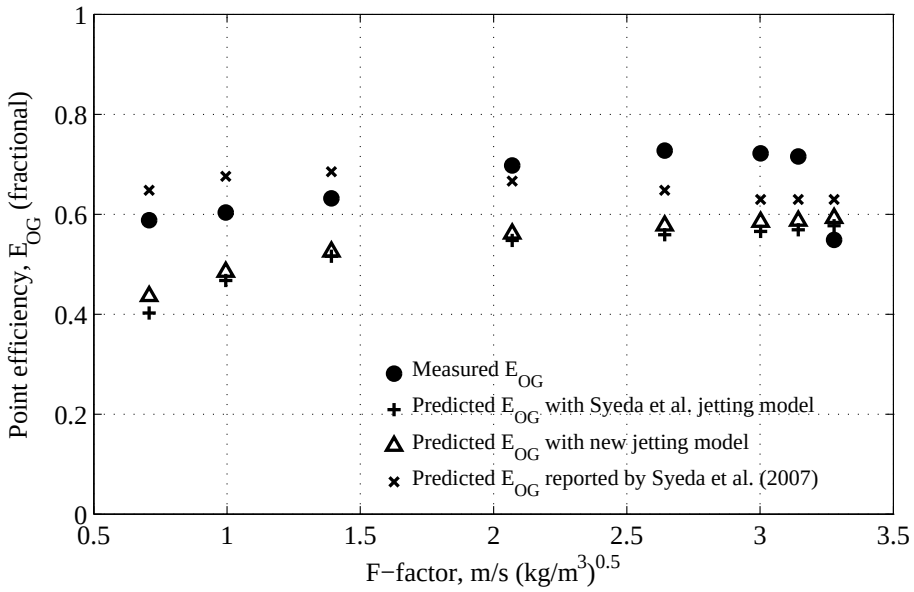

Figure 4.8: Comparison of efficiency predictions for the C6/C7 system 165 kPa, 8.3% open hole area

Table 4.7: C6/C7 system 165 kPa, 8.3% hole area. Comparison of the bubbling and jetting efficiencies.

F_b (m/s)(kg/m^3)$^{0.5}$	FSB	f_j (Syeda et al.)	f_j (new model)	E_b	E_j	E_{OG} (Syeda et al.)	E_{OG} (new model)
0.708	0.077	0.449	0.499	0.099	0.775	0.403	0.436
0.995	0.094	0.570	0.597	0.111	0.737	0.468	0.485
1.392	0.115	0.672	0.689	0.128	0.705	0.516	0.525
2.070	0.167	0.756	0.783	0.177	0.668	0.548	0.561
2.642	0.244	0.785	0.831	0.252	0.644	0.559	0.577
3.002	0.307	0.794	0.853	0.315	0.631	0.566	0.585
3.143	0.340	0.796	0.861	0.347	0.626	0.569	0.587
3.278	0.393	0.798	0.867	0.400	0.622	0.577	0.593

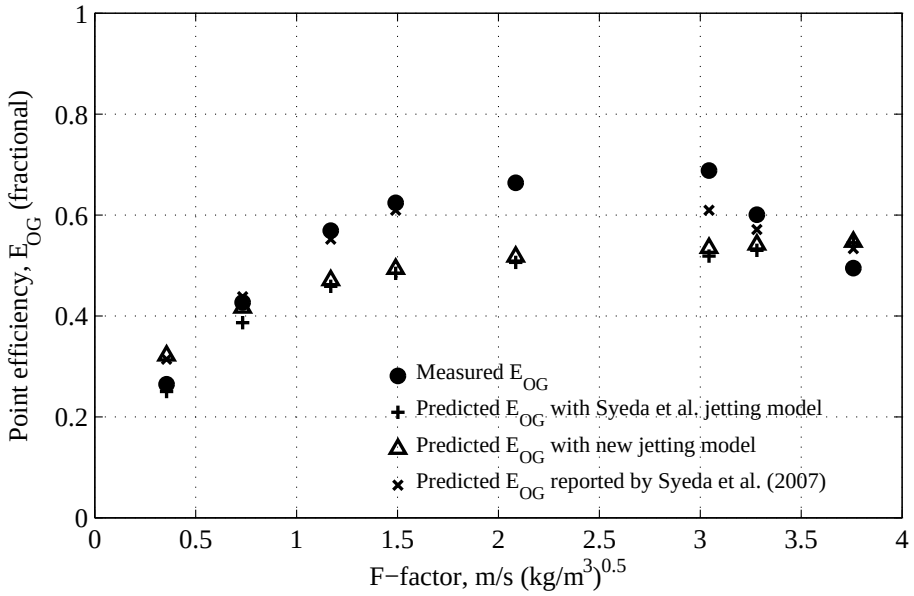

Figure 4.9: Comparison of efficiency predictions for the C6/C7 system 165 kPa, 14% open hole area

Table 4.8: C6/C7 system 165 kPa, 14% hole area. Comparison of the bubbling and jetting efficiencies.

F_b (m/s)(kg/m^3)$^{0.5}$	FSB	f_j (Syeda et al.)	f_j (new model)	E_b	E_j	E_{OG} (Syeda et al.)	E_{OG} (new model)
0.356	0.058	0.215	0.322	0.108	0.772	0.251	0.322
0.733	0.087	0.462	0.512	0.115	0.704	0.387	0.416
1.170	0.108	0.622	0.645	0.127	0.661	0.459	0.471
1.491	0.128	0.690	0.708	0.144	0.637	0.485	0.493
2.086	0.188	0.757	0.785	0.200	0.604	0.506	0.518
3.044	0.310	0.794	0.858	0.319	0.571	0.519	0.535
3.281	0.390	0.798	0.868	0.398	0.563	0.530	0.542
3.759	0.523	0.803	0.889	0.529	0.549	0.545	0.547

4.4.3 Impact of fraction jetting on point efficiency

The new fraction jetting model also provides insight into how the mechanisms of vapor transport affect efficiency with changes in rate and physical properties. The degree of large bubbling, small bubbling, and jetting for each of the datasets is shown, using both Syeda's fraction jetting model and the new fraction jetting model, in Figures 4.10–4.23.

When there is more than one mode of transport available, the effect of physical properties on efficiency is two-fold. The change in the physical properties themselves cause a change in the efficiency of mass transfer due to change in diffusivities and the driving force for mass transfer. Additionally, they also cause a change in the resistance to vapor flow through the dispersion and therefore the relative preferred modes of vapor transport. This is evident from the Figures 4.10–4.23, where it can be seen that the fraction jetting decreases with an increase in the pressure and small bubbling increases with increase in pressure.

As explained before, due to the sensitivity of the point efficiency to fraction jetting, the change in the fraction jetting with change in physical properties can be seen as the way the efficiency change with physical properties is predicted in the model. With an increase in the pressure, the break up of large bubbles increases the effective bubble regime efficiency and, at the same time, increases the contributions of the bubbling zone to the point efficiency due to decreased fraction jetting. This explains why, even with a reduction in the vapor diffusivity and relative volatilities with increasing pressure, an overall increase in efficiency is observed with increase in pressure.

The fraction jetting predictions also explain rate effects in a new light. Traditionally, the drop in efficiency at higher rates was attributed to the decreasing contact times or entrainment. In addition to those effects, from the Figures 4.10–4.23, it appears that with increase in rates, the fraction jetting increases, the bubble efficiency increases due to break

up of large bubbles, and the jetting efficiency decreases due to decreased contact times. The result of these effects is that there is net drop in efficiency because more of the vapor is transported in the form of jets, which is generally less efficient than bubble transport. This explains the gradual drop in efficiency at higher rates by attributing it to jetting.

The implications of understanding the rate and physical property effects in the context of the new fraction jetting model are that they provide a better understanding of the impact of fraction jetting on point efficiency. For instance, the drop in efficiency due to high fraction jetting at high rates can be regained with a increase in resistance on the tray (a higher weir perhaps) to promote bubbling. Modest changes to design aimed at reducing fraction jetting may potentially lead to noticeable changes in efficiency as explained in this chapter.

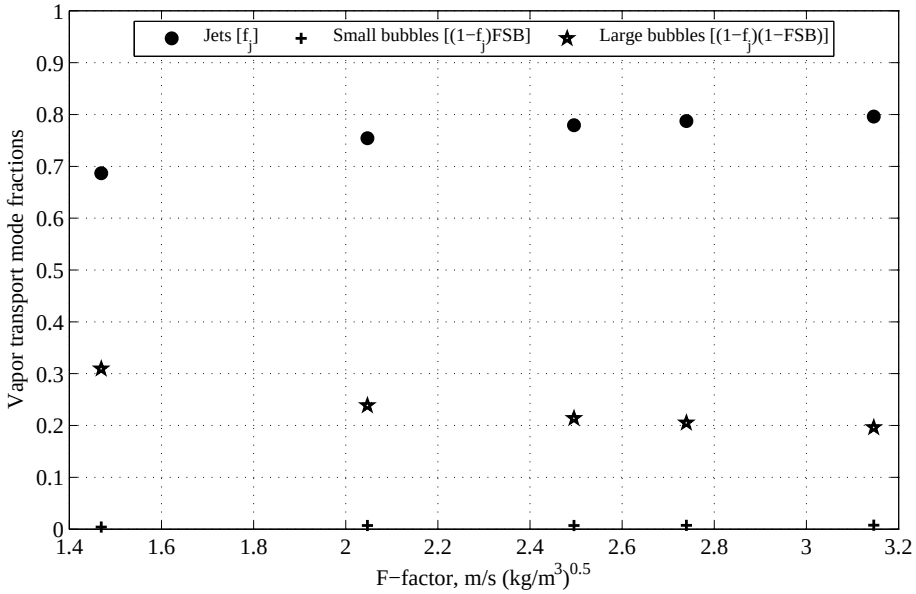

Figure 4.10: Predicted fraction jetting, small bubbling, and large bubbling for the C6/C7 system 34 kPa, 14% open hole area using the Syeda et al. fraction jetting model.

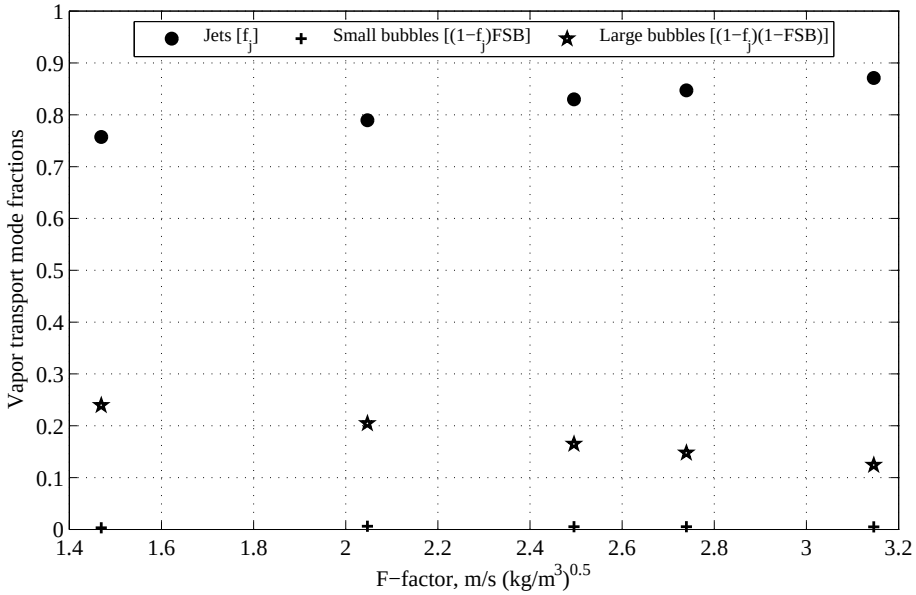

Figure 4.11: Predicted fraction jetting, small bubbling, and large bubbling for the C6/C7 system 34 kPa, 14% open hole area using the new fraction jetting model.

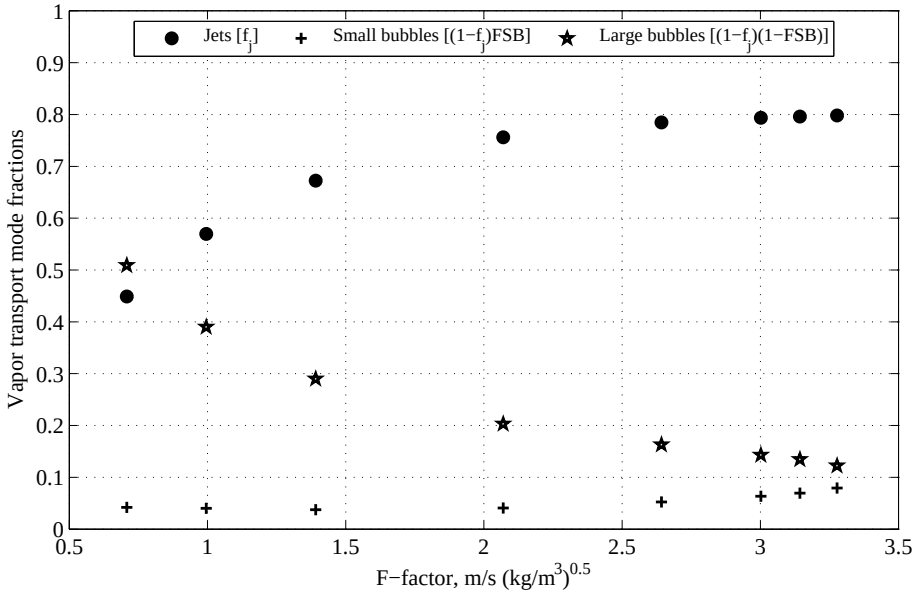

Figure 4.12: Predicted fraction jetting, small bubbling, and large bubbling for the C6/C7 system 165 kPa, 8.3% open hole area using the Syeda et al. fraction jetting model.

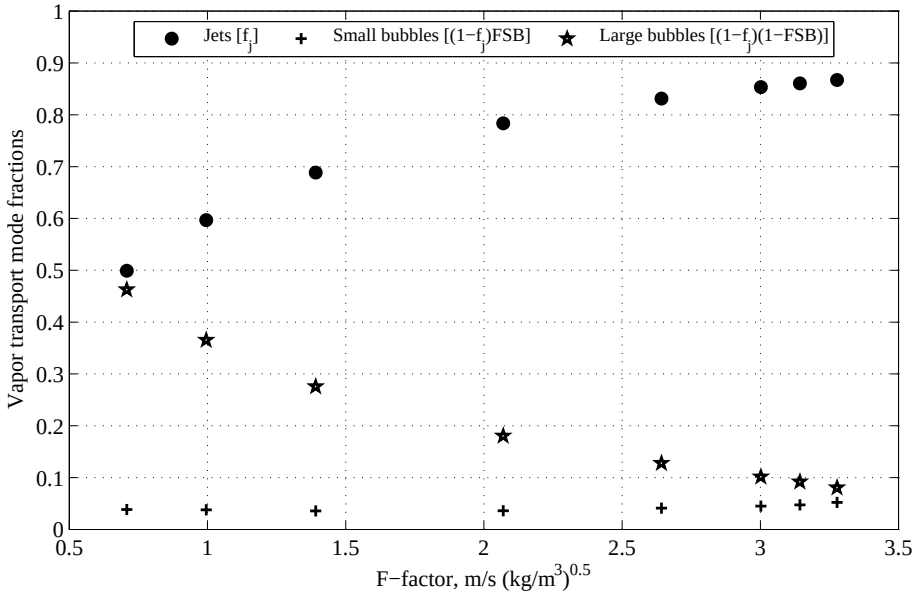

Figure 4.13: Predicted fraction jetting, small bubbling, and large bubbling for the C6/C7 system 165 kPa, 8.3% open hole area using the new fraction jetting model.

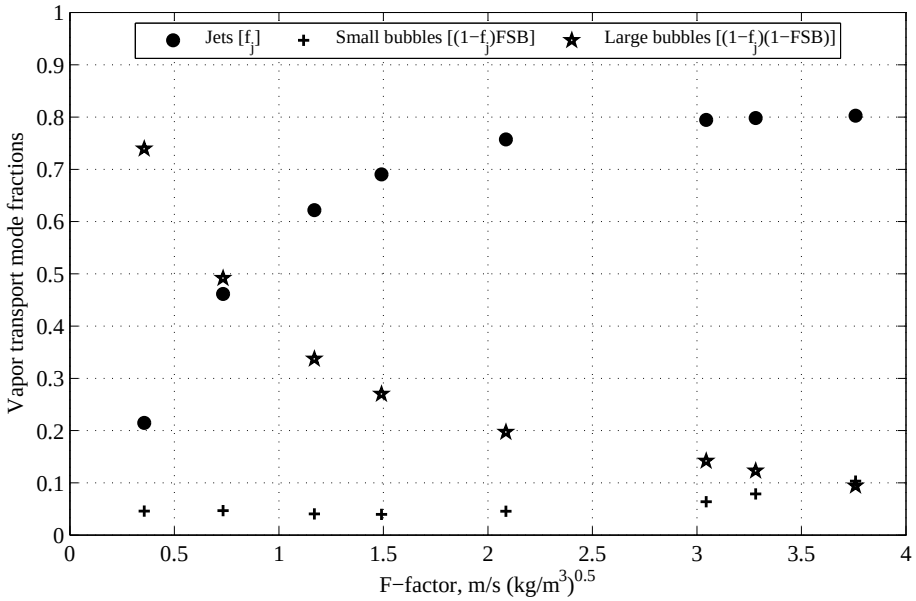

Figure 4.14: Predicted fraction jetting, small bubbling, and large bubbling for the C6/C7 system 165 kPa, 14% open hole area using the Syeda et al. fraction jetting model.

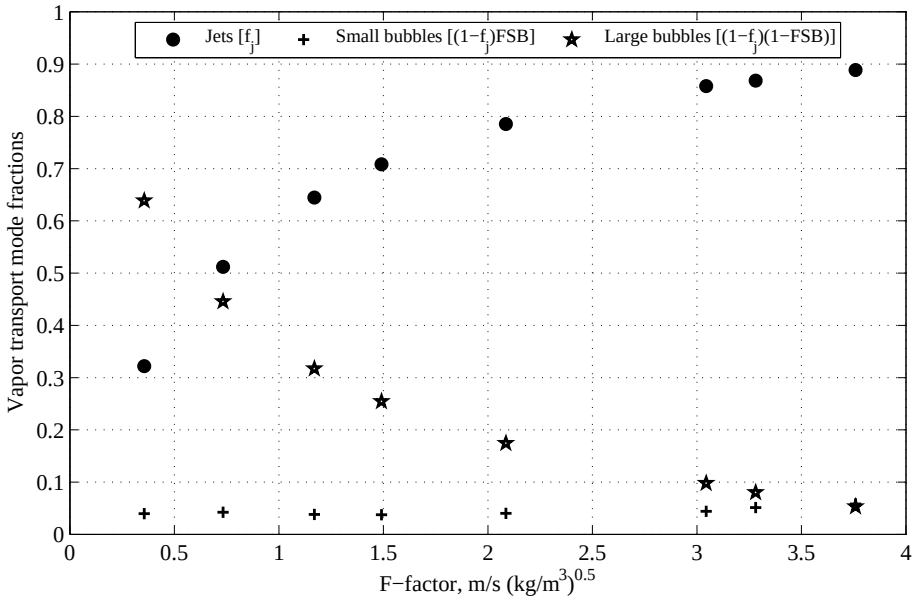

Figure 4.15: Predicted fraction jetting, small bubbling, and large bubbling for the C6/C7 system 165 kPa, 14% open hole area using the new fraction jetting model.

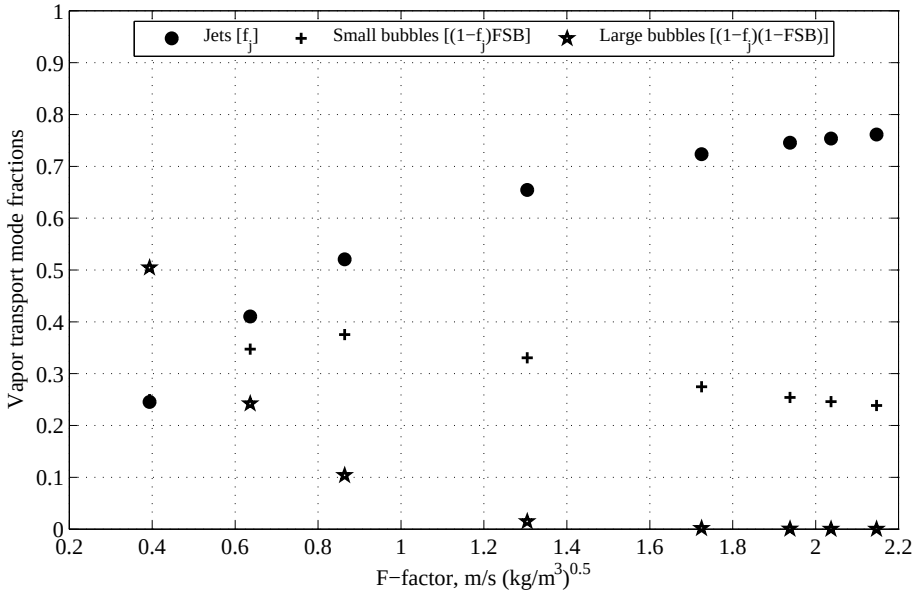

Figure 4.16: Predicted fraction jetting, small bubbling, and large bubbling for the IC4/NC4 system 1138 kPa, 8.3% open hole area using the Syeda et al. fraction jetting model.

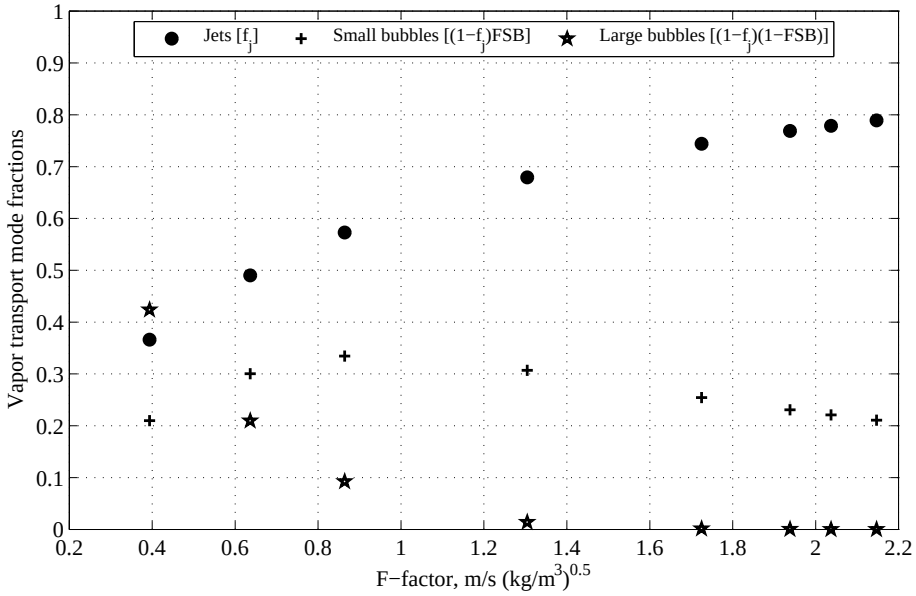

Figure 4.17: Predicted fraction jetting, small bubbling, and large bubbling for the IC4/NC4 system 1138 kPa, 8.3% open hole area using the new fraction jetting model.

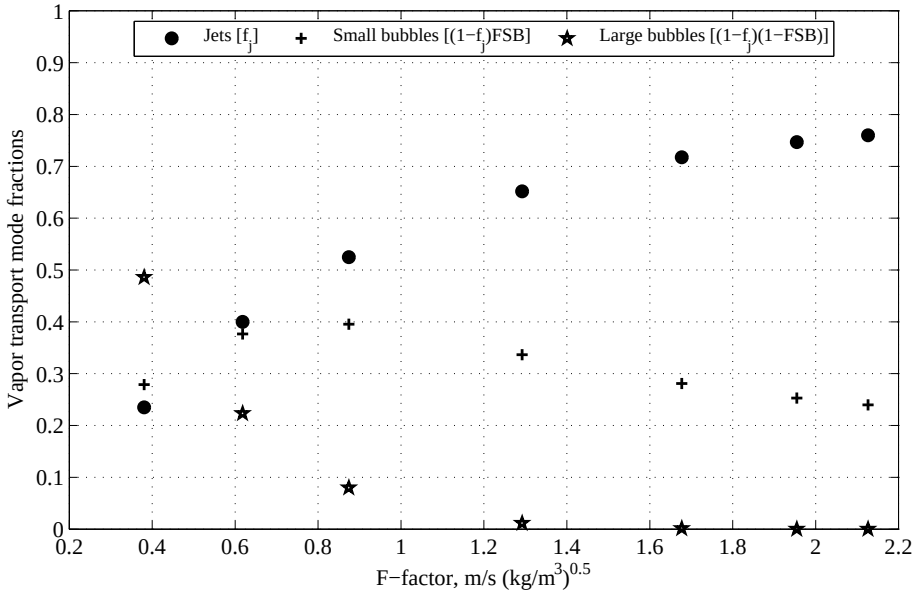

Figure 4.18: Predicted fraction jetting, small bubbling, and large bubbling for the IC4/NC4 system 1138 kPa, 14% open hole area using the Syeda et al. fraction jetting model.

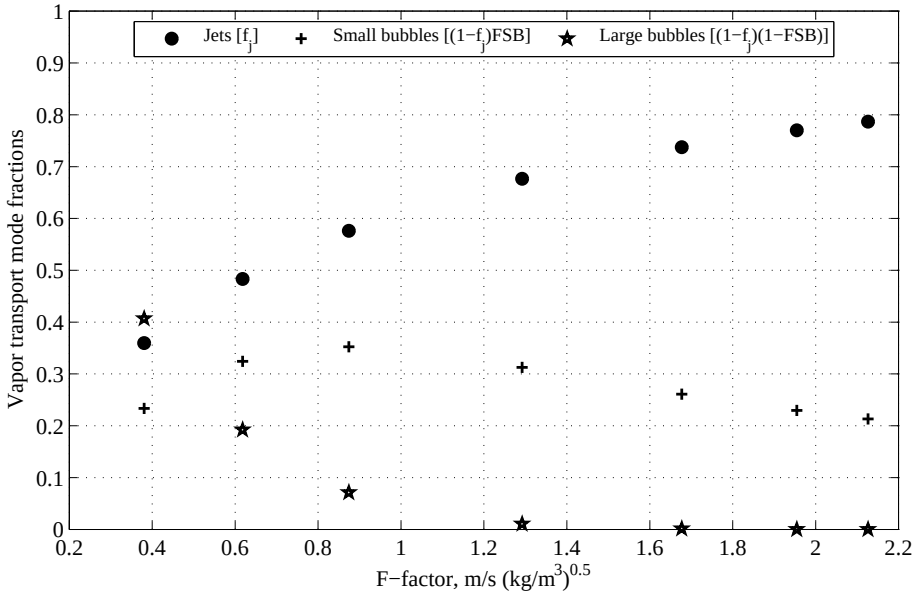

Figure 4.19: Predicted fraction jetting, small bubbling, and large bubbling for the IC4/NC4 system 1138 kPa, 14% open hole area using the new fraction jetting model.

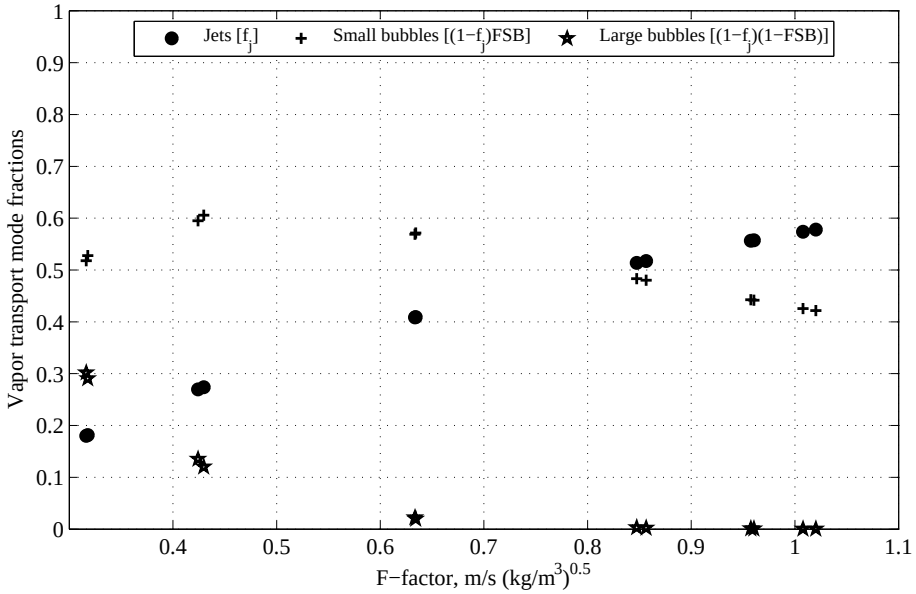

Figure 4.20: Predicted fraction jetting, small bubbling, and large bubbling for the IC4/NC4 system 2068 kPa, 8.3% open hole area using the Syeda et al. fraction jetting model.

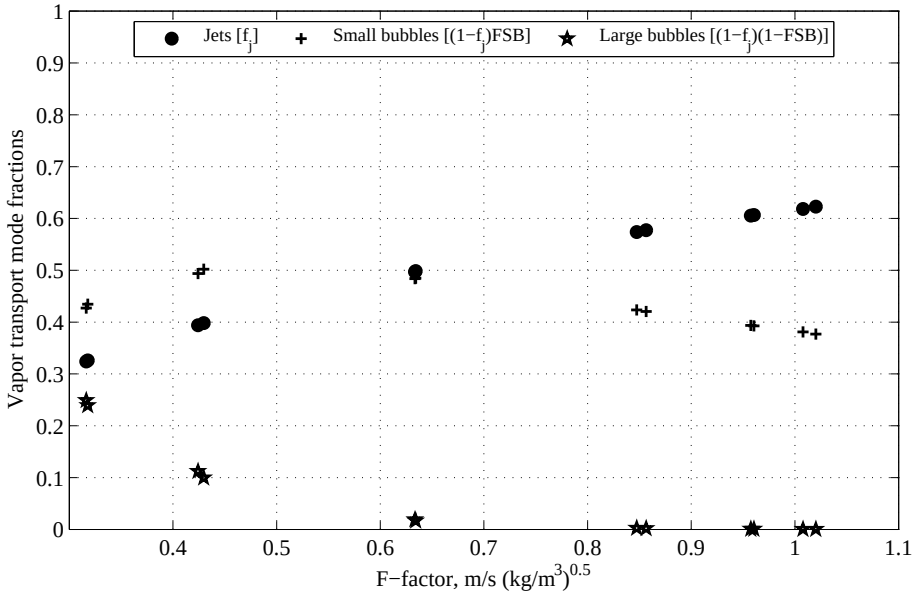

Figure 4.21: Predicted fraction jetting, small bubbling, and large bubbling for the IC4/NC4 system 2068 kPa, 8.3% open hole area using the new fraction jetting model.

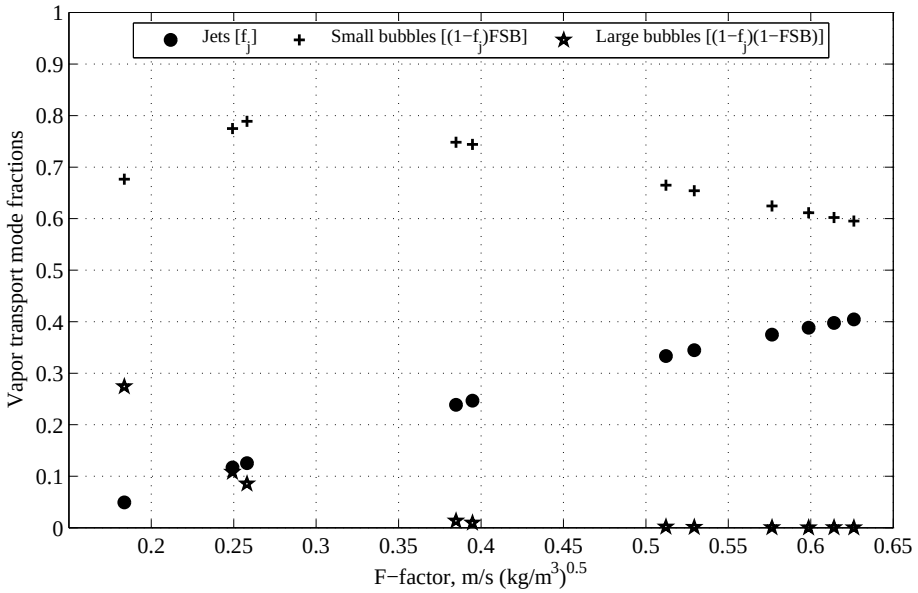

Figure 4.22: Predicted fraction jetting, small bubbling, and large bubbling for the IC4/NC4 system 2758 kPa, 8.3% open hole area using the Syeda et al. fraction jetting model.

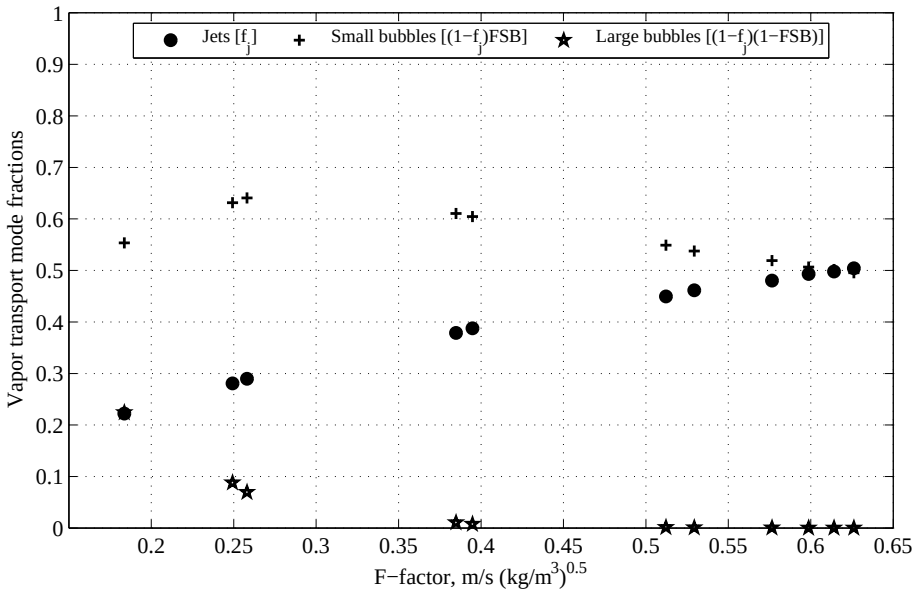

Figure 4.23: Predicted fraction jetting, small bubbling, and large bubbling for the IC4/NC4 system 2758 kPa, 8.3% open hole area using the new fraction jetting model.

4.5 Scope of the study

The fraction jetting model described here is limited to binary systems. When physical properties of the systems involved are dissimilar, surface tension, surface tension gradient, and froth stabilization forces also come into play. For aqueous systems with high surface tension and association forces such as hydrogen bonding, the dependence on concentration may be important.

The data used for the model is from air-water and therefore the extension to hydrocarbon systems in not tested. However other hydraulic studies using the modified Froude number indicate that such an extension might be possible (Hofhuis and Zuiderweg, 1979).

The fraction jetting at any operating condition is assumed to be constant. The fraction jetting remains the same even if the operating condition is approached from a higher rate or at a lower rate. This has not been tested and there is a need to study the fraction jetting model factors in more detail.

Although the fraction jetting data of Raper et al. include two valve tray points and two bubble cap tray points for comparison, the fraction jetting model is primarily for sieve trays. However, the model structure is amenable for extension to other tray types. For instance, the resistance on valve trays due to valve caps inhibits the jetting and results in reduced fraction jetting. This expectation is consistent with the literature observations that valve trays tend to operate more in the bubble regime than spray (Dhulesia, 1983, 1984; Kister, 1992).

The effect of hydraulic phenomenon like oscillations in the two phase mixture described by Biddulph (1975) are also not considered.

All of the Raper et al. data are from a 0.5 m diameter column. The fraction jetting data obtained from a small diameter column may be different than those obtained on a larger diameter column found in industrial columns. The vapor distribution and hydraulic gradients on large trays are different than those observed on small trays (Lockett, 1986;

Tang et al., 1987). The fraction jetting changes with a change in the column diameter are also outside the scope of this study.

4.6 Summary

In this chapter, the new fraction jetting model described in Chapter 3 was applied in the Syeda et al. sieve tray efficiency model in place of their original model. The results were compared with those of the Syeda et al. predictions. The new model also takes into effect the weir height and the liquid load using the clear liquid height. The new model is directly applicable to the existing multi-regime efficiency models and provides a phenomenological basis for predicting fraction jetting unlike the existing empirical fraction jetting models.

In addition, the new model provides phenomenological explanations for the indirect effects of rate and physical properties on efficiency in terms of fraction jetting. This can potentially lead to better design and operation by engineering for lower fraction jetting where efficiency loss at high rates are attributed to jetting rather than entrainment.

CHAPTER 5

SUMMARY AND CONCLUSIONS

In this chapter the major findings and contributions of this work are discussed, conclusions, and directions for future work are presented.

5.1 Major findings

The contributions and major findings are summarized below.

- A new fraction jetting model for sieve trays has been developed with the following features:
  - Has a simple model structure, which is based on the modified Froude number, that is also consistent with existing empirical correlations is developed.
  - Incorporates the vapor velocity, clear liquid height, vapor and liquid densities affecting the fraction jetting in a phenomenological manner using the modified Froude number.
  - Is asymptotically consistent unlike the existing Syeda et al. fraction jetting model
  - Can directly be used in place of the Syeda et al. fraction jetting model in the Syeda et al. sieve tray efficiency model.
  - Explains the physical significance of the single parameter of the fraction jetting model.
  - Explains the rate of change of fraction jetting with F-factor phenomenologically in terms of the dominant mode of vapor transport.

- Provided a basis for explaining the indirect effects of rate on sieve tray efficiency attributing the gradual drop in efficiency at high rates to fraction jetting

- Provided a basis for explaining the indirect effects of physical properties on sieve tray efficiency attributing the higher efficiencies at higher pressures, despite a drop in diffusivity and driving force, to reduced fraction jetting.

5.2 Conclusions

Incorporating fraction jetting leads to tray efficiency models that are based on a contact mechanism in accordance with actual phenomenon on a tray. Gradual changes in efficiency and capacity can be explained. Indirect effects of rate and physical properties have also been attributed to changes in fraction jetting.

The proposed fraction jetting model has a phenomenological basis, agrees with the current models, and has the ability to replace the existing fraction jetting models used in multi-regime tray efficiency models.

The modified Froude number based model structure has been developed and used to correlate Raper et al.'s fraction jetting data. The model describes Raper's data over the entire experimental range.

Based on the analysis of the residual fraction jetting (fraction jetting predicted using the new model - measured fraction jetting), it follows that the new model has no systemic bias and adequately captures the variability in the fraction jetting.

The value of the fraction jetting model parameter (0.0449), which signifies a change in the dominant mode of vapor transport in terms of the modified Froude number, agrees with completely independent set of data of Hofhuis and Zuiderweg (1979).

The new fraction jetting model can directly replace the Syeda's fraction jetting model in Syeda's sieve tray efficiency model. The average absolute deviations between the Syeda sieve tray efficiency model predictions using the Syeda fraction jetting model and the new

fraction jetting model do not exceed 0.031 for all of the seven hydrocarbon data sets considered. Furthermore, the new fraction jetting model can predict the fraction jetting for hydrocarbon systems without being artificially limited to a fraction jetting of 0.8 at high F-factors.

The Syeda sieve tray efficiency model retains the crowned pattern predictive capability when the new fraction jetting model is incorporated into it.

The fraction jetting model is expected to lead to improved models for predicting multi-regime efficiency as it is based on a phenomenological understanding of the mechanisms that lead to bubbling and jetting.

The methodology and the model structure developed can be a basis for further improvement of the model with the availability of additional data.

5.3 Future work

Fraction jetting data are needed on systems other than air-water to allow verification that the proposed new fraction jetting model has broad applicability. The data collection should be aimed at measuring various factors on fraction jetting as outlined in this work. In addition, the data collected on commercial scale columns will be valuable to capture the vapor flow patterns on large trays.

As an extension to this model framework, the general form of the modified Froude number may be used to develop a more sophisticated fraction jetting model by implementing gas velocity and the clear liquid profiles. Such an approach will provide a means to model mechanisms such as jet breakup by considering the jet stability at various locations on the tray.

A valued addition to this work would be the study of fraction jetting on different tray types. The presence of additional construction above the holes on valve trays results in additional resistance to jetting on valve trays. Raper's data, however, includes only two points for valve trays and two points for bubble cap trays. The fraction jetting on valve

trays appears to be similar to that of the sieve trays, but there is a need for additional experimental work that includes effect of valve tray specific geometric parameters such as slot area, valve lift, and valve weight.

The effect of fractional hole area on fraction jetting is another direction of study for improving the fraction jetting model. Variations in the fractional hole area due to (i) variation in the hole diameter for the same number of holes, and (ii) variation in the number of holes for the same diameter must be studied separately.

It is also recommended that the fraction jetting data collections be accompanied with froth height, clear liquid height, and dispersion density measurements. This will allow the use of measured hydraulic variables rather than estimated variables from clear liquid height or froth density correlations.

REFERENCES

AIChE (1958). Bubble tray design manual. Technical report, AIChE, New York.

Al-Masry, W. A., Ali, E. M., and Al-Kalbani, M. N. (2007). Prediction of regime transitions in bubble columns using acoustic and differential pressure signals. *Chemical Engineering Journal*, 133(1-3):139–149.

Andrew, S. (1969). Hydrodynamics of sieve plates at high liquid and vapor throughputs. *Institute of Chemical Engineers Symposium Series*, 32:2:49.

Ashley, M. J. and Haselden, G. G. (1972). Effectiveness of vapor-liquid contacting on a sieve plate. *Transactions of the Institution of Chemical Engineers and the Chemical Engineer*, 50(2):119–124.

Barber, A. and Wijn, E. F. (1979). Foaming in crude distillation units. *Institute of Chemical Engineers Symposium Series*, 56:3.1/15.

Bekassymolnar, E. and Mustafa, H. (1991). Clear liquid height on sieve plates in the froth, mixed and spray regimes. *Chemical Engineering Research & Design*, 69(1):14–20.

Bennett, D. L., Agrawal, R., and Cook, P. J. (1983). New pressure-drop correlation for sieve tray distillation-columns. *AIChE Journal*, 29(3):434–442.

Bennett, D. L., Watson, D. N., and Wiescinski, M. A. (1997). New correlation for sieve-tray point efficiency, entrainment, and section efficiency. *AIChE Journal*, 43(6):1611–1626.

Biddulph, M. (1975). Oscillating behavior on distillation trays -2. *American Institute of Chemical Engineers Journal*, 21(1):41–49.

Burgess, J. and Calderbank, P. (1975). The measurement of bubble parameters in two-phase dispersion-2. *Chemical Engineering Science*, 30:1107–1121.

Calderbank, B. (1978). Limitations of burgess-calderbank probe technique for characterization of gas liquid dispersions on sieve trays. *Chemical Engineering Science*, 33:1405–1406.

Calderbank, P. H. and Pereira, J. (1977). Prediction of distillation plate efficiencies from froth properties. *Chemical Engineering Science*, 32(12):1427–1433.

Chan, H. and Fair, J. R. (1984). Prediction of point efficiencies on sieve trays .1. binary-systems. *Industrial and Engineering Chemistry Process Design and Development*, 23(4):814–819.

Chen, G. X., Afacan, A., and Chuang, K. T. (1994). Effects of surface-tension on tray point efficiencies. *The Canadian Journal of Chemical Engineering*, 72(4):614–621.

Chen, G. X. and Chuang, K. T. (1993). Prediction of point efficiency for sieve trays in distillation. *Industrial and Engineering Chemistry Research*, 32(4):701–708.

Colwell, C. J. (1981). Clear liquid height and froth density on sieve trays. *Industrial and Engineering Chemistry Process Design and Development*, 20(2):298–307.

Dhulesia, H. (1983). Operating flow regimes on the valve tray. *Chemical Engineering Research and Design*, 61(5):329–332.

Dhulesia, H. (1984). Clear liquid height on sieve and valve trays. *Chemical Engineering Research and Design*, 62(5):321–326.

Drazin, P. (2002). *Introduction to hydrodynamic stability*. Cambridge university press, Cambridge.

FRI (2010). Fractionation Research Inc., Personal communication.

Garcia, J. A. and Fair, J. R. (2000a). A fundamental model for the prediction of distillation sieve tray efficiency. 1. Database development. *Industrial and Engineering Chemistry Research*, 39(6):1809–1817.

Garcia, J. A. and Fair, J. R. (2000b). A fundamental model for the prediction of distillation sieve tray efficiency. 2. Model development and validation. *Industrial and Engineering Chemistry Research*, 39(6):1818–1825.

Hesketh, R. P., Etchells, A. W., and Russell, T. W. F. (1991). Experimental observations of bubble breakage in turbulent flow. *Industrial and Engineering Chemistry Research*, 30(5):835–841.

Hoek, P. J. and Zuiderweg, F. J. (1982). Influence of vapor entrainment on distillation tray efficiency at high-pressures. *AIChE Journal*, 28(4):535–541.

Hofhuis, P. A. M. and Zuiderweg, F. J. (1979). Sieve plates: dispersion density and flow regimes. *Institute of Chemical Engineers Symposium Series*, 56:2.2/1.

Hu, B., Yang, H.-m., and Hewitt, G. F. (2007). Measurement of bubble size distribution using a flying optical probe technique: Application in the highly turbulent region above a distillation plate. *Chemical Engineering Science*, 62(10):2652–2662.

Hughmark, G. A. (1965). Point efficiencies for tray distillations. *Chemical Engineering Progress*, 61(7):97–100.

Jeronimo, M. A. and Sawistowski, H. (1973). Phase inversion correlation for sieve trays. *Transactions of the Institution of Chemical Engineers*, 51(3):265–266.

Johnson, K. (1981). Phase inversion for gas-liquid dispersions on sieve trays. Master's thesis, The University of Texas at Austin, Austin.

Kister, H. Z. (1992). *Distillation Design*. McGraw Hill, NY.

Kunesh, J. G., Kister, H. Z., Lockett, M. J., and Fair, J. R. (1995). Distillation - still towering over other options. *Chemical Engineering Progress*, 91(10):43–54.

Lockett, M. J. (1981). The froth to spray transition on sieve trays. *Transactions of the Institution of Chemical Engineers*, 59(1):26–34.

Lockett, M. J. (1986). *Distillation Tray Fundamentals*. Cambridge University Press, Cambridge.

Lockett, M. J. and Ahmed, I. S. (1983). Tray and point efficiencies from a 0.6 meter diameter distillation column. *Chemical Engineering Research & Design*, 61(2):110–118.

Loon, R. E., Pinczewski, W. V., and Fell, C. J. D. (1973). Dependence of froth-to-spray transition of sieve tray design parameters. *Transactions of the Institution of Chemical Engineers*, 51(4):374–376.

Mix, T. J., Dweck, J. S., Weinberg, M., and Armstrong, R. C. (1978). Energy conservation in distillation. *Chemical Engineering Progress*, 74(4):49–55.

Payne, G. and Prince, R. G. H. (1975). The transition from jetting to bubbling at a submerged orifice. *Transactions of the Institution of Chemical Engineers*, 53:209.

Payne, G. and Prince, R. G. H. (1977). The relationship between the froth and spray regimes, and the orifice processes occuring on perforated distillation plates. *Transactions of the Institution of Chemical Engineers*, 55:266.

Pinczewski, W. and Fell, C. (1982). Froth to spray transition on sieve trays. *Industrial and Engineering Chemistry Process Design and Development*, 21:774–776.

Pinczewski, W. V. and Fell, C. J. D. (1972). Transition from froth-to-spray regime on commercially loaded sieve trays. *Transactions of the Institution of Chemical Engineers and the Chemical Engineer*, 50(2):102.

Porter, K. E. and Wong, P. F. Y. (1969). Transition from spray to bubbling on sieve plates. *Institute of Chemical Engineers Symposium Series*, 32:2:23.

Prado, M. and Fair, J. R. (1987). Fundamental model for the prediction of sieve tray efficiency. In *EFCE Publication Series (European Federation of Chemical Engineering)*, pages 529–553, Univ of Texas at Austin, Austin, TX, USA. Publ by European Federation of Chemical Engineering, Amarousion-Pefki, Greece.

Prado, M. and Fair, J. R. (1990). Fundamental model for the prediction of sieve tray efficiency. *Industrial and Engineering Chemistry Research*, 29(6):1031–1042.

Prado, M., Johnson, K. L., and Fair, J. R. (1987). Bubble to spray transition on sieve trays. *Chemical Engineering Progress*, 83(3):32–40.

Prince, R. G. H., Jones, A. P., and Panic, R. (1979). The froth-spray transition. *Institute of Chemical Engineers Symposium Series*, 56:2.2/27.

Raper, J., Hai, N., Pinczewski, W. V., and Fell, C. J. D. (1979). Mass transfer efficiency on simulated industrial sieve trays operating in the spray regime. *Institute of Chemical Engineers Symposium Series*, 56:2.2/57–74.

Raper, J., Kearney, M., Burgess, J., and Fell, C. (1982). The structure of industrial sieve tray froths. *Chemical Engineering Science*, 37(4):501–506.

Sakata, M. and Yanagi, T. (1972). Performance of a commercial scale sieve tray. *Institute of Chemical Engineers Symposium Series*, 56:3.2/21–24.

Seader, J. D. and Henley, E. J. (2006). *Separation Process Principles (2nd edition)*. John Wiley & Sons Inc.

Spells, K. and Bakowski, S. (1950). A study of bubble formation at single slots submerged in water. *Transactions of the Institution of Chemical Engineers*, 28:38.

Sundar, R. and Tan, R. B. H. (1999). A model for bubble-to-jet transition at a submerged orifice. *Chemical Engineering Science*, 54(18):4053–4060.

Syeda, S. R. (2010). Personal communication.

Syeda, S. R., Afacan, A., and Chuang, K. T. (2004). Effect of surface tension gradient on froth stabilization and tray efficiency. *Chemical Engineering Research and Design*, 82(A6):762–769.

Syeda, S. R., Afacan, A., and Chuang, K. T. (2007). A fundamental model for prediction of sieve tray efficiency. *Chemical Engineering Research and Design*, 85(A2):269–277.

Tan, R. B. H. and Sundar, R. (2001). On the froth-spray transition at multiple orifices. *Chemical Engineering Science*, 56(21-22):6337–6340.

Tang, W., Li, Q., and Shen, F. (1987). Non-uniform entrainment distribution of large trays and its effect on efficiency. In *EFCE Publication Series (European Federation of Chemical Engineering)*, pages 449–459, East China Petroleum Inst, Beijing, China. Publ by European Federation of Chemical Engineering, Amarousion-Pefki, Greece.

Todd, W. G. and Van Winkle, M. (1972). Correlation of valve tray efficiency data. *Industrial and Engineering Chemistry Process Design and Development*, 11(4):589–604.

Van Sinderen, A. H., Wijn, E. F., and Zanting, R. W. J. (2003). Entrainment and maximum vapour flow rate of trays. *Chemical Engineering Research and Design*, 81(1):94–107.

Wijn, E. F. (1998). On the lower operating range of sieve and valve trays. *Chemical Engineering Journal*, 70(2):143–155.

Wong, P. F. Y. and Kwan, W. K. (1979). Generalized method for predicting the spray-bubbling transition on sieve plates. *Transactions of the Institution of Chemical Engineers*, 57(3):205–209.

Yanagi, T. and Sakata, M. (1982). Performance of a commercial scale 14-percent hole area sieve tray. *Industrial and Engineering Chemistry Process Design and Development*, 21(4):712–717.

Yang, G. Q., Du, B., and Fan, L. S. (2007). Bubble formation and dynamics in gas-liquid-solid fluidization–a review. *Chemical Engineering Science*, 62(1-2):2–27.

Zaritzky, N. E. and Calvelo, A. (1979). Internal mass transfer coefficient within single bubbles. theory and experiment. *The Canadian Journal of Chemical Engineering*, 57(1):58–64.

Zuiderweg, F. J. (1982). Sieve trays - A view on the state of the art. *Chemical Engineering Science*, 37(10):1441–1464.

Zuiderweg, F. J. and Harmens, A. (1958). The influence of surface phenomena on the performance of distillation columns. *Chemical Engineering Science*, 9(2-3):89.

APPENDIX A

Fraction jetting data

Table A.1: Raper et al. fraction jetting data. plate active area = 0.18 m^2, plate thickness = 1.7 mm, Weir load = 10 (m^3/h/m), column diameter = 0.5 m.

F_b	ϕ	h_w	TT	ρ_G	ρ_L	h_{cl}	Fr'	f_j
0.193	0.05	0.15	sieve	1.3	997	0.1421	0.0052	0.023
0.504	0.05	0.15	sieve	1.3	997	0.1210	0.0146	0.363
0.504	0.07	0.075	bubble cap	1.3	997	0.0649	0.0200	0.233
0.504	0.05	0.075	sieve	1.3	997	0.0649	0.0200	0.306
0.506	0.07	0.025	bubble cap	1.3	997	0.0277	0.0307	0.452
0.913	0.11	0.075	Glitsch V-1 valve	1.3	997	0.0537	0.0398	0.494
1.228	0.06	0.075	sieve	1.3	997	0.0468	0.0574	0.646
0.913	0.11	0.025	Glitsch V-1 valve	1.3	997	0.0236	0.0601	0.549
1.308	0.11	0.075	sieve	1.3	997	0.0452	0.0622	0.727
1.008	0.05	0.025	sieve	1.3	997	0.0228	0.0675	0.574
1.500	0.10	0.075	sieve	1.3	997	0.0417	0.0743	0.626
1.500	0.06	0.075	sieve	1.3	997	0.0417	0.0743	0.678
1.117	0.10	0.025	sieve	1.3	997	0.0219	0.0763	0.543
1.556	0.11	0.075	sieve	1.3	997	0.0407	0.0780	0.766
1.228	0.06	0.025	sieve	1.3	997	0.0210	0.0857	0.522
1.254	0.11	0.025	sieve	1.3	997	0.0208	0.0879	0.729
1.704	0.15	0.075	sieve	1.3	997	0.0383	0.0880	0.657
1.837	0.16	0.075	sieve	1.3	997	0.0363	0.0975	0.719
1.440	0.15	0.025	sieve	1.3	997	0.0195	0.1043	0.662
1.500	0.06	0.025	sieve	1.3	997	0.0191	0.1098	0.553
1.500	0.11	0.025	sieve	1.3	997	0.0191	0.1098	0.727
1.500	0.11	0.025	sieve	1.3	997	0.0191	0.1098	0.766
2.002	0.16	0.075	sieve	1.3	997	0.0340	0.1098	0.710
1.550	0.11	0.025	sieve	1.3	997	0.0188	0.1144	0.541
1.704	0.15	0.025	sieve	1.3	997	0.0178	0.1291	0.708
1.723	0.11	0.025	sieve	1.3	997	0.0177	0.1310	0.755
1.745	0.11	0.025	sieve	1.3	997	0.0176	0.1331	0.714
1.792	0.16	0.025	sieve	1.3	997	0.0173	0.1378	0.736
2.004	0.16	0.025	sieve	1.3	997	0.0161	0.1596	0.759

F_b F-factor, m/s (kg/m^3)$^{0.5}$ ϕ Fractional hole area h_w Outlet weir height, m TT Tray type

ρ_G Vapor density, kg/m^3 h_{cl} Clear liquid height from Bennett et al. (1983) correlation, m

ρ_L Liquid density, kg/m^3 Fr' Modified Froude number f_j Measured fraction jetting

APPENDIX B

Syeda et al. sieve tray efficiency model - corrected equations

This appendix lists the corrected versions of the equations in the Syeda et al. (2007) model that have been identified with the help of the first author of the article (Syeda, 2010).

Equation	Remark
$k\bar{\Delta}t = 0.16\frac{3.8\rho_L^{0.1}\rho_G^{0.3}}{\sigma^{0.4}}(u_b g)^{0.6}t_{GLB}$	t_{GLB} was not printed in the dissociation rate equation for the fraction of small bubbles
$h_L = 0.6h_w^{0.5}\left(\frac{p}{b}FP\right)^{0.25}$	Exponent of the weir height was not printed in the Zuiderweg spray regime equations.

where

k is the first order bubble breakage rate constant (1/s),

$\bar{\Delta}t$ is the time when half of the total secondary bubbles are formed in the froth from the initial number of bubbles (s) rho_G and ρ_L are the vapor and liquid densities (kg/m^3),

p is the hole pitch (m),

b is the weir length per unit bubbling area (1/m),

FP is the flow parameter, $\left(\frac{\rho_G}{\rho_L}\right)^{0.5}$ at total reflux, and

t_{GLB} is the residence time of the large bubbles (s)

APPENDIX C

Residual analysis of the fraction jetting model

In this appendix, bias plots of the residual fraction jetting calculated from the new fraction jetting model predictions and the Raper et al. data are plotted against (i) clear liquid height (Figure C.1), (ii) the vapor velocity based on the bubbling area (Figure C.2), and (iii) the fractional open hole area (Figure C.3).

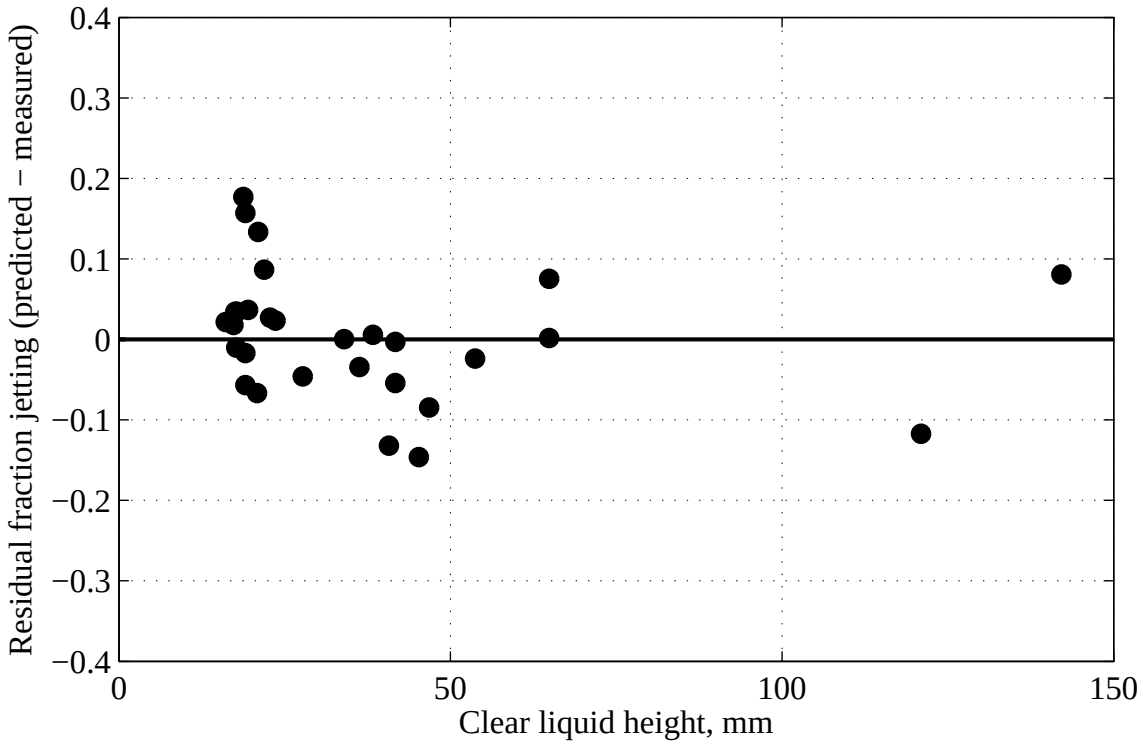

Figure C.1: Bias plot of the new jetting fraction model with respect to the calculated clear liquid height from the Bennett et al. (1983) clear liquid height correlation for sieve trays. The residual is calculated as predicted-measured. Raper et al. data.

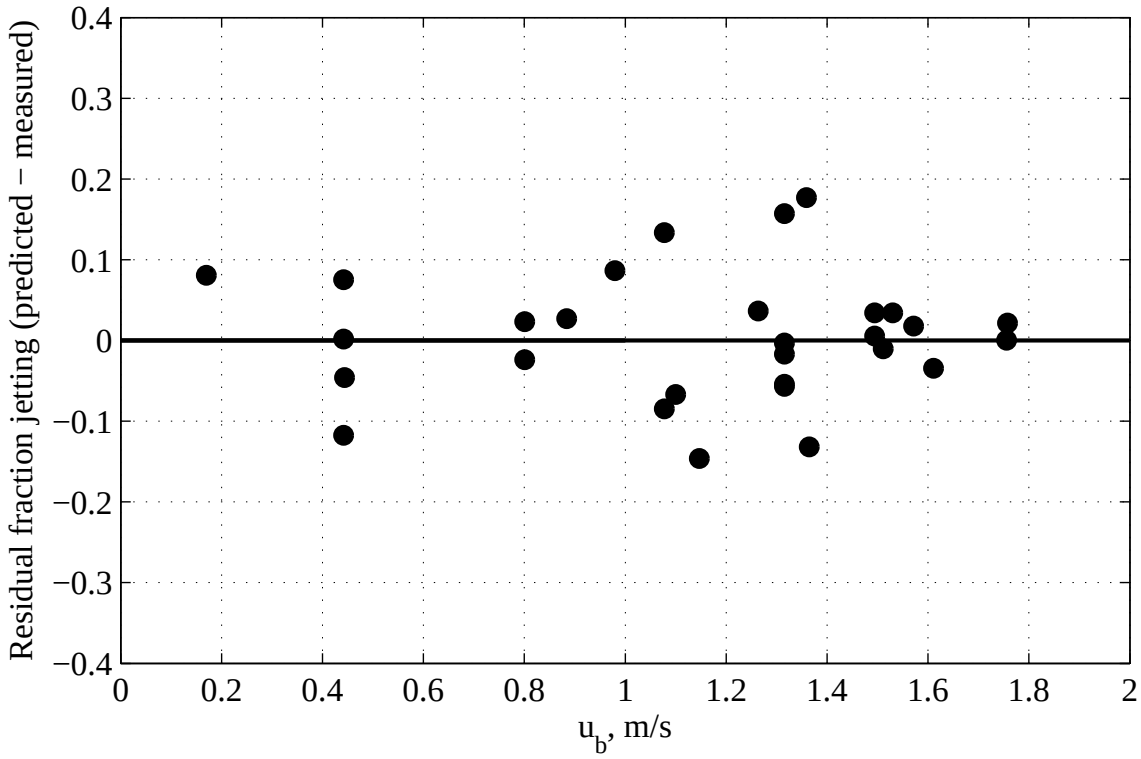

Figure C.2: Bias plot of the new jetting fraction model with respect to the vapor velocity based on the bubbling area. The residual is calculated as predicted-measured. Raper et al. data.

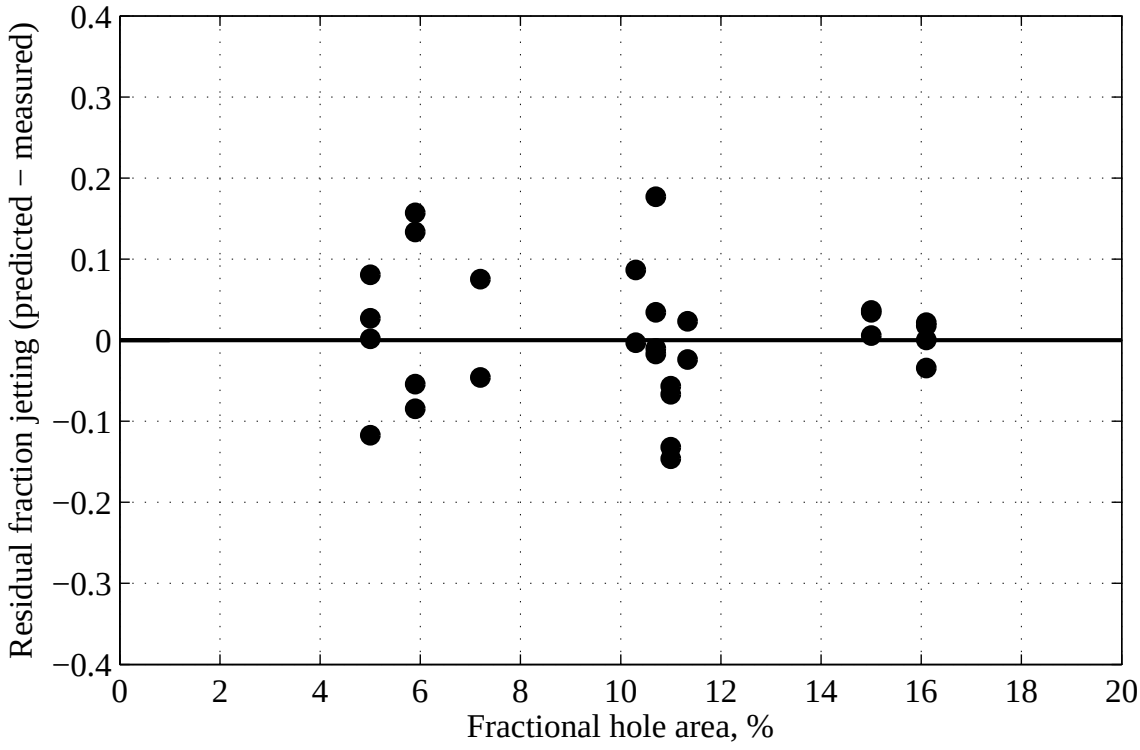

Figure C.3: Bias plot of the new jetting fraction model with respect to the fractional hole area which is the ratio of the open area to the bubbling area. The residual is calculated as predicted-measured. Raper et al. data.

APPENDIX D

Sieve tray efficiency data

The data tables for the sieve tray efficiency data used in Chapter 4 are presented here. Tables D.1, D.3, D.5, D.7, D.9, D.11, and D.13 present the sieve tray efficiency data used by Syeda et al. (2007) for the sieve tray efficiency model. Tables D.2, D.4, D.6, D.8, D.10, D.12, and D.14 present the Syeda et al. (2007) sieve tray efficiency model predictions with the new fraction jetting model.

Table D.1: C6/C7 system 34 kPa, sieve tray efficiency data, 14% hole area

L_f	G_f	E_{OGm}	α	D_L	D_G	ρ_L	ρ_G	μ_L	μ_G	σ	m	λ	D	d_h	TS	h_w	W	A_b	A_n
4,022	4,852	0.5242	1.83	4.12E-09	8.06E-06	714.3	1.14	3.40E-04	7.40E-06	0.0194	0.8044	0.9780	1.22	0.0127	0.61	0.0508	0.94	0.859	0.991
6,017	6,759	0.5664	1.83	4.26E-09	8.19E-06	710.4	1.14	3.40E-04	7.30E-06	0.0191	0.9134	1.0313	1.22	0.0127	0.61	0.0508	0.94	0.859	0.991
7,792	8,239	0.5951	1.83	4.28E-09	8.21E-06	710.4	1.14	3.40E-04	7.30E-06	0.0191	0.9134	0.9719	1.22	0.0127	0.61	0.0508	0.94	0.859	0.991
8,851	9,085	0.5509	1.83	4.36E-09	8.29E-06	708.7	1.15	3.40E-04	7.30E-06	0.0190	0.9271	0.9599	1.22	0.0127	0.61	0.0508	0.94	0.859	0.991
10,171	10,433	0.3695	1.83	4.49E-09	8.41E-06	703.9	1.15	3.40E-04	7.30E-06	0.0190	0.9187	0.9580	1.22	0.0127	0.61	0.0508	0.94	0.859	0.991

L_f	Liquid mass flow rate, kg/hr	σ	Surface tension, N/m
G_f	Vapor mass flow rate, kg/hr	m	m = dy/dx (Slope of equilibrium line)
E_{OGm}	Point efficiency (fractional)	λ	Stripping factor
α	Relative volatility	D	Column diameter, m
D_L	Liquid diffusivity, m^2/s	d_h	Hole diameter, m
D_G	Vapor diffusivity, m^2/s	TS	Tray spacing, m
ρ_L	Liquid density, kg/m^3	h_w	Weir height, m
ρ_G	Vapor density, kg/m^3	W	Weir length, m
μ_L	Liquid viscosity, Pa-s	A_b	Active or bubbling area, m^2
μ_G	Vapor viscosity, Pa-s	A_n	Net area, m^2

Table D.2: C6/C7 system 34 kPa, sieve tray efficiency data, 14% hole area, model predictions with the Syeda et al. sieve tray efficiency model and the new fraction jetting model.

F_b	d_{32L}	t_{GLB}	E_{LB}	F_{SB}	E_{SB}	E_B	f_j	E_j	E_{OGc}
1.470	0.036	0.021	0.014	0.013	1.000	0.027	0.757	0.598	0.459
2.047	0.038	0.030	0.018	0.029	1.000	0.046	0.789	0.601	0.484
2.495	0.040	0.029	0.016	0.032	1.000	0.047	0.830	0.582	0.491
2.740	0.041	0.028	0.015	0.034	1.000	0.049	0.847	0.573	0.493
3.146	0.042	0.028	0.014	0.038	1.000	0.052	0.871	0.561	0.495

F_b	F-factor, $(Pa)^{0.5}$	E_{SB}	Efficiency of the small bubbles, fractional
d_{32L}	Sauter mean diameter of the large bubbles, m	E_B	Efficiency of the bubble zone, fractional
t_{GLB}	Residence time of the large bubbles, s	f_j	Fraction jetting, fractional
E_{LB}	Efficiency of the large bubbles, fractional	E_j	Efficiency of the jetting zone, fractional
F_{SB}	Fraction of small bubbles in the bubble zone, fractional	E_{OGc}	Predicted point efficiency, fractional

Table D.3: C6/C7 system 165 kPa, sieve tray efficiency data, 8.3% hole area

L_f	G_f	E_{OGm}	α	D_L	D_G	ρ_L	ρ_G	μ_L	μ_G	σ	m	λ	D	d_h	TS	h_w	W	A_b	A_n
4,767	4,905	0.5883	1.57	7.61E-09	2.28E-06	662.0	5.02	2.72E-04	8.50E-06	0.0141	0.8813	0.9202	1.22	0.0127	0.61	0.0508	0.94	0.859	0.991
6,649	6,918	0.6036	1.57	7.61E-09	2.28E-06	657.7	5.05	2.72E-04	8.50E-06	0.0139	0.9298	0.9783	1.22	0.0127	0.61	0.0508	0.94	0.859	0.991
9,087	9,671	0.6320	1.57	7.59E-09	2.28E-06	658.0	5.05	2.73E-04	8.50E-06	0.0140	0.9306	1.0002	1.22	0.0127	0.61	0.0508	0.94	0.859	0.991
13,555	14,369	0.6977	1.57	7.50E-09	2.26E-06	658.6	5.04	2.77E-04	8.50E-06	0.0139	0.9334	0.9986	1.22	0.0127	0.61	0.0508	0.94	0.859	0.991
17,786	18,361	0.7277	1.57	7.62E-09	2.28E-06	658.0	5.05	2.72E-04	8.50E-06	0.0139	0.9409	0.9808	1.22	0.0127	0.61	0.0508	0.94	0.859	0.991
20,024	20,862	0.7221	1.57	7.63E-09	2.28E-06	658.0	5.05	2.72E-04	8.50E-06	0.0139	0.9409	0.9900	1.22	0.0127	0.61	0.0508	0.94	0.859	0.991
21,038	21,843	0.7159	1.57	7.66E-09	2.29E-06	657.1	5.05	2.70E-04	8.50E-06	0.0139	0.9465	0.9924	1.22	0.0127	0.61	0.0508	0.94	0.859	0.991
22,343	22,867	0.5488	1.57	7.80E-09	2.31E-06	651.4	5.09	2.59E-04	8.50E-06	0.0137	0.9603	0.9959	1.22	0.0127	0.61	0.0508	0.94	0.859	0.991

L_f	Liquid mass flow rate, kg/hr	σ	Surface tension, N/m
G_f	Vapor mass flow rate, kg/hr	m	m = dy/dx (Slope of equilibrium line)
E_{OGm}	Point efficiency (fractional)	λ	Stripping factor
α	Relative volatility	D	Column diameter, m
D_L	Liquid diffusivity, m^2/s	d_h	Hole diameter, m
D_G	Vapor diffusivity, m^2/s	TS	Tray spacing, m
ρ_L	Liquid density, kg/m^3	h_w	Weir height, m
ρ_G	Vapor density, kg/m^3	W	Weir length, m
μ_L	Liquid viscosity, Pa-s	A_b	Active or bubbling area, m^2
μ_G	Vapor viscosity, Pa-s	A_n	Net area, m^2

Table D.4: C6/C7 system 165 kPa, sieve tray efficiency data, 8.3% hole area, model predictions with the Syeda et al. sieve tray efficiency model and the new fraction jetting model.

F_b	d_{32L}	t_{GLB}	E_{LB}	F_{SB}	E_{SB}	E_B	f_j	E_j	E_{OGc}
0.708	0.029	0.089	0.024	0.077	1.000	0.099	0.499	0.775	0.436
0.995	0.031	0.080	0.019	0.094	1.000	0.111	0.597	0.737	0.485
1.392	0.034	0.072	0.015	0.115	1.000	0.128	0.689	0.705	0.525
2.070	0.037	0.067	0.012	0.167	1.000	0.177	0.783	0.668	0.561
2.642	0.039	0.067	0.011	0.244	1.000	0.252	0.831	0.644	0.577
3.002	0.040	0.069	0.010	0.307	1.000	0.315	0.853	0.631	0.585
3.143	0.040	0.070	0.010	0.340	1.000	0.347	0.861	0.626	0.587
3.278	0.040	0.072	0.011	0.393	1.000	0.400	0.867	0.622	0.593

F_b	F-factor, $(Pa)^{0.5}$	E_{SB}	Efficiency of the small bubbles, fractional
d_{32L}	Sauter mean diameter of the large bubbles, m	E_B	Efficiency of the bubble zone, fractional
t_{GLB}	Residence time of the large bubbles, s	f_j	Fraction jetting, fractional
E_{LB}	Efficiency of the large bubbles, fractional	E_j	Efficiency of the jetting zone, fractional
F_{SB}	Fraction of small bubbles in the bubble zone, fractional	E_{OGc}	Predicted point efficiency, fractional

Table D.5: C6/C7 system 165 kPa, sieve tray efficiency data, 14% hole area

L_f	G_f	E_{OGm}	α	D_L	D_G	ρ_L	ρ_G	μ_L	μ_G	σ	m	λ	D	d_h	TS	h_w	W	A_b	A_n
2,433	2,490	0.2647	1.57	7.95E-09	2.33E-06	645.5	5.11	2.50E-04	8.40E-06	0.0136	0.9299	0.9632	1.22	0.0127	0.61	0.0508	0.94	0.859	0.991
5,022	5,124	0.4267	1.57	7.55E-09	2.27E-06	645.5	5.11	2.62E-04	8.40E-06	0.0136	0.9309	0.9570	1.22	0.0127	0.61	0.0508	0.94	0.859	0.991
7,306	8,152	0.5690	1.57	7.52E-09	2.26E-06	650.0	5.08	2.69E-04	8.40E-06	0.0138	0.9120	1.0235	1.22	0.0127	0.61	0.0508	0.94	0.859	0.991
9,536	10,391	0.6243	1.57	7.51E-09	2.26E-06	651.0	5.08	2.70E-04	8.40E-06	0.0138	0.9140	1.0045	1.22	0.0127	0.61	0.0508	0.94	0.859	0.991
14,305	14,555	0.6639	1.57	7.73E-09	2.30E-06	649.1	5.09	2.60E-04	8.40E-06	0.0137	0.9312	0.9617	1.22	0.0127	0.61	0.0508	0.94	0.859	0.991
18,900	21,196	0.6882	1.57	7.44E-09	2.25E-06	652.7	5.07	2.74E-04	8.40E-06	0.0139	0.9010	1.0137	1.22	0.0127	0.61	0.0508	0.94	0.859	0.991
21,590	22,867	0.6009	1.57	7.64E-09	2.29E-06	650.1	5.08	2.64E-04	8.40E-06	0.0138	0.9131	0.9712	1.22	0.0127	0.61	0.0508	0.94	0.859	0.991
23,763	26,250	0.4950	1.57	7.56E-09	2.27E-06	647.5	5.10	2.64E-04	8.40E-06	0.0137	0.9219	1.0219	1.22	0.0127	0.61	0.0508	0.94	0.859	0.991

L_f	Liquid mass flow rate, kg/hr	σ	Surface tension, N/m
G_f	Vapor mass flow rate, kg/hr	m	m = dy/dx (Slope of equilibrium line)
E_{OGm}	Point efficiency (fractional)	λ	Stripping factor
α	Relative volatility	D	Column diameter, m
D_L	Liquid diffusivity, m^2/s	d_h	Hole diameter, m
D_G	Vapor diffusivity, m^2/s	TS	Tray spacing, m
ρ_L	Liquid density, kg/m^3	h_w	Weir height, m
ρ_G	Vapor density, kg/m^3	W	Weir length, m
μ_L	Liquid viscosity, Pa-s	A_b	Active or bubbling area, m^2
μ_G	Vapor viscosity, Pa-s	A_n	Net area, m^2

Table D.6: C6/C7 system 165 kPa, sieve tray efficiency data, 14% hole area, model predictions with the Syeda et al. sieve tray efficiency model and the new fraction jetting model.

F_b	d_{32L}	t_{GLB}	E_{LB}	F_{SB}	E_{SB}	E_B	f_j	E_j	E_{OGc}
0.356	0.023	0.116	0.053	0.058	1.000	0.108	0.322	0.772	0.322
0.733	0.026	0.092	0.031	0.087	1.000	0.115	0.512	0.704	0.416
1.170	0.029	0.077	0.021	0.108	1.000	0.127	0.645	0.661	0.471
1.491	0.031	0.072	0.018	0.128	1.000	0.144	0.708	0.637	0.493
2.086	0.033	0.069	0.015	0.188	1.000	0.200	0.785	0.604	0.518
3.044	0.036	0.068	0.013	0.310	1.000	0.319	0.858	0.571	0.535
3.281	0.036	0.072	0.013	0.390	1.000	0.398	0.868	0.563	0.542
3.759	0.037	0.075	0.013	0.523	1.000	0.529	0.889	0.549	0.547

F_b	F-factor, $(Pa)^{0.5}$	E_{SB}	Efficiency of the small bubbles, fractional
d_{32L}	Sauter mean diameter of the large bubbles, m	E_B	Efficiency of the bubble zone, fractional
t_{GLB}	Residence time of the large bubbles, s	f_j	Fraction jetting, fractional
E_{LB}	Efficiency of the large bubbles, fractional	E_j	Efficiency of the jetting zone, fractional
F_{SB}	Fraction of small bubbles in the bubble zone, fractional	E_{OGc}	Predicted point efficiency, fractional

Table D.7: IC4/NC4 system 1138 kPa, sieve tray efficiency data, 8.3% hole area

L_f	G_f	E_{OGm}	α	D_L	D_G	ρ_L	ρ_G	μ_L	μ_G	σ	m	λ	D	d_h	TS	h_w	W	A_b	A_n
6,424	6,440	0.558	1.23	1.03E-08	5.62E-07	493.0	28.0	9.00E-05	9.50E-06	0.0050	1.0562	1.0588	1.22	0.0127	0.61	0.0508	0.94	0.859	0.991
10,428	10,359	0.7342	1.23	1.03E-08	5.61E-07	494.0	27.7	9.00E-05	9.50E-06	0.0050	1.0562	1.0491	1.22	0.0127	0.61	0.0508	0.94	0.859	0.991
14,100	14,139	0.7888	1.23	1.03E-08	5.62E-07	493.0	28.0	9.00E-05	9.50E-06	0.0050	1.0562	1.0591	1.22	0.0127	0.61	0.0508	0.94	0.859	0.991
21,376	21,270	0.8177	1.23	1.03E-08	5.62E-07	493.0	27.8	9.00E-05	9.50E-06	0.0050	1.0562	1.0509	1.22	0.0127	0.61	0.0508	0.94	0.859	0.991
28,200	28,377	0.8229	1.23	1.04E-08	5.63E-07	493.0	28.3	9.00E-05	9.50E-06	0.0050	1.0562	1.0628	1.22	0.0127	0.61	0.0508	0.94	0.859	0.991
31,670	31,828	0.8100	1.23	1.03E-08	5.62E-07	493.0	28.2	9.00E-05	9.50E-06	0.0050	1.0562	1.0614	1.22	0.0127	0.61	0.0508	0.94	0.859	0.991
33,351	33,452	0.7700	1.23	1.04E-08	5.63E-07	493.0	28.2	9.00E-05	9.50E-06	0.0050	1.0562	1.0594	1.22	0.0127	0.61	0.0508	0.94	0.859	0.991
35,028	35,256	0.7500	1.23	1.05E-08	5.69E-07	493.0	28.2	9.00E-05	9.50E-06	0.0050	1.0562	1.0631	1.22	0.0127	0.61	0.0508	0.94	0.859	0.991

L_f	Liquid mass flow rate, kg/hr	σ	Surface tension, N/m
G_f	Vapor mass flow rate, kg/hr	m	m = dy/dx (Slope of equilibrium line)
E_{OGm}	Point efficiency (fractional)	λ	Stripping factor
α	Relative volatility	D	Column diameter, m
D_L	Liquid diffusivity, m^2/s	d_h	Hole diameter, m
D_G	Vapor diffusivity, m^2/s	TS	Tray spacing, m
ρ_L	Liquid density, kg/m^3	h_w	Weir height, m
ρ_G	Vapor density, kg/m^3	W	Weir length, m
μ_L	Liquid viscosity, Pa-s	A_b	Active or bubbling area, m^2
μ_G	Vapor viscosity, Pa-s	A_n	Net area, m^2

Table D.8: IC4/NC4 system 1138 kPa, sieve tray efficiency data, 8.3% hole area, model predictions with the Syeda et al. sieve tray efficiency model and the new fraction jetting model.

F_b	d_{32L}	t_{GLB}	E_{LB}	F_{SB}	E_{SB}	E_B	f_j	E_j	E_{OGc}
0.394	0.022	0.164	0.019	0.331	1.000	0.344	0.366	0.806	0.513
0.636	0.024	0.160	0.015	0.589	1.000	0.596	0.490	0.766	0.679
0.864	0.025	0.160	0.014	0.783	1.000	0.786	0.573	0.737	0.758
1.305	0.028	0.167	0.012	0.957	1.000	0.957	0.679	0.700	0.782
1.725	0.029	0.180	0.012	0.994	1.000	0.994	0.744	0.672	0.754
1.938	0.030	0.188	0.012	0.998	1.000	0.998	0.769	0.661	0.739
2.037	0.030	0.192	0.012	0.999	1.000	0.999	0.779	0.656	0.732
2.147	0.031	0.197	0.012	0.999	1.000	0.999	0.789	0.651	0.725

F_b	F-factor, $(Pa)^{0.5}$	E_{SB}	Efficiency of the small bubbles, fractional
d_{32L}	Sauter mean diameter of the large bubbles, m	E_B	Efficiency of the bubble zone, fractional
t_{GLB}	Residence time of the large bubbles, s	f_j	Fraction jetting, fractional
E_{LB}	Efficiency of the large bubbles, fractional	E_j	Efficiency of the jetting zone, fractional
F_{SB}	Fraction of small bubbles in the bubble zone, fractional	E_{OGc}	Predicted point efficiency, fractional

Table D.9: IC4/NC4 system 1138 kPa, sieve tray efficiency data, 14% hole area

L_f	G_f	E_{OGm}	α	D_L	D_G	ρ_L	ρ_G	μ_L	μ_G	σ	m	λ	D	d_h	TS	h_w	W	A_b	A_n
6,290	6,468	0.4921	1.23	1.06E-08	5.62E-07	485.0	30.2	9.00E-05	9.40E-06	0.0050	0.9894	1.0174	1.22	0.0127	0.61	0.0508	0.94	0.859	0.991
10,254	10,258	0.6783	1.23	1.06E-08	5.63E-07	489.0	28.8	9.00E-05	9.40E-06	0.0050	0.9894	0.9898	1.22	0.0127	0.61	0.0508	0.94	0.859	0.991
14,470	14,505	0.7363	1.23	1.02E-08	5.57E-07	490.0	28.8	9.00E-05	9.40E-06	0.0050	0.9894	0.9918	1.22	0.0127	0.61	0.0508	0.94	0.859	0.991
21,456	21,332	0.7565	1.23	1.02E-08	5.56E-07	492.0	28.5	9.00E-05	9.40E-06	0.0050	0.9894	0.9837	1.22	0.0127	0.61	0.0508	0.94	0.859	0.991
27,823	27,785	0.7632	1.23	1.02E-08	5.56E-07	492.0	28.7	9.00E-05	9.40E-06	0.0050	0.9894	0.9881	1.22	0.0127	0.61	0.0508	0.94	0.859	0.991
32,408	32,380	0.7598	1.23	1.02E-08	5.57E-07	492.0	28.7	9.00E-05	9.50E-06	0.0050	0.9894	0.9886	1.22	0.0127	0.61	0.0508	0.94	0.859	0.991
35,311	35,284	0.6890	1.23	1.04E-08	5.63E-07	492.0	28.8	9.00E-05	9.50E-06	0.0050	0.9894	0.9887	1.22	0.0127	0.61	0.0508	0.94	0.859	0.991

L_f	Liquid mass flow rate, kg/hr	σ	Surface tension, N/m
G_f	Vapor mass flow rate, kg/hr	m	m = dy/dx (Slope of equilibrium line)
E_{OGm}	Point efficiency (fractional)	λ	Stripping factor
α	Relative volatility	D	Column diameter, m
D_L	Liquid diffusivity, m^2/s	d_h	Hole diameter, m
D_G	Vapor diffusivity, m^2/s	TS	Tray spacing, m
ρ_L	Liquid density, kg/m^3	h_w	Weir height, m
ρ_G	Vapor density, kg/m^3	W	Weir length, m
μ_L	Liquid viscosity, Pa-s	A_b	Active or bubbling area, m^2
μ_G	Vapor viscosity, Pa-s	A_n	Net area, m^2

Table D.10: IC4/NC4 system 1138 kPa, sieve tray efficiency data, 14% hole area, model predictions with the Syeda et al. sieve tray efficiency model and the new fraction jetting model.

F_b	d_{32L}	t_{GLB}	E_{LB}	F_{SB}	E_{SB}	E_B	f_j	E_j	E_{OGc}
0.381	0.019	0.174	0.026	0.365	1.000	0.381	0.360	0.752	0.515
0.618	0.021	0.168	0.020	0.628	1.000	0.635	0.483	0.713	0.673
0.874	0.023	0.168	0.018	0.832	1.000	0.835	0.576	0.681	0.746
1.292	0.025	0.174	0.015	0.967	1.000	0.967	0.677	0.645	0.749
1.677	0.026	0.185	0.015	0.995	1.000	0.995	0.738	0.619	0.718
1.955	0.027	0.196	0.015	0.999	1.000	0.999	0.770	0.605	0.695
2.126	0.027	0.205	0.015	1.000	1.000	1.000	0.787	0.596	0.682

F_b	F-factor, $(Pa)^{0.5}$	E_{SB}	Efficiency of the small bubbles, fractional
d_{32L}	Sauter mean diameter of the large bubbles, m	E_B	Efficiency of the bubble zone, fractional
t_{GLB}	Residence time of the large bubbles, s	f_j	Fraction jetting, fractional
E_{LB}	Efficiency of the large bubbles, fractional	E_j	Efficiency of the jetting zone, fractional
F_{SB}	Fraction of small bubbles in the bubble zone, fractional	E_{OGc}	Predicted point efficiency, fractional

Table D.11: IC4/NC4 system 2068 kPa, sieve tray efficiency data, 8.3% hole area

L_f	G_f	E_{OGm}	α	D_L	D_G	ρ_L	ρ_G	μ_L	μ_G	σ	m	λ	D	d_h	TS	h_w	W	A_b	A_n
7,446	7,388	0.7898	1.16	2.01E-08	3.81E-07	426.0	56.5	6.50E-05	1.01E-05	0.0025	0.8729	0.8661	1.22	0.0127	0.61	0.0508	0.94	0.859	0.991
10,108	10,086	0.8790	1.16	1.77E-08	3.75E-07	424.0	57.6	6.50E-05	1.01E-05	0.0025	0.8729	0.8710	1.22	0.0127	0.61	0.0508	0.94	0.859	0.991
14,823	14,925	0.8466	1.16	1.68E-08	3.72E-07	424.0	57.9	6.50E-05	1.01E-05	0.0025	0.8729	0.8789	1.22	0.0127	0.61	0.0508	0.94	0.859	0.991
20,021	20,100	0.8582	1.16	1.74E-08	3.74E-07	424.0	57.6	6.50E-05	1.01E-05	0.0025	0.8729	0.8764	1.22	0.0127	0.61	0.0508	0.94	0.859	0.991
22,576	22,483	0.8567	1.16	1.69E-08	3.71E-07	425.0	57.3	6.50E-05	1.01E-05	0.0025	0.8729	0.8693	1.22	0.0127	0.61	0.0508	0.94	0.859	0.991
23,815	24,069	0.8440	1.16	1.69E-08	3.72E-07	423.0	58.2	6.50E-05	1.01E-05	0.0025	0.8729	0.8822	1.22	0.0127	0.61	0.0508	0.94	0.859	0.991
7,258	7,216	0.7314	1.16	1.33E-08	3.61E-07	432.0	54.4	6.50E-05	1.02E-05	0.0025	0.9718	0.9661	1.22	0.0127	0.61	0.0508	0.94	0.859	0.991
9,662	9,703	0.8270	1.16	1.31E-08	3.60E-07	430.0	54.7	6.50E-05	1.02E-05	0.0025	0.9718	0.9758	1.22	0.0127	0.61	0.0508	0.94	0.859	0.991
14,448	14,555	0.8380	1.16	1.30E-08	3.60E-07	430.0	55.2	6.50E-05	1.02E-05	0.0025	0.9718	0.9789	1.22	0.0127	0.61	0.0508	0.94	0.859	0.991
19,329	19,467	0.8130	1.16	1.31E-08	3.60E-07	430.0	55.2	6.50E-05	1.02E-05	0.0025	0.9718	0.9787	1.22	0.0127	0.61	0.0508	0.94	0.859	0.991
21,866	21,958	0.8135	1.16	1.28E-08	3.59E-07	430.0	55.0	6.50E-05	1.02E-05	0.0025	0.9718	0.9759	1.22	0.0127	0.61	0.0508	0.94	0.859	0.991
23,035	23,112	0.8098	1.16	1.31E-08	3.61E-07	430.0	55.0	6.50E-05	1.02E-05	0.0025	0.9718	0.9750	1.22	0.0127	0.61	0.0508	0.94	0.859	0.991

L_f	Liquid mass flow rate, kg/hr	σ	Surface tension, N/m
G_f	Vapor mass flow rate, kg/hr	m	m = dy/dx (Slope of equilibrium line)
E_{OGm}	Point efficiency (fractional)	λ	Stripping factor
α	Relative volatility	D	Column diameter, m
D_L	Liquid diffusivity, m^2/s	d_h	Hole diameter, m
D_G	Vapor diffusivity, m^2/s	TS	Tray spacing, m
ρ_L	Liquid density, kg/m^3	h_w	Weir height, m
ρ_G	Vapor density, kg/m^3	W	Weir length, m
μ_L	Liquid viscosity, Pa-s	A_b	Active or bubbling area, m^2
μ_G	Vapor viscosity, Pa-s	A_n	Net area, m^2

Table D.12: IC4/NC4 system 2068 kPa, sieve tray efficiency data, 8.3% hole area, model predictions with the Syeda et al. sieve tray efficiency model and the new fraction jetting model.

F_b	d_{32L}	t_{GLB}	E_{LB}	F_{SB}	E_{SB}	E_B	f_j	E_j	E_{OGc}
0.318	0.019	0.196	0.019	0.645	1.000	0.652	0.326	0.871	0.723
0.430	0.020	0.198	0.017	0.834	1.000	0.837	0.398	0.848	0.842
0.634	0.022	0.205	0.015	0.967	1.000	0.967	0.498	0.817	0.893
0.856	0.024	0.215	0.014	0.995	1.000	0.995	0.577	0.793	0.878
0.960	0.024	0.221	0.014	0.998	1.000	0.998	0.607	0.784	0.868
1.020	0.024	0.226	0.014	0.999	1.000	0.999	0.623	0.777	0.861
0.316	0.019	0.194	0.018	0.632	1.000	0.638	0.324	0.861	0.710
0.424	0.020	0.195	0.016	0.815	1.000	0.818	0.394	0.839	0.826
0.634	0.022	0.201	0.014	0.962	1.000	0.963	0.497	0.806	0.885
0.847	0.024	0.210	0.013	0.994	1.000	0.994	0.574	0.781	0.872
0.957	0.024	0.216	0.013	0.998	1.000	0.998	0.605	0.771	0.860
1.008	0.024	0.219	0.013	0.998	1.000	0.998	0.618	0.767	0.855

F_b	F-factor, $(Pa)^{0.5}$	E_{SB}	Efficiency of the small bubbles, fractional
d_{32L}	Sauter mean diameter of the large bubbles, m	E_B	Efficiency of the bubble zone, fractional
t_{GLB}	Residence time of the large bubbles, s	f_j	Fraction jetting, fractional
E_{LB}	Efficiency of the large bubbles, fractional	E_j	Efficiency of the jetting zone, fractional
F_{SB}	Fraction of small bubbles in the bubble zone, fractional	E_{OGc}	Predicted point efficiency, fractional

Table D.13: IC4/NC4 system 2758 kPa, sieve tray efficiency data, 8.3% hole area

L_f	G_f	E_{OGm}	α	D_L	D_G	ρ_L	ρ_G	μ_L	μ_G	σ	m	λ	D	d_h	TS	h_w	W	A_b	A_n
7,560	7,408	0.8682	1.11	2.30E-08	3.09E-07	378.0	86.2	5.00E-05	1.05E-05	0.0011	0.9110	0.8927	1.22	0.0127	0.61	0.0508	0.94	0.859	0.991
11,377	11,486	0.8991	1.11	2.05E-08	3.05E-07	374.0	88.5	5.00E-05	1.05E-05	0.0011	0.9110	0.9197	1.22	0.0127	0.61	0.0508	0.94	0.859	0.991
15,241	15,451	0.9245	1.11	2.07E-08	3.06E-07	373.0	89.1	5.00E-05	1.05E-05	0.0011	0.9110	0.9236	1.22	0.0127	0.61	0.0508	0.94	0.859	0.991
17,274	17,446	0.9124	1.11	2.02E-08	3.05E-07	373.0	88.8	5.00E-05	1.05E-05	0.0011	0.9110	0.9201	1.22	0.0127	0.61	0.0508	0.94	0.859	0.991
18,169	18,133	0.8883	1.11	2.12E-08	3.06E-07	374.0	87.7	5.00E-05	1.05E-05	0.0011	0.9110	0.9092	1.22	0.0127	0.61	0.0508	0.94	0.859	0.991
5,163	5,039	0.8513	1.11	1.55E-08	2.98E-07	392.0	78.7	5.00E-05	1.07E-05	0.0011	0.9904	0.9666	1.22	0.0127	0.61	0.0508	0.94	0.859	0.991
6,967	6,917	0.9158	1.11	1.49E-08	2.94E-07	389.0	80.5	5.00E-05	1.06E-05	0.0011	0.9904	0.9832	1.22	0.0127	0.61	0.0508	0.94	0.859	0.991
10,688	10,815	0.9066	1.11	1.48E-08	2.94E-07	386.0	82.6	5.00E-05	1.07E-05	0.0011	0.9904	1.0020	1.22	0.0127	0.61	0.0508	0.94	0.859	0.991
14,230	14,360	0.9154	1.11	1.48E-08	2.94E-07	387.0	82.2	5.00E-05	1.07E-05	0.0011	0.9904	0.9994	1.22	0.0127	0.61	0.0508	0.94	0.859	0.991
15,946	16,164	0.8764	1.11	1.49E-08	2.95E-07	386.0	82.2	5.00E-05	1.07E-05	0.0011	0.9904	1.0039	1.22	0.0127	0.61	0.0508	0.94	0.859	0.991
16,559	17,238	0.8668	1.11	1.49E-08	2.95E-07	386.0	82.4	5.00E-05	1.07E-05	0.0011	0.9904	1.0310	1.22	0.0127	0.61	0.0508	0.94	0.859	0.991

L_f	Liquid mass flow rate, kg/hr	σ	Surface tension, N/m
G_f	Vapor mass flow rate, kg/hr	m	m = dy/dx (Slope of equilibrium line)
E_{OGm}	Point efficiency (fractional)	λ	Stripping factor
α	Relative volatility	D	Column diameter, m
D_L	Liquid diffusivity, m^2/s	d_h	Hole diameter, m
D_G	Vapor diffusivity, m^2/s	TS	Tray spacing, m
ρ_L	Liquid density, kg/m^3	h_w	Weir height, m
ρ_G	Vapor density, kg/m^3	W	Weir length, m
μ_L	Liquid viscosity, Pa-s	A_b	Active or bubbling area, m^2
μ_G	Vapor viscosity, Pa-s	A_n	Net area, m^2

Table D.14: IC4/NC4 system 2758 kPa, sieve tray efficiency data, 8.3% hole area, model predictions with the Syeda et al. sieve tray efficiency model and the new fraction jetting model.

F_b	d_{32L}	t_{GLB}	E_{LB}	F_{SB}	E_{SB}	E_B	f_j	E_j	E_{OGc}
0.258	0.018	0.217	0.020	0.902	1.000	0.904	0.290	0.924	0.910
0.395	0.019	0.225	0.017	0.988	1.000	0.988	0.388	0.898	0.953
0.529	0.020	0.236	0.016	0.998	1.000	0.998	0.462	0.878	0.943
0.599	0.021	0.242	0.015	0.999	1.000	0.999	0.493	0.870	0.936
0.626	0.021	0.244	0.015	1.000	1.000	1.000	0.504	0.868	0.933
0.184	0.016	0.210	0.020	0.712	1.000	0.717	0.222	0.938	0.767
0.249	0.018	0.212	0.018	0.878	1.000	0.880	0.281	0.922	0.892
0.385	0.019	0.219	0.016	0.983	1.000	0.983	0.379	0.896	0.950
0.512	0.020	0.226	0.014	0.997	1.000	0.997	0.449	0.878	0.944
0.577	0.021	0.231	0.014	0.999	1.000	0.999	0.480	0.870	0.937
0.614	0.021	0.232	0.014	0.999	1.000	0.999	0.498	0.865	0.932

F_b	F-factor, $(Pa)^{0.5}$	E_{SB}	Efficiency of the small bubbles, fractional
d_{32L}	Sauter mean diameter of the large bubbles, m	E_B	Efficiency of the bubble zone, fractional
t_{GLB}	Residence time of the large bubbles, s	f_j	Fraction jetting, fractional
E_{LB}	Efficiency of the large bubbles, fractional	E_j	Efficiency of the jetting zone, fractional
F_{SB}	Fraction of small bubbles in the bubble zone, fractional	E_{OGc}	Predicted point efficiency, fractional

VITA

Anand N. Vennavelli

Candidate for the Degree of

Doctor of Philosophy

Dissertation: A PHENOMENOLOGICAL MODEL FOR FRACTION JETTING ON DISTILLATION SIEVE TRAYS FOR MULTI-REGIME MASS TRANSFER MODELING APPLICATIONS

Major Field: Chemical Engineering

Biographical:

Personal Data: Born in Hyderabad, AP, India on February 24, 1981.

Education:

Received the B.Tech degree from Osmania University, Hyderabad, AP, India, 2002, in Chemical Engineering

Received the M.S. degree from Oklahoma State University, Stillwater, Oklahoma, United States of America, 2006, in Chemical Engineering

Completed the requirements for the degree of Doctor of Philosophy with a major in Chemical Engineering at the Oklahoma State University in May, 2011.

Experience:

Worked at the ConocoPhillips San Francisco Refinery during the summers of 2006, 2007, and 2008.

Name: Anand N. Vennavelli Date of Degree: May, 2011

Institution: Oklahoma State University Location: Stillwater, Oklahoma

Title of Study: A PHENOMENOLOGICAL MODEL FOR FRACTION JETTING ON DISTILLATION SIEVE TRAYS FOR MULTI-REGIME MASS TRANSFER MODELING APPLICATIONS

Pages in Study: 109 Candidate for the Degree of Doctor of Philosophy

Major Field: Chemical Engineering

Scope and Method of Study: Predicting the fraction of the vapor transported as jets, or fraction jetting, on a distillation tray operating in the mixed-froth regime has several advantages. The fraction jetting model can explain the gradual changes in tray efficiency during the froth-spray transition and eliminate the need to predict the froth-spray transition point when separate froth and spray regime models are used. Fraction jetting models facilitate multi-regime efficiency models, such as the Syeda, Afacan, and Chuang (2007) sieve tray efficiency model, that are valid for both froth and spray regimes. In this work, a new phenomenological model to predict fraction jetting is presented. The model is developed using the air-water fraction jetting data of Raper et al. (1982) on sieve trays. The fraction jetting model is developed such that it can be directly used in multi-regime mass transfer modeling applications.

Findings and Conclusions: A single parameter phenomenological model, based on the modified Froude number, has been developed. The model structure is consistent with existing empirical fraction jetting models and the model parameter signifies a change in the dominant mode of vapor transport from bubbles to jets. In addition, the model predictions of the Syeda et al. sieve tray efficiency model with (a) the new fraction jetting model and (b) the Syeda et al. fraction jetting model are compared to show that the new fraction jetting model can directly replace the Syeda et al. fraction jetting model in the Syeda et al. sieve tray efficiency model while retaining the unique crowned efficiency-rate patterns of the Syeda et al. efficiency model. The new fraction jetting model is expected to lead to improved models for predicting multi-regime efficiency as it is based on a phenomenological understanding of the mechanisms that lead to bubbling and jetting.

ADVISOR'S APPROVAL: Dr. James R. Whiteley